MEASUREMENT OF STRESS AND DISEASE MARKERS IN BIOLOGICAL FLUIDS BY FAST SCAN CYCLIC VOLTAMMETRY AND HPLC-UV

By

MEHJABIN ABDUL MAJID KATHIWALA

A DISSERTATION PRESENTED TO THE GRADUATE SCHOOL
OF THE UNIVERSITY OF FLORIDA IN PARTIAL FULFILLMENT
OF THE REQUIREMENTS FOR THE DEGREE OF
DOCTOR OF PHILOSOPHY

UNIVERSITY OF FLORIDA

2009

To my loving husband & lovely son,
Krupant & Isa Vora

ACKNOWLEDGMENTS

It is a pleasure to thank all the people involved in making this dissertation possible. First and foremost, I would like to thank my advisor, Dr. Anna Brajter-Toth, for her help and guidance throughout my work. Dr. Brajter-Toth has been not only my advisor, but also my friend. It's been a wonderful relationship. I would like to thank my committee members Dr. Vaneica Young, Dr. Charles Martin, Dr. Benjamin Smith and Dr. Richard Melker for their guidance over the years.

I would like to thank Dr. Charles Martin once again along with Dr. Fatih Buyukserin for helping me obtain the SEM images of my sensor. Next, I would like to thank Dr. Richard J. Johnson for partial funding of the work presented in this thesis. I would like to express my heartfelt gratitude to Dr. Anne Simmonds from Guy Hospital, UK, for helpful discussions and the xanthinuric urine sample. I would also like to thank Dr. Sergey Jharikov from the Veterans Affairs Hospital for preparing the cell samples and teaching me to do the same. Very special thanks to Dr. Kathryn Williams, Lori Clark, Jeanne Karably and Antoinette Knight for their continued support through my years at UF.

Being away from my son Isa during this past year was the best motivation to complete this dissertation. My husband, Krupant has always been by my side with kind and encouraging words. He has been with me on this exciting journey and I love him for being there for me.

A very special thanks to my parents, to whom I owe everything I am today. My father, Late Abdul Majid Kathiwala inspired me to be my best in everything I did. I am sure he is proud of me today. My mother Mrs Naeema Kathiwala's unending love and support made the hardest task seem easy. With her blessings I will always have the courage to move ahead in life. I would like to thank my father-in-law Mr Dinesh Jayantilal Vora and mother-in law Mrs Mallika Vora for helping me take care of Isa and for their love and support.

I would also like to extend my gratitude to my brothers, sisters, brothers-in-law, sisters-in-law, nieces and nephews, who have loved and supported me always. Thanks to Dr. Roberto Bravo, Dr. Kholoud Abou El-Nour, Dr. Nare Alpheus Mautjana, Andrews Obeng Affum, Abraham Boateng, Jason Perry, Abbigail Davenport, Rachel Cohen, Kulvir Nandra, David Price and Gelin Looi for their help, friendship and support. I would like to thank my dear friend Dr. Rekha Pai for her love and support.

I also want to thank this great country, The United States of America, where I have met so many lovely people, including my wonderful husband, and I have fulfilled my dreams and more. Above all I would like to thank Allah for his guidance and love in every step of my life.

TABLE OF CONTENTS

LIST OF TABLES

LIST OF FIGURES

LIST OF SCHEMES

Abstract of Dissertation Presented to the Graduate School
of the University of Florida in Partial Fulfillment of the
Requirements for the Degree of Doctor of Philosophy

MEASUREMENT OF STRESS AND DISEASE MARKERS IN ENDOTHELIAL CELL SUPERNATANT AND BIOLOGICAL FLUIDS BY FAST SCAN CYCLIC VOLTAMMETRY AND HPLC

By

Mehjabin Abdul Majid Kathiwala

August 2009

Chair: Anna Brajter-Toth
Major: Chemistry

Changes in the concentrations of purine metabolites released from endothelial cells of the pulmonary artery (PAECs) and aorta (AECs) exposed to oxidative stress were studied to identify possible stress markers. Detection of purine metabolites was achieved using HPLC-UV and fast scan cyclic voltammetry (FSV) at nanostructured carbon fiber sensor (N-CFS).

An N-CFS that was compatible in the measurements in biological media was obtained by potential cycling in phosphate buffer between +1.5 V and -1.0 V for 30 min. Initial compatibility of the N-CFS with FSV was performed in diluted urine sample. Xanthinuria is a rare disease, in which xanthine oxidase deficiency leads to the accumulation of xanthine (XA) in urine. Sensitivity of XA measurements at the N-CFS with FSV was optimized and XA was measured in 2000-fold diluted xanthinuric urine. This work demonstrated that the sensor could be used to measure XA as a disease marker. Results showed good agreement for measurement of metabolites in urine sample by HPLC-UV. However, for measurement of metabolites in cell supernatants, the fabrication of N-CFS and the FSV signal acquisition method required further optimization to obtain a low and stable background signal. The optimization procedure for the measurements in cell supernatants involved fabrication of the nanostructured sensor surface in

simple physiological media and FSV signal acquisition in diluted cell supernatant to minimize matrix effects. The dilution was possible due to the high sensitivity of the sensor with FSV methods.

The optimized FSV method with the N-CFS was used for the measurements of the metabolites in cell supernatants. The results showed a large sensor response in supernatants of PAECs and AECs exposed to oxidative stress, and indicated the presence of a mixture of metabolites, which were identified by a HPLC-UV method. Metabolites included uracil (Ur), 2,8-dihydroxyadenine (2,8-DHA), uric acid (UA), hypoxanthine (Hy) and XA, with 2,8-DHA present at highest concentrations. This was the first time 2,8-DHA was detected and identified in endothelial cell supernatant exposed to oxidative stress. The HPLC-UV results indicated that the analyte detected with the N-CFS and FSV in the cell supernatants was 2,8-DHA, since the levels of Ur, UA, Hy and XA were low compared to those of 2,8-DHA. A preliminary method using the N-CFS was developed for the measurement of 2,8-DHA in cell supernatants.

CHAPTER 1
INTRODUCTION

Oxidative Stress

Oxidative stress is defined as an imbalance between reactive oxygen species (ROS) and antioxidants, with the former prevailing. In chemical terms, oxidative stress is a large rise in cellular reduction potential.[1] The effect of oxidative stress depends on the magnitude of these changes. At times cells are able to regain their original state by overcoming stress, but severe oxidative stress can cause cell death or necrosis, and in some cases even moderate oxidative stress can bring about apoptosis.

Hypoxia is defined as a pathological condition in which the entire body or a region (tissue or cells) is deprived of oxygen supply. Cells can be categorized as hypoxia tolerant or hypoxia sensitive. Hypoxia tolerant cells would depress the ATP turnover, while the hypoxia sensitive cells would cause ATP depletion and increased concentrations of the metabolites of ATP: namely, adenosine (Ado), inosine (Ino), hypoxanthine (Hy), xanthine (XA) and uric acid (UA).

Hypoxia

Hypoxia is suggested to cause oxidative stress *in vivo* and *in vitro* based on the observation that exposure to hypoxic conditions causes an increase in platelet activating factor (PAF), a potent phospholipids activator and mediator of many leucocyte functions, including platelet aggregation, inflammation and anaphylaxis *in vivo*. These conditions are in turn, caused by accumulation of reactive oxygen species (ROS).[2] The primary sources of these ROS are the mitochondria, peroxisomes, cytochrome P450 enzymes, and the endothelial white blood cells.[3, 4] Under normal conditions there is a healthy balance of the ROS and the antioxidants. However, under the influence of various external factors, such as pollution, stress and chronic conditions, the balance is no longer maintained, and there is an increase in the ROS. Another source of ROS

is the xanthine oxidase-xanthine dehydrogenase system, which is highly localized in the endothelial cells and converts Hy to XA to UA. Under oxidative stress, xanthine dehydrogenase is converted to xanthine oxidase, and free radicals are generated as a byproduct. Cigarette smoke, polluted air and some drugs are known to provoke free radical reactions. The ROS produced may induce permeability of Ca^{2+}, which in turn results in perturbation of endothelial cells and results in PAF synthesis.[5]

The decrease in the production of ATP to meet the energy demands of the cell causes membrane depolarization and an influx of Ca^{2+} through voltage-gated Ca^{2+} channels. Accumulation of ROS is initiated early during ischemia or hypoxia as the cytosolic Ca^{2+} concentration increases and upsets the mitochondrial handling of Ca^{2+}. Nuclear and mitochondrial DNA are known targets of free radical attack, which can result in base hydroxylation and strand cleavage leading to ATP degradation.[6, 7] ATP is further broken down to Ado by the enzymes ecto-ATP apyrase (CD39) and ecto-5'-AMP nucleotidases (CD73).[8] As their names suggest these enzymes are bound to the cell surface. Ado released into the interstitial spaces is rapidly metabolized to inosine (Ino), Hy, XA and UA.[9] Another important effect of hypoxia is the increased activity of the enzyme xanthine oxidase which is responsible for the conversion of Hy to XA and finally to UA. Under hypoxia, xanthine oxidase activity is increased due to posttranslational modulation of the enzyme.[10] Under ischemia, the concentration of UA in the brain increases from basal levels to approximately 40 nmol/g of wet tissue after 24 -48 hrs.[11] Levels of Hy have also been found to increase in heart perfusate after occlusion[9] and in smooth muscle cells exposed to hypoxia.[12] The increased enzyme activity leads to increased XA and UA production via the purine catabolism pathway. Thus, hypoxia may lead to increases in the

concentrations of the major metabolites in the purine pathway; of specific interest are Ado, Ino, Hy, XA and UA.

We can thus divide the effect of hypoxia into three stages, the first stage being the inability of ATP production to meet the energy demand of the cells, leading to ATP depletion and increases in purine metabolites in the case of hypoxia-sensitive cells. Next, hypoxia will lead to membrane depolarization and increased Ca^{2+}concentrations.[13, 14] Since ROS are produced at the onset of hypoxia, this will further increase Ca^{2+} permeability and perturb the cell membrane resulting in DNA and RNA degradation. Finally, the situation is further accelerated by the increased activity of xanthine oxidase which provides a constant supply of ROS as a byproduct. The mechanism by which the cells struggle to survive (or in some cases to delay death) must be studied in depth in terms of the levels of purine metabolites to identify metabolite as markers of stress leading to cell death. Measurement of the levels of Ado and its metabolites may further help in investigating their roles in hypoxia/ischemia induced oxidative stress.

Hyperoxia

Oxidative stress is known to contribute to tissue injury following irradiation and hyperoxia.[15, 16] Oxidative stress can result from either diminished levels of antioxidants or increased production of ROS.[17] The resulting oxidative damage can have any of the following effects: a) adaptation of the cell by upregulation of defense systems, b) cell injury, i.e. damage to molecular targets like lipids, DNA, carbohydrates, proteins etc; and c) cell death. Following cell injury, the cell may recover or survive with persistent damage, while damage to DNA may trigger cell death by apoptosis or necrosis.

Hyperoxic ventilation (oxygen supply to the affected organ) during surgeries can diminish the chances of wound infections and has shown to reduce brain damage after experimental stroke (occluded blood supply to brain).[18, 19] But high oxygen pressures have been found to have

harmful effects on the lungs in humans and deaths in lab animals due to hyperoxic lung injury.[20,21,22] It is thought that hyperoxia causes its harmful effects via ROS formation.[17] As mentioned earlier, this can cause an imbalance between free radicals and antioxidants and may lead to cell damage, which in turn causes purine and pyrimidine metabolites to be released. Measurement of the changes in their levels caused by high oxygen pressures on pulmonary artery endothelial cells may help to identify a marker of hyperoxic lung injury and may contribute to investigating cellular mechanisms under high oxygen tensions. In order to determine the effects of varying oxygen tensions on the cellular metabolism, we will study the effect of hypoxia and hyperoxia on the release of purine and pyrimidine metabolites in the extracellular fluid of the pulmonary artery endothelial cells (PAECs) and aortic endothelial cells (AECs).

Effect of Oxidative Stress on Endothelial Cell Metabolism

Endothelial cells serve as a barrier between blood and the tissues and thus are the first to experience composition changes in the extracellular environment, such as changes in normal levels of glucose and in oxygen pressure associated with stress and disease.[23] Under physiological conditions, PAECs are exposed to low oxygen pressures of 3-5 %[24] since the pulmonary artery carries deoxygenated blood from the heart to the lungs for purification. Consequently PAECs are highly tolerant to low oxygen pressure, which in other cells is associated with hypoxic stress. The tolerance to low oxygen pressure in PAECs is likely due to cellular processes which preserve ATP and GTP by increasing glycolytic metabolism for the production of the nucleotides.[25,26] On the other hand, endothelial cells which line the aorta (AECs), which carries oxygenated blood from the heart to blood vessels, are exposed to normal oxygen pressures of around 14-20 %. Changes in oxygen pressure to higher than normal at PAECs or lower than normal at AECs expose the cells to hyperoxia and hypoxia, respectively.

Recent analysis of glucose deprivation at AECs showed an increase in the levels of purine metabolites in the cell supernatant. During glucose deprivation, the cells can use triglycerides as the energy source to upregulate purine *de novo* synthesis.[27] In the assay, the incorporation of [^{14}C]formate at position 8 of the purine ring was measured.[27, 28] Normal conditions in the cells are marked by purine and pyrimidine catabolism and salvage pathways occuring in conjunction. The energy cost of synthesizing a nucleotide *de novo* is higher in ATP equivalents than that of reutilizing an intact purine or pyrimidine ring.

After 24 -48 hr of hypoxia in rat brain, levels of UA increase, while the levels of XA and Hy decrease, suggesting high activity of xanthine oxidase during hypoxia.[29, 30, 30, 31] In smooth muscle [32]and endothelial cells,[33] the levels of Hy and XA increase under hypoxia while the levels of UA remain unchanged. UA and uracil (Ur) have been found to increase during energy stress in smooth muscle.[34] The activity of xanthine oxidase decreases under hyperoxia in rat PAECs.[31]

Hypoxia and hyperoxia can cause an increase in the production of reactive oxygen species (ROS) from molecular oxygen, forming superoxide radicals ($O_2^{\bullet-}$), hydrogen peroxide (H_2O_2) and hydroxyl radicals ($OH^{\bullet}$).[35] Sources of ROS are the electron transport chain in the mitochondria and metabolic pathways, such as the NADPH oxidase and xanthine oxidase/dehydrogenase systems.[4, 36, 37] Under hypoxia, endothelial nitrogen oxide synthase (eNOS), which is located in the Golgi complex and the cell membrane,[38] is activated due to Ca^{2+} influx to generate nitric oxide ($NO^{\bullet}$) above basal levels in order to promote vasodilation. Hyperoxia in ovine fetal-PAECs causes a 2.7-fold increase in the expression of eNOS.[39] However, under reduced intracellular levels of eNOS[40] or absence of either the substrate L-arginine (possibly due to argininosuccinate synthetase deficiency) or the cofactor tetrahydrobiopterin (BH_4) (due to defect in synthesis and/or regeneration), BH_4 is also

susceptible to oxidation and degrades to 7,8-dihydrobiopterin. Heme reduction in the enzyme results in the uncoupling of eNOS and consequently leads to the production of $O_2^{\bullet-}$ rather than $NO^{\bullet}$,[41, 42] and decreased levels of $NO^{\bullet}$. In addition, the reaction of $O_2^{\bullet-}$ and $NO^{\bullet}$ at diffusion-limited rates to form peroxinitrite radicals ($ONOO^-$) drops the levels of $NO^{\bullet}$ even more.[43] Under normal conditions there is a balance between ROS production and the levels of cellular antioxidants which scavenge the radicals such as superoxide dismutase, catalase and glutathione peroxidase.[44, 45] But, an imbalance between ROS production and antioxidant levels induces oxidative stress. It has been suggested that UA can scavenge $O_2^{\bullet-}$, $ONOO^-$, and $NO^{\bullet}$ to form allantoin, triuret and 6-aminouracil, respectively, in urine.[46] However, since $ONOO^-$ is formed at diffusion-limited rates, the formation of 6-aminouracil and allantoin should be limited.[46, 47] In γ-irradiated plasma, UA has been suggested to scavenge nitrogen dioxide radical ($NO^{\bullet}_2$) formed from $ONOO^-$.[48, 49]

Oxidative stress can result in adaptation of cells by up/down regulation of signaling molecules and metabolism, while extended periods of stress can cause cell injury via damage to lipids, proteins, RNA, and finally DNA, which may trigger cell death by apoptosis or necrosis.

Experimental observations have shown that under oxidative stress, production of ROS is enhanced as seen in (Figure 1-1), which causes the Na^+/Ca^{2+} exchanger and voltage-gated Ca^{2+} channels to operate in the reverse mode leading to an influx of extracellular Ca^{2+}.[50] Further, the elevated levels of ROS in the mitochondria can cause the Ca^{2+}-ATPase motor to stop functioning due to increased demand for ATP, and this also increases Ca^{2+} levels in the mitochondria and increases levels of ROS.[13, 14] The rising Ca^{2+} concentration in the cytoplasm causes Ca^{2+} influx into the nucleus through the pores in the nuclear envelope.[13] Furthermore, under hypoxia and hyperoxia, intracellular Ca^{2+} acts as a signaling molecule which signals the release of ATP into

the extracellular fluid via the membrane hemichannels[51, 52] and vesicles.[53] Extracellular ATP signaling activates purine receptors which activate kinases. The activated purine receptors mediate glucose uptake for cell survival, and the activated kinases have protective effects and inhibit apoptosis.[52, 54] However, after 2 hr the extracellular ATP levels decrease, resulting in the degradation of ATP to Ado. The extracellular Ado can re-enter the endothelial cells and is degraded by adenosine deaminase and nucleoside phosphorylase to Ino and Hy.[55] Finally, under hypoxia, there is a decrease in the production of ATP (in an effort to conserve energy), to meet the energy demands of stressed cells. This generates AMP and ADP, which are degraded to purine metabolites.[9]

In addition, extended exposure to oxidative stress can cause DNA damage by fragmentation, hydroxylation and strand cleavage, leading to base degradation.[6, 7, 56] Since RNA is more abundant in cells than DNA, it is damaged more easily by ROS. Because of defects in RNA molecules, there are subsequent errors in protein synthesis,[57] which are, however, less lethal than mutations in the genome of the cell. Thus the cells can tolerate higher levels of damage in RNA than in DNA. RNA degradation is the major mechanism of removal of damaged RNA.[58] Ur and XA are the final degradation products of the RNA pyrimidines (Ur and cytosine) and the purines [adenine (Ade) and guanine (Gua)], respectively.[59] Degradation of DNA and RNA is regulated by metabolic pathways, which control production of purine and pyrimidine nucleotides as shown in (Figure. 1-2).

Oxidative stress can cause disruptions in the normal purine and pyrimidine cycle, which can cause an increase in the levels of purines and pyrimidines due to decreased use and increased degradation of cellular purines.[60] The disruption of the purine and pyrimidine pathways elevates levels of metabolites and makes the metabolites susceptible to oxidation by ROS.

Different methods have been used to measure purine and pyrimidine metabolites. Capillary electrophoresis (CE) has been used in the analysis of Ado with LOD's ranging from 0.9 fmol for cAMP to 30 fmol for Ado.[61] Electrochemical sensors show good sensitivity and selectivity toward purine metabolites in urine samples.[62, 63] The most widely used method for measurement of purine and pyrimidine metabolites is gradient elution HPLC with UV-detection, with limits of detection of 0.50 μM for purine metabolites.[64] In this work, reverse phase HPLC-UV with isocratic elution allows a good separation of the purine and pyrimidine metabolites of interest within 20 min with limited loss or sample decomposition.

Under oxidative stress when ROS are produced, the chain of events described above is expected to lead to changes in the concentrations of purine and pyrimidine metabolites released in the cell supernatant. In this work, the feasibility of measuring changes in the concentrations of purine and pyrimidine metabolites in cell supernatant of PAECs and AECs as markers of oxidative stress/damage due to abnormal oxygen pressures from normal was tested using HPLC-UV. The concentration changes of these metabolites can provide an insight into the survival technique adapted by the cells to delay death, or the changes occurring in the cells as a function of oxidative stress.

Purine and Pyrimidine Cycle in Oxidative Stress

Purine and pyrimidine nucleotide synthesis *de novo* and salvage reactions provide alternative but concerted means for regulating production of purine and pyrimidine nucleotides to meet cellular requirements. The energy cost of synthesizing a nucleotide *de novo* is six times higher in ATP equivalents than that of reutilizing an intact ring. As a result, cells have an extremely efficient mechanism, which involves the degradation and recycling of daily waste products of normal muscle work and wound healing. This is called the salvage pathway.

Normal conditions are marked by purine and pyrimidine catabolism and the salvage pathway occuring in conjunction. Anomalous conditions, however, either activate or disable a certain pathway and result in accumulation or depletion of metabolite(s). As mentioned above, oxidative stress can be one of the conditions, and enzyme deficiency is also known to affect the levels of purine and pyrimidine metabolites.

Deficiency of an enzyme results in an imbalance of product and substrate in purine and pyrimidine catabolism leading to severe disorders. Deficiency of xanthine oxidase (enzyme responsible for the conversion of Hy to XA to UA) results in the accumulation of XA and to a lesser extent Hy, and leads to a condition referred to as xanthinuria. XA is a by-product of several pathways, and thus is present in high concentrations. Hy is not present in large amounts, as its chief metabolic fate is phosphorylation to IMP via the salvage pathway.[65-68]

There are other examples of disorders in the purine cycle. Severe combined immunodeficiency disease (SCID) is caused by a deficiency of adenosine deaminase, the enzyme responsible for converting Ado to Ino in the catabolism of the purines. A deficiency of adenosine deaminase selectively leads to the destruction of B and T lymphocytes, the cells that mount immune responses.[67] The most common purine disorder is gout which results from an excess of purine or partial deficiency of the salvage enzyme HGPRT which converts Hy to IMP. Deficiency of adenine phosphoribosyltransferase causes accumulation of Ade and thus formation of 2,8-DHA, and leads to a condition referred to as 2,8-dihydroxyadenine lithiasis.[69, 70]

In the pyrimidine cycle there are two disorders due to enzyme deficiency: orotic aciduria type I, which is due to deficiencies of orotate phosphoribosyl transferase and OMP decarboxylase; and orotic aciduria type II, which is due to a deficiency of OMP decarboxylase. Both of these disorders lead to retarded growth and severe anemia.

Carbon Fiber Ultramicroelectrodes

Carbon fiber sensors have been used with great success for measurements *in vitro* and *in vivo* of metabolites such as dopamine (DA), UA, ascorbic acid (AA), XA and Hy.[62, 63, 71-79] Due to their small size, they can be used in conjunction with fast scan cyclic voltammetry (FSV). Carbon fiber sensors are especially popular due to their ease of construction, small size and rapid response times.[73, 80-83] Carbon fibers are made from different precursor materials, most commonly polyacrilonitrile (PAN), viscose rayon, petroleum or coal tar pitch, and phenolic resin.[84, 85]

Manufacture of carbon fibers involves polymerization, spinning of fibers, thermal stabilization, carbonization and finally graphitization. The properties of carbon fibers can be modified to improve mechanical properties by increasing the crystallinity and orientation of the atoms and also by reducing the defects.[86-88] The cross sections of carbon fibers can have different structures, defined as the "onion", "radial" or "random" types.[85] The carbon fiber surface is very complex and has a high fraction of edge planes.[88] It is proposed that most of the electron transfer at the carbon fiber occurs at the edges of the plane due to the presence of functional groups such as phenol, carbonyl, carboxyl, quinine and lactone as shown in (Figure 1-3).

The sensitivities of carbon fibers can be increased by pretreatment methods.[89] In spite of their popularity for the study of biological systems, one drawback to the use of carbon electrodes is that they often foul, causing a loss in the observed electrochemical response and/or a decrease in the observed charge transfer kinetics. Accurate analytical determination of electroactive species is difficult under such conditions. Consequently, various electrode activation schemes have been developed in order to enhance the observed rate of electron transfer at the electrode-solution interface. The high sensitivity at treated carbon fibers is achieved by chemical or physical modification to enhance the desirable properties of the surface. The most commonly

used techniques for activation of the carbon fiber surface are mechanical, electrochemical, thermal, and chemical.

Mechanical polishing of the carbon fiber involves polishing of the surface with 600-grit emery paper to remove surface defects and impurities. The surface is then polished with 0.05 mm alumina using a polishing wheel to produce a mirror like surface. Once the electrode surface is polished, the electrode is dipped in 1:1 propanol water and sonicated to remove the surface impurities.[90] Diamond particles in place of alumina have been used to avoid contamination of the carbon fiber surface. In this work, mechanical polishing was combined with electrochemical activation, as developed earlier by Bravo et al.[73]

Fabrication of an active surface at the carbon fiber through electrochemical methods has been found to be highly effective in enhancing the sensitivity and selectivity. Bravo et al and Kholoud et al have reported a remarkable improvement in the sensitivities of UA, Ado, Hy and XA after electrochemical fabrication procedures, in which the carbon fiber was continuously cycled between -1.0 and + 1.5 V vs SCE for 3600 cycles at 10 V s^{-1}.[63, 71, 73, 91-93] Electrochemical procedures for carbon fibers can be divided in two main categories: mild and strong. Electrochemical fabrication which involves potential limits of 2.0 V or less are referred to as mild, whereas those involving potential limits greater than 2.0 V are considered strong.[87] Mild procedures produce surface oxide functionalities which may increase the sensitivity for positively charged analytes compared to negatively charged analytes. Strong electrochemical procedures, on the other hand, may overoxidize the surface and produce an insulating oxide film over the carbon fiber surface. The cell time constant of the carbon fiber with the oxide film is large due to high resistivity. Strong methods of electrochemical activation can also result in lower resolution of analytes, especially in a mixture.

Heat treatment at 540 °C for 4.5 hr at 1 torr improved the kinetics of AA at the carbon fiber electrode.[94] Activation of the carbon fiber with a nitrogen laser improved the voltammetric responses of dopamine, 4-methylcatechol and 3,4-dihdroxyphenylacetate.[81]

Despite the large number of different techniques that have been used to accomplish activation of carbon fiber surface, there is no universally accepted method of activation.

Carbon fiber surface activation has been attributed to the removal of impurities from the electrode surface, an increase in the electrode area due to roughening and or cracking of the surface, an increase of oxygen-containing functional groups that may act as electron transfer mediators, and the exposure of edge plane carbon and/or lattice defects that may act as sites for electron transfer.[73] The total observed effect of any given activation procedure is most likely due to a combination of these phenomena.

In almost all studies where carbon fiber electrodes are used, it is a common practice to pretreat/fabricate, or activate the electrode surface prior to obtaining electrochemical data. In this work, we have used the fabrication procedure which was developed in our laboratory, in which the carbon fiber sensor is electrochemically oxidized by continuously cycling between -1.0 and + 1.5 V vs SCE for 3600 cycles at 10 V s^{-1}.[73] This procedure produces a very active nanostructured carbon fiber sensor (N-CFS) with increased surface area and improved sensitivity for the analytes. There is efficient mass transport at the surface which facilitates steady state electrochemistry, and this can be observed at scan rates lower than 1 V s^{-1}. (Figure 1-4) shows the voltammogram of 5 mM potassium ferricyanide in 0.5 M KCl, pH 6.0 at the N-CFS before and after the surface fabrication procedure. At a conventional-sized electrode, a peak shaped curve would be obtained due to the greater initial rate of electrolysis compared to the rate of diffusion of the analyte from the bulk. Another advantage of the N-CFS is that the iR effects and

cell time constant are reduced due to the small size of the electrode compared to conventional electrodes.

Fast Scan Cyclic Voltammetry (FSV)

In fast scan cyclic voltammetry (FSV), the voltage is ramped very rapidly, upto 10^6 V s^{-1}. It is extremely difficult, almost impossible, to perform FSV using conventional sized electrodes due to the cell time constant and the iR drop. The cell time constant is the time required to charge the double layer after the potential is applied. The iR drop at conventional sized electrodes distorts the data in electrochemical experiments. The iR and the cell time constant are both dependent on the area of the electrode and are thus greatly reduced at the N-CFS, thus permitting experiments to be performed at very high scan rates.[74, 77, 95] Experimentally scan rates of 1,000,000 V s^{-1} have been used, representing a considerable improvement over 10 V s^{-1}, the rate used at conventional sized electrodes.[96] FSV is a powerful analytical tool. Since the introduction of FSV in the 1980's many voltammetric investigations using FSV at ultramicroelectrodes have shown its advantages over conventional electroanalytical techniques. High temporal resolution allows real time determination,[76] which can be extremely important in measuring concentration changes *in vivo*. The signal averaging capability of FSV improves the S/N ratio. FSV can also be used as a kinetic filter, where a slowly reacting analyte can be differentiated from a rapidly reacting analyte at the N-CFS. Due to the continuous cycling, the surface of the N-CFS is regenerated, thus limiting electrode passivation and increasing the lifetime and quality of the sensor. The most important advantage of FSV is that it stabilizes the N-CFS and limits follow-up reactions, and in turn leads to increased sensitivity of the analytes being measured. Compared to other techniques like chronoamperometry, FSV can provide more information for a particular analyte, which can help in confirming its identity with confidence.

High Performance Liquid Chromatography (HPLC)

Liquid chromatography was discovered in the late 1890's by the Russian botanist, M.S. Tswett. High performance liquid chromatography is a highly improved form of liquid column chromatography, where a solvent is forced through the column under high pressures, instead of allowing it to drip through a column under gravity. In HPLC, the solution containing the mixture of analytes is injected into the column (stationary phase), and a pump moves the solvent (mobile phase) through the stationary phase. During this process, called elution, the components are separated and they are detected by a suitable means to the compounds as they emerge from the column. The resulting chromatogram is a plot of signal intensity versus retention time in the column.

The main components of an HPLC system are the pump, injector, column and detector, as shown in (Figure 1-5). The pump consists of one or more pistons/pump-head assemblies. The pump head is made of stainless steel and has a cavity into which the pistons move in and out, causing the mobile phase to be pushed into the column. The injector port provides a well defined volume of the sample to be introduced into the mobile phase. Injection of sample is achieved manually using a syringe or via automated injection. Normally a guard column is placed at the head of the column to prevent particulate matter from the mobile phase or highly retained sample components from reaching the analytical HPLC column. The most common type of column packing (i.e. stationary phase) is composed of 5 μm silica spheres with octyl ($-(CH_2)_7\ CH_3$) or octadecyl ($-(CH_2)_{17}\ CH_3$) groups bonded to the surface. Because of the nonpolar nature of the stationary phase surface, the retention times of the components increase as their polarity decreases. Commonly used detectors for HPLC are electrochemical, ultraviolet absorption,

fluorescence, mass spectrometric and conductimetric. In this work a UV-detector operated at 254 and 293 nm was used.

Study Overview

The goal of this work was the development of nanostructured carbon fiber sensors (N-CFS) from PAN-based carbon fibers. The aim was to exploit the advantages of N-CFS in metabolite analysis in physiological media such as Hank's Balanced Salt Solution (HBSS) and Dulbecco's Modified Eagle Medium (DMEM).The final goal was the development of the sensor and method for rapid measurements of metabolites released into the supernatants of endothelial cells exposed to oxidative stress, induced by changing the oxygen pressure at the cells.

Fast scan cyclic voltammetry (FSV) at N-CFS has been developed by our group for the measurement of small metabolites in biological fluids e.g. urine, and in physiological buffers. However, in physiological buffers FVS at N-CFS was not successful due to high LODs and sensor passivation. In this work the method was optimized and was successfully applied to measurements of small metabolites in physiological and cellular media.

This introductory chapter has provided information about oxidative stress and the events that occur as a result of oxidative stress at the cellular level. A brief description of pulmonary and aortic endothelial cells was also provided. The techniques that are used throughout the work, FSV and HPLC-UV, were also discussed briefly.

Chapter 2 explains the experimental methods and instrumentation. Details of the instruments, including schematics, are provided and described to help the reader reproduce any of the experiments conducted in this work. Chapter 3 describes the modifications that were performed in the fabrication procedure of the N-CFS with FSV to make the sensor compatible in cellular media.

Chapter 4 describes the application of the N-CFS to the measurement of UA and XA in 2000-fold diluted normal and xanthinuric urine, respectively. The results obtained with FSV were verified with HPLC-UV and standard addition for the urine samples. This chapter also shows the reproducibility of the sensor and the accuracy of the measurements without the need for standard additions. Chapter 4 also includes a method for choosing an electrode for use in biological media. This chapter also describes the surface features of the sensor with the help of SEM images obtained before and after the optimization procedure.

Chapter 5 describes the HPLC-UV results obtained in the supernatants of endothelial cells exposed to oxidative stress. HPLC-UV was performed on the cell supernatant due to sample complexity. The results obtained in this section helped in identification of stress markers in the supernatant of the cells, including a new stress marker, 2,8-dihydroxyadenine (2,8-DHA), which is proposed to be a byproduct of the polyamine synthesis pathway and is accumulated under stress due to upregulation of this pathway in combination with reduced salvage of Ade.

Chapter 6 describes the FSV results obtained at the N-CFS in the cell supernatants and how they compare to the HPLC-UV results. Finally, chapter 7 summarizes the conclusions drawn from the thesis work and proposes ideas for future investigations.

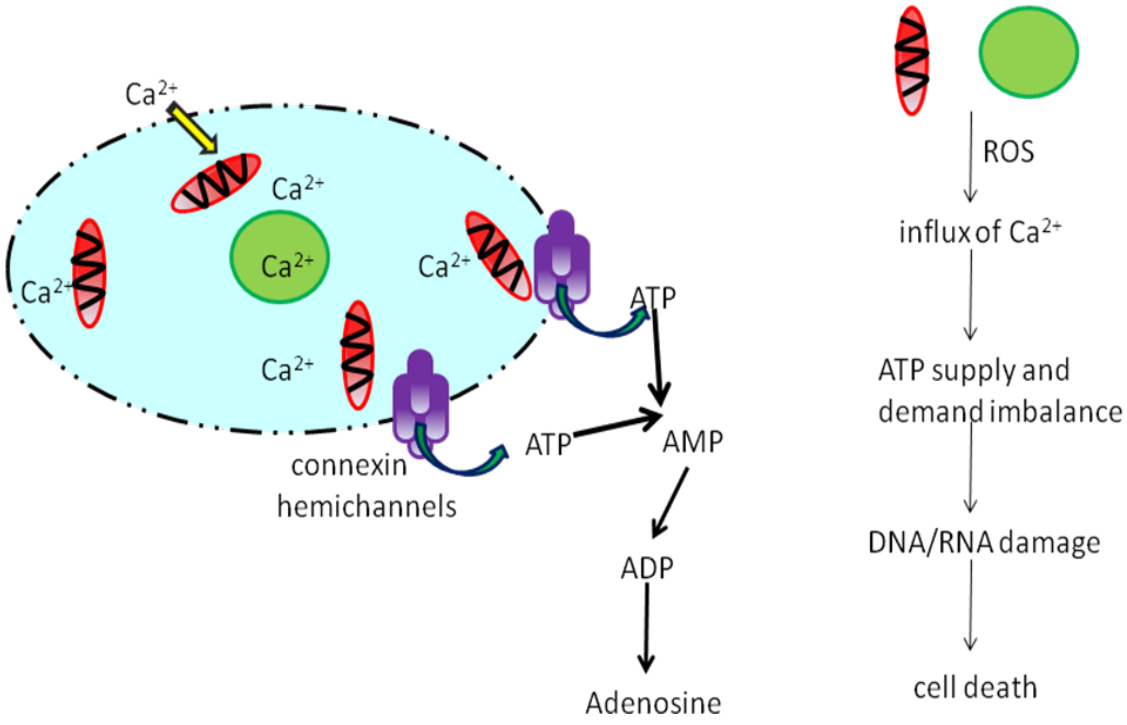

Figure 1-1. Cell diagram showing the effect of oxidative stress on mitochondria (shown in red), and the nucleus (shown in green), leading to DNA and RNA damage and cell death. Under oxidative stress of hypoxia or hyperoxia an influx of extracellular Ca^{2+} (the Na^{+}/Ca^{2+} exchanger and voltage gated Ca^{2+} channels operate in the reverse mode) can increase production of ROS. Elevated levels of ROS in the mitochondria can cause the Ca^{2+}-ATPase motor to stop functioning, due to the increased demand for ATP, and this further increases Ca^{2+} levels, including in the nucleus (through the pores in the nuclear envelope) and further increases ROS production. In addition, under hypoxia or hyperoxia, intracellular Ca^{2+} signals the release of ATP and UTP into the extracellular fluid via the plasma membrane hemichannels (shown in purple), and vesicles. Extracellular ATP and UTP activate purine receptors, which mediate glucose uptake for cell survival and activate kinases which inhibit apoptosis. However, after 2 hr, the extracellular ATP levels decrease, resulting in the degradation of ATP to Ado. The extracellular Ado can re-enter the endothelial cells and is degraded by adenosine deaminase and nucleoside phosphorylase to inosine and hypoxanthine. Finally, under hypoxia, there is a decrease in the production of ATP (in an effort to conserve energy) to meet the energy demands of stressed cells. This generates AMP and ADP, which are degraded to final metabolites. Similarly UTP can degrade to uracil via the action of the ectonucleases

Figure 1-2. Metabolic pathways of purines and pyrimidines. Enzymes in purine pathway: 1. 5-nucleotidase. 2. Purine nucleoside phosphorylase. 3. Xanthine oxidase. 4. Hypoxanthine-guanine phosphoribosyltransferase. 5. Inosine 5'-monophosphate dehydrogenase. 6. Guanine monophosphate synthetase. 7. Guanine deaminase. 8. Adenine phosphoribosyltransferase. 9. Adenosine deaminase. 10. AMP monoadenylate deaminase. 11. Xanthine phosphoribosyltransferase. Enzymes in pyrimidine pathway: 1. Pyrimidine 5'-nucleotidase. 2. Uridine phosphorylase. 3. Dihydropyrimidine dehydrogenase. 4. Dihydropyriminidase. 5. β- Ureidopropionase. 6. Thymidine phosphorylase. 7. Cytidine deaminase. 8. Uridine phosphorylase. 9. Uracil/orotate phosphoribosyltransferase. 10. Uridine/thymidine kinase

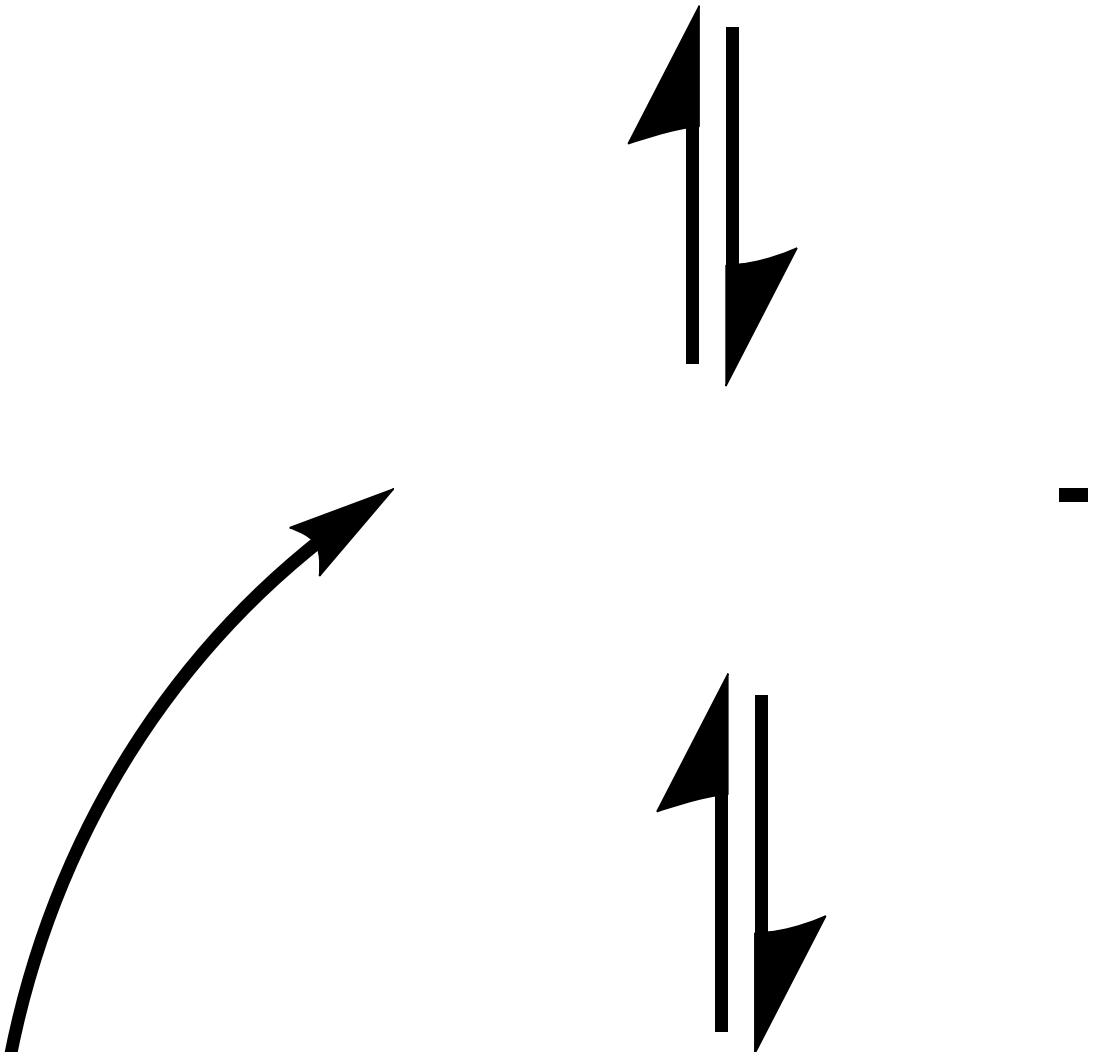

Figure 1-3. A possible structure of oxygen containing functional groups on an electrochemically fabricated nanostructured carbon fiber sensor

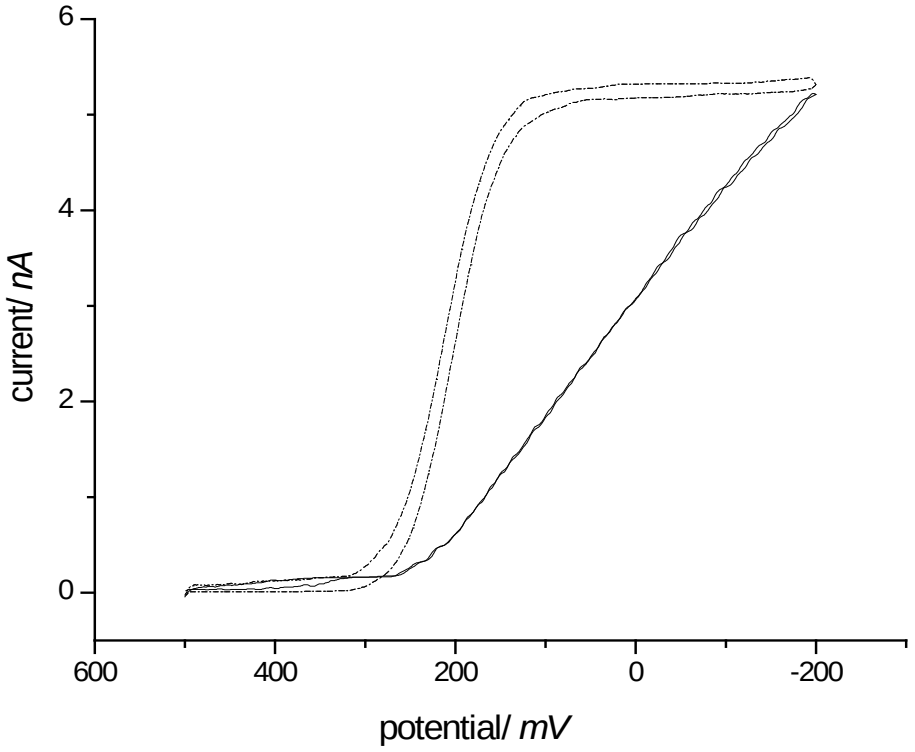

Figure 1-4. Cyclic voltammogram of carbon fiber sensor in 5 mM $K_3Fe(CN)_6$ in 0.5 M pH 6.0 KCl before (solid) and after (dotted) surface fabrication procedure. 50 cycles at 50 mV s^{-1}

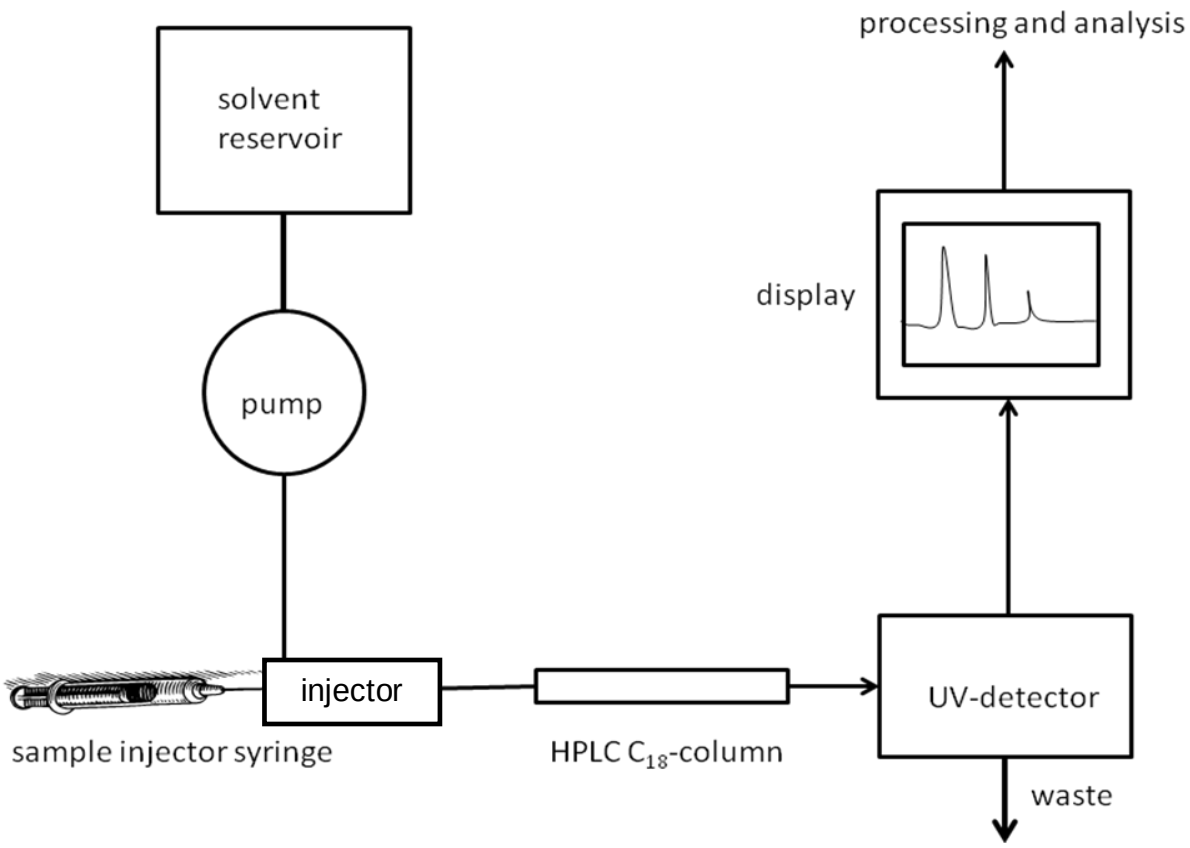

Figure 1-5. Schematic of HPLC instrument

CHAPTER 2
EXPERIMENTAL

Reagents and Solutions

All chemicals were obtained from Fisher (Pittsburgh, PA) and Sigma-Aldrich (St. Louis, MO). Sodium phosphate buffer, pH 7.4, was prepared with sodium phosphate monobasic monohydrate ($NaH_2PO_4 \cdot H_2O$) and sodium phosphate dibasic anhydrate (Na_2HPO_4). pH was adjusted with 0.1 M NaOH or KOH (for HPLC) before the experiments. The mobile phase buffer, pH 5.1, was prepared from KH_2PO_4 and the pH was adjusted with 0.1 M H_3PO_4. HBSS (Hank's Balanced Salt Solution) ($CaCl_2$ 1.26 mM, $MgCl_2.6H_2O$ 0.493 mM, $MgSO_4.7H_2O$ 0.407 mM, KCl 5.33 mM, KH_2PO_4 0.441 mM, $NaHCO_3$ 4.17 mM, NaCl 137.93 mM, Na_2HPO_4 0.338 mM, and D-glucose 5.56 mM) and Dulbecco's Modified eagle Medium (DMEM) (Glycine 0.4 mM, L-Arginine hydrochloride 0.398 mM, L-Cystine.2HCl 0.201 mM, L-Glutamine 4.0 mM, L-Histidine hydrochloride.H_2O 0.2 mM, L-Isoleucine 0.802 mM, L-Leucine 0.802 mM, L-Lysine hydrochloride 0.798 mM, L-Methionine 0.201 mM, L-Phenylalanine 0.4 mM, L-Serine 0.4 mM, L-Threonine 0.798 mM, L-Tryptophan 0.0784 mM, L-Tyrosine disodium salt dehydrate 0.398 mM, L-Valine 0.803 mM, Choline chloride 0.026 mM, D-Calcium pantothenate 0.00839 mM, Folic acid 0.00907 mM, i-Inositol 0.04 mM, Niacinamide 0.0328 mM, Pyridoxine hydrochloride 0.0196 mM, Riboflavin 0.00106 mM, Thiamine hydrochloride 0.0119 mM, $CaCl_2$ 1.8 mM, $Fe(NO_3)_3.9H_2O$ 0.000248 mM, $MgSO_4$ 0.814 mM, KCl 5.33 mM, $NaHCO_3$ 44.05 mM, NaCl 110.34 mM,$NaH_2PO_4.H_2O$ 0.906 mM, D-glucose 5.56 mM, Phenol Red 0.0399 mM and sodium pyruvate 1.0 mM) were purchased from Invitrogen (Carlsbad, CA). Xanthine oxidase (EC 1.17.3.2.) 0.73 units/mL and uricase (EC 1.7.3.3.) 0.78 units/mL, were used in enzyme assays. All determinations were performed at room temperature. Doubly deionized water (dDI) was used

to prepare solutions, which were prepared fresh before the experiments. HPLC filters were from Millipore (Billerica, MA) and GE Osmonics Labstore (Minnetonka, MN).

Cyclic Voltammetry

In cyclic voltammetry, a triangular waveform is applied to an electrode under controlled diffusion of the analyte, and the current is measured. The potential of a working electrode is scanned linearly from an initial potential, where no faradaic reaction of the analyte occurs, to a final potential where a maximum current i_p is reached due to oxidation or reduction of the analyte. After the maximum current is reached the direction of the linear sweep is reversed and the reduced or oxidized species can be detected. The rate of potential change is the scan rate, ν ($V\ s^{-1}$), and the range between the initial and final potentials is the potential window, which depends on the electrochemical properties of the analyte, electrode and electrolyte. In a cyclic voltammogram the current increases as the potential reaches the reduction/oxidation potential of the analyte depending on the direction of the scan, and falls off as the concentration of the analyte depletes close to the electrode surface. The potential difference between the reduction E_{pc} and oxidation E_{pa} is expressed as

$$\Delta Ep = E_{pc} - E_{pa} \tag{2-1}$$

The theoretical peak current i_p for a diffusion controlled, reversible reaction is given by the Randles-Sevcik equation:

$$i_p = (2.69 \times 10^5)\ n^{1/2}\ A\ D_0^{1/2}\ \nu^{1/2}\ C_0^* \tag{2-2}$$

and for an irreversible reaction is given by:

$$i_p = (2.99 \times 10^5)\ n\ (\alpha n_\alpha)^{1/2}\ A\ D_0^{1/2}\ \nu^{1/2}\ C_0^* \tag{2-3}$$

where n is the number of moles of electrons transferred per mole of compound. A is the area of the electrode in cm^2, D_0 is the diffusion coefficient in $cm^2\ s^{-1}$, ν is the scan rate in $V\ s^{-1}$, C_0^* is the

bulk concentration of the analyte in mol cm^{-3}, α is the transfer coefficient, and $n\alpha$ is the number of electrons in the rate determining step.

The voltammograms at the carbon fiber electrode are sigmoidal in shape as shown in (Figure 2-1B) and are independent of the scan rate up to 1 V s^{-1}. The limiting current i_L at the steady state is given by the equation:

$$i_L = 4nFDCr \qquad (2\text{-}2)$$

where n is the number of electrons, F is the Faraday's constant (9.648531 x 10^4 coulombs mol^{-1}), D is the diffusion coefficient in cm^2 s^{-1}, C is the concentration of the analyte in mol cm^{-3} and r is the radius of the electrode in cm. At higher scan rates the voltammograms are peak shaped as shown in (Figure 2-1A) and the peak current is dependent on the scan rate employed. The radius of the carbon fiber electrode was determined using $Fe(CN)_6^{-3}$ as the redox probe. The diffusion coefficient of 7.7 x 10^{-6} cm^2 s^{-1} was used for $Fe(CN)_6^{-3}$ in 0.5 M KCl.

Fast Scan Cyclic Voltammetry (FSV)

In FSV, a high frequency triangular potential waveform is applied to the cell. A 100 Hz waveform from -1.0 to 1.5 V applied in this work gives a scan rate of 500 V s^{-1}. The time required for each scan is 10 ms. The potential is swept from -1.0 to +1.5 V, which generates a background current at the carbon fiber electrode even without the analyte present, due to double layer charging. The signal obtained at the carbon fiber in the presence of an electroactive analyte such as XA is dependent on the oxidation potential(s) of the analyte which in the case of XA are 0.6 V and 0.9 V vs SCE. The background signal is subtracted from the analyte signal to give the cyclic voltammogram of the analyte as shown in (Figure 2-2).

Instrumental Setup

A Bioanalytical Systems Electrochemical Analyzer (BAS-100, West Lafayette, IN) was used for all the voltammetric determinations at scan rates lower than 1 V s^{-1}. The data were

downloaded to a computer and analyzed using Microcal Origin 6.0 (Microcal Software Inc., North Hampton, MA). A home made preamplifier formed by an input operational amplifier (AD515, Analog Devices),[97] various resistors and capacitors, and a second operational amplifier (OP27) was connected to the BAS-100 as shown in (Figure 2-3).

The minimum current measurable by BAS-100 was 0.1 μA. However, with the preamplifier it could measure currents as low as 0.1 nA due to the gain of the amplifier, which ranged from 100 to 10,000. At low scan rates (less than 40 mV s^{-1}), the time constant of the system was set to 100 μs to minimize distortion of the differences in peak potential, ΔE_p.

The fast scan voltammetry (FSV) system is illustrated in (Figure 2-2) and (Figure 2-4). Here a continuous triangular potential waveform is applied to the SCE reference electrode using a function generator (Universal Programmer, Model 175, EG&G Princeton, NJ, USA) in a two-electrode configuration system. A home built current transducer measured the current at the electrode in fast scan voltammetry.[97] A copper mesh Faraday cage was used to minimize noise. The current was converted to voltage, amplified, recorded and stored by a digital oscilloscope (LeCroy Model 9310A, Chestnut Ridge, NY). The applied waveform was simultaneously monitored using Channel 1 of the oscilloscope. Stored data were transferred from the oscilloscope to a PC for display and analysis.

A syringe was used to inject all solutions into an ~80-μL electrochemical cell which was used in fast scan voltammetric experiments, and the injections allowed the solutions to be pumped into the cell to maintain permanent contact between the solution and electrode. First the background current was recorded in buffer followed by the analyte solution in the same buffer. The oscilloscope allowed for the subtraction of the background current from the total analyte current to produce a background subtracted voltammogram as shown in (Figure 2-4).

To minimize noise, signal averaging with digital processing of the data was used. A total of 250 scans from -1.0 to + 1.5 V were recorded at 500 V s^{-1} for both the buffer and the analyte solution in buffer, which were averaged and stored for digital background subtraction. The number of scans (cycles) recorded was a compromise to achieve a high signal-to-noise ratio in a short time.[74]

Electrodes

Polyacrylonitrile (PAN) based carbon fiber (7.5 μm diameter; Textron Specialty Materials, Lowell, MA) was the working electrode material. A single carbon fiber was attached to a copper wire with silver epoxy (EPO-TEK 410 E, Epoxy Technology, Billerica, MA). The epoxy was allowed to dry for 24-48 hr, and the fiber and copper wire were sealed in a micro pipet tip and allowed to dry for another 48 hr. The previous procedure[73] was modified by touch polishing of the sealed fiber on 600-grit SiC paper (Mark V Laboratory, East Granby, CT) on a polishing wheel (Ecomet I, Buehler Laboratory, Evanston, IL), and washing with dDI before the electrochemical measurements. Sensors that gave a response in 5 mM $K_3Fe(CN)_6$ in 0.5M KCl (pH 6.0) at 50 mVs^{-1} corresponding to the theoretical diameter of the carbon fiber (7.5 μm) were used for analysis. A disk geometry was assumed, and the diffusion coefficient of $Fe(CN)_6^{3-}$ is 7.7 x 10^{-6} cm^2s^{-1}.[98] The capacitance of the sensor is higher if the resin packing surrounding the fiber contains voids and/or if there is excess of the conducting epoxy, used to connect the carbon fiber to copper wire,[99] but these problems can be avoided during fabrication. Saturated calomel (SCE) was the reference electrode (Fisher Scientific, Pittsburg, PA). The electrode surface was electrochemically fabricated by continuous cycling at 10 Vs^{-1} for 3600 cycles between -1.0 to 1.5 V vs SCE.

SEM Imaging

SEM images were obtained using a Hitachi S4000 FE-SEM. The carbon fiber was coated along its length with nail varnish to expose the disk surface. Carbon fibers insulated with the varnish were treated by the electrochemical oxidation and reduction in buffer, as described.[73] After the surface fabrication procedure, before the SEM analysis, the fibers were dipped in doubly deionized water for cleaning. The cleaved fibers, which were coated with nail varnish, but were not electrochemically treated, were also imaged. To improve the quality of the SEM images, the fibers were sputtered with a thin Au/Pd film, using a Desk II Cold Sputter instrument (Denton Vacuum, LLC).

Concentration Determination

A 50-μL urine sample was diluted to 100 mL with 31 mM phosphate buffer, pH 7.4. Standard addition was performed for 2 or 4 μM final concentration in 10 mL. The solubility of XA is 130 mg/L or 8.5 $x10^{-4}$ M at pH 7.0. XA stock solutions (50 μM) were sonicated for at least 15-20 min. UA stock solutions (30 mM) were stirred for at least 10 min.

HPLC-UV Measurements

The HPLC system was comprised of a Hewlett Packard Series 1050 pulseless pump (Avondale, PA) with a valve and a manual 20.0 μL injection loop and MACS 700 (EM Sciences) UV-detector operated at 254 and 293 nm and interfaced to a PC through an analog-to-digital convertor (Pico Technology, UK). The software used for data acquisition was Picoscope (Pico Technology, UK) and the data were analyzed by Microcal Origin 6.0 (OriginLab Corporation Northampton, MA) software. All HPLC solvents were filtered and degassed. The Burdick & Jackson (Muskegon, MI) C-18 column, 4.6 mm width x 250 mm length with particle size of 5 μm, was maintained at room temperature and was conditioned with methanol (60 min), 1:1

methanol: dDI water (30 min), dDI water (60 min) and last with mobile phase (45 min)[100] at a flow rate of 1.0 mL min^{-1}. With 20 mM KH_2PO_4, pH 5.1, mobile phase, retention times were: Ur (6.8 ± 0.1) min, UA (8.4 ± 0.2) min, 2,8-DHA (10.7 ± 0.1) min, Hy (12.6 ± 0.1) min and XA (14.6 ± 0.1) min. A schematic of the HPLC-UV set up is shown in (Figure 1-5)

Chromatograms of adenosine monophosphate (AMP), allantoin, uridine, Ade, Ur, 2,8-DHA, Ado, guanine and Ino were obtained as described above to measure the retention times of these metabolites. Ade was not detected by the method used. Ade has been measured with ion pair HPLC-UV with gradient elution.[69, 101] Other retention times were: allantoin (eluted with the solvent front), AMP (13.5 ± 0.2) min, Ade, Ino and Gua coeluted (13.5 ±0.1) min, uridine (14.7 ± 0.2) min and 2,8-DHA (10.7 ± 0.1) min. The 2,8-DHA peak in the cell supernatant was also confirmed by addition of internal standard.

Retention times of Hy (12.6 ± 0.1) min and XA (14.6 ± 0.1) min were close to those of AMP, Ado, Ino, Gua and uridine. Internal standards were used and xanthine oxidase assay was performed to confirm their presence in cell supernatants.

Enzyme Assays

Xanthine oxidase selectively oxidizes Hy to XA and XA to UA.[102] An HPLC chromatogram was obtained for a mixture of XA and Hy (ca. 30 μM each in HBSS, pH 7.5 buffer). Addition of xanthine oxidase verified the formation of UA (8.4 ± 0.2) min by HPLC-UV. This confirmed the presence of Hy and XA. In the cell supernatant the assay not only confirmed the presence of Hy and XA, but also confirmed the absence of the metabolites that were retained at (13.5 ± 0.1) min and (14.7 ± 0.2) min by the complete disappearance of the Hy and XA peaks. Further, the assay did not cause an increase in the 2,8-DHA peak suggesting absence of Ade in the supernatant. Similarly uricase, which selectively oxidizes UA to

allantoin,[103] confirmed the presence of UA in the standard and in the cell supernatant by appearance of the allantoin peak.

Furthermore, the identities of the analytes in the cell supernatants were confirmed using absorption spectra for Hy (254 nm), XA (270 nm), UA (293 nm), Ur (260 nm) and 2,8-DHA (305 nm). Analyte concentrations were measured by comparing absorbances of standards [Ur (10 μM), UA (5 μM), 2,8-DHA (11 μM), Hy (15 μM) and XA (15 μM)] at 254 nm to the respective metabolite absorbance in the cell supernatant using Beer's law.

Cells

The cell culture was as described by Block and Patel.[104] In brief, endothelial cells were scraped from the main pulmonary artery or aorta of 6- to 7-mo-old pigs, and the cells were propagated in a monolayer. All monolayers were initially identified as endothelial cells by phase-contrast microscopy. Selected dishes of cells were characterized further by electron microscopy or by indirect immunofluorescent staining for factor VIII antigen or both. By use of these techniques, monolayer cultures were estimated to be pure endothelial cells. Fifth- to seventh-passage cells in post confluent monolayers, maintained in RPMI 1640 medium (Life Technologies, Grand Island, NY) containing 4% fetal bovine serum (HyClone Labs, Logan, UT) and antibiotics (100 U/ml of penicillin, 100 μg/ml of streptomycin, 20 μg/ml of gentamicin and 2 μg/ml of fungizone) (maintenance medium) were used.

The RPMI 1640 media were discarded from the confluent monolayers and the cells were washed in HBSS buffer 2-3 times. 5 mL of HBSS buffer was placed over the cells and the cells were exposed to: 1) 3% O_2-5% CO_2-92% N_2 (normoxia for PAECs, hypoxia for AECs); or 2) 20% O_2-5% CO_2-75% N_2 (normoxia for AECs, hyperoxia for PAECs) at 37°C for 24 and 48 hr. After the specified time the cells were observed under the microscope for viability. The PAECs

and AECs were adhered to the petri plate after 24 hr exposure to normoxia and hypoxia. A few PAEC's and AECs were seen floating after normoxia of 48 hr. After 48 hr of hypoxia most of the AECs were afloat. Cell supernatant was collected and used for the measurements. Numbers of cells per dish were ca. 1 x 10^6 determined by direct counting method.

Statistical Analysis

Four petri dishes were prepared for each condition and the supernatants from 3 or 4 petri dishes for each condition were used. When 2 sets of results were obtained from each petri dish, for PAECs exposed to 20% O_2 for 48 hr, the standard deviation (SD) for the concentrations of the metabolites that were detected was negligible. Thereafter, the results from different petri dishes for a particular condition were pooled. For FSV experiments at least 5 voltammograms were obtained for each condition. Values are reported as mean ± SD. Sensitivity is reported as the average slope of the calibration curve for at least 4 concentrations and 3 determinations at each concentration. The limit of detection (LOD) is for a signal-to-noise ratio of 3. Normal urine samples were obtained from 6 healthy individuals. Since xanthinuria is a rare disease, only one sample was available for analysis. For HPLC experiments at least 5 chromatograms were obtained for each condition at both 254 and at 293 nm. Values are reported as mean ± SD.

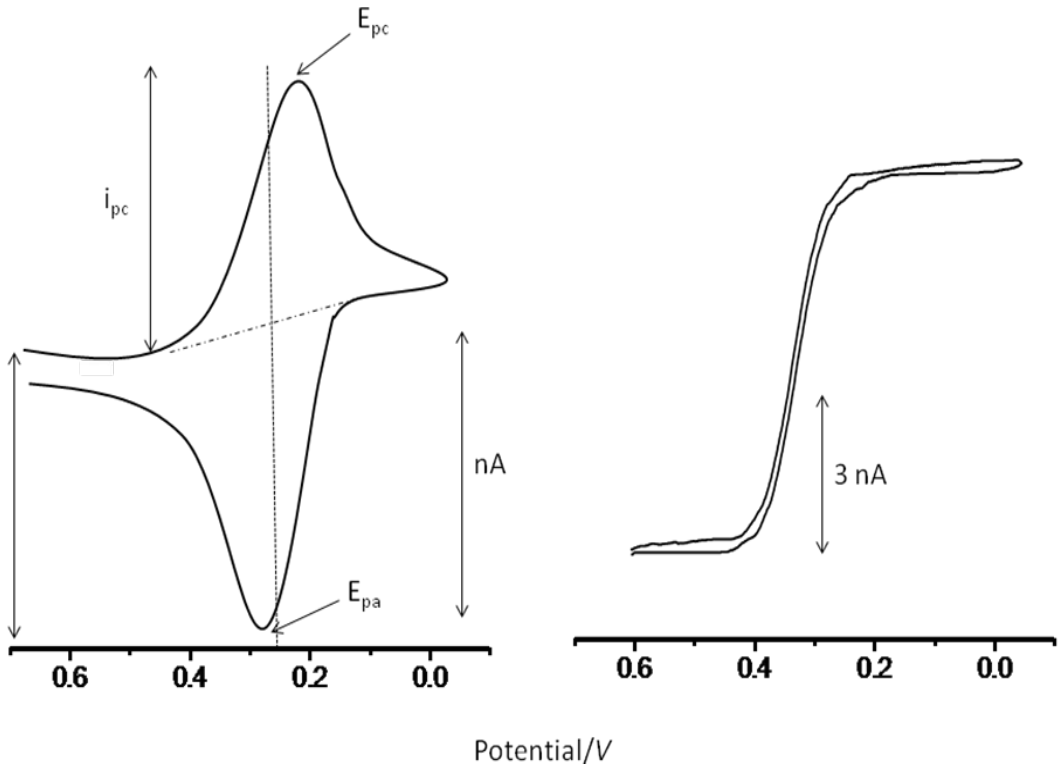

Figure 2-1. Cyclic Voltammetry: A) conventional sized electrode; E_{pc}: cathodic peak potential, E_{pa}: anodic peak potential, i_{pc}: cathodic peak current, i_{pa}: anodic peak current; B) ultramicroelectrode (N-CFS, r = 3.75 μm); 5 mM $Fe(CN)_6^{3-}$ in 0.5 M KCl (pH 6.0). Scan rate 50 mV s^{-1}

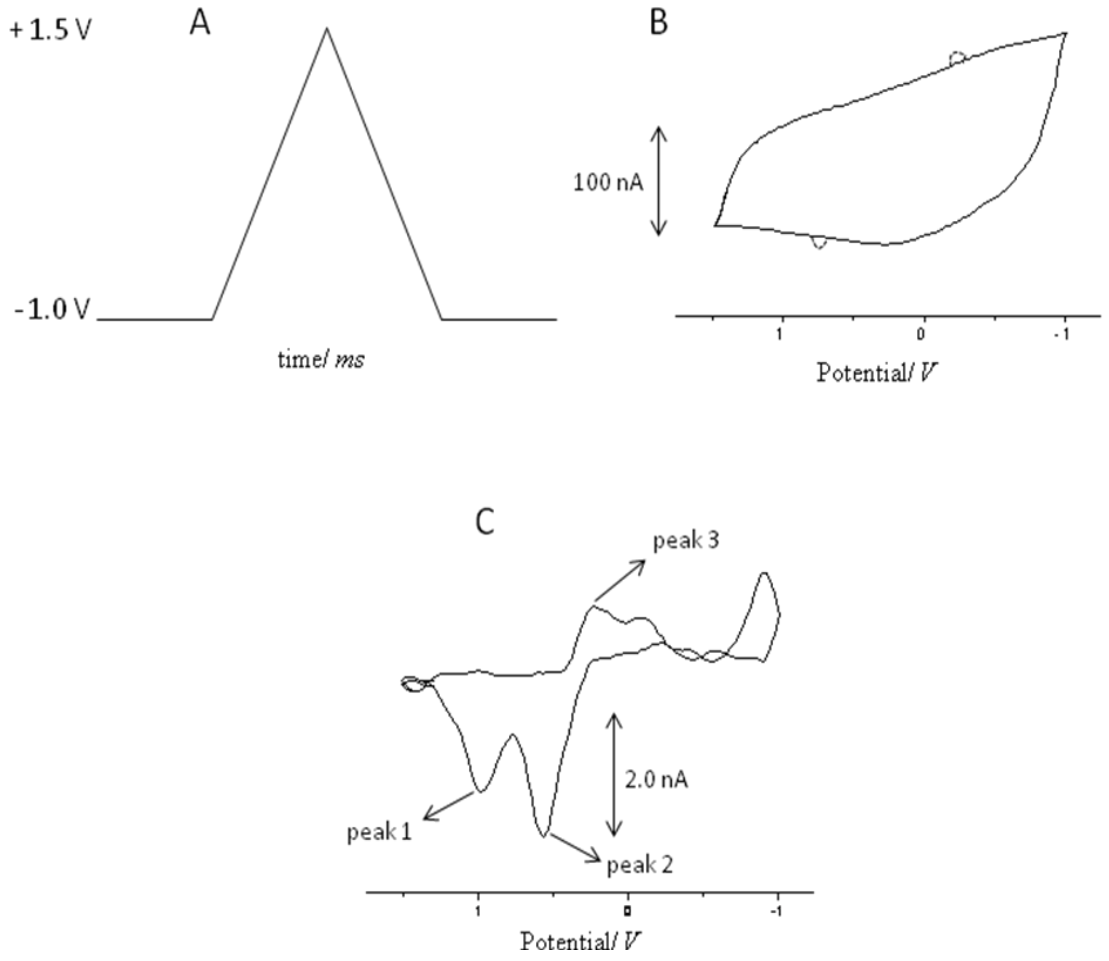

Figure 2-2. Fast scan voltammetry of xanthine in buffer: A) continuous applied potential waveform from -1.0 to +1.5 V vs SCE; B) large background and analyte current in buffer at 500 V s^{-1}; C) background subtracted voltammogram of 2.6 µM xanthine. 31 mM phosphate, pH 7.4; average of 250 scans; 500 V s^{-1}; carbon fiber sensor radius 3.5 µm. The peak at 0.85 V (peak 1) represents xanthine oxidation and the peak at 0.5 V (peak 2) is the oxidation peak of uric acid generated from xanthine oxidation; reduction of uric acid oxidation product (diimine) is at peak 3

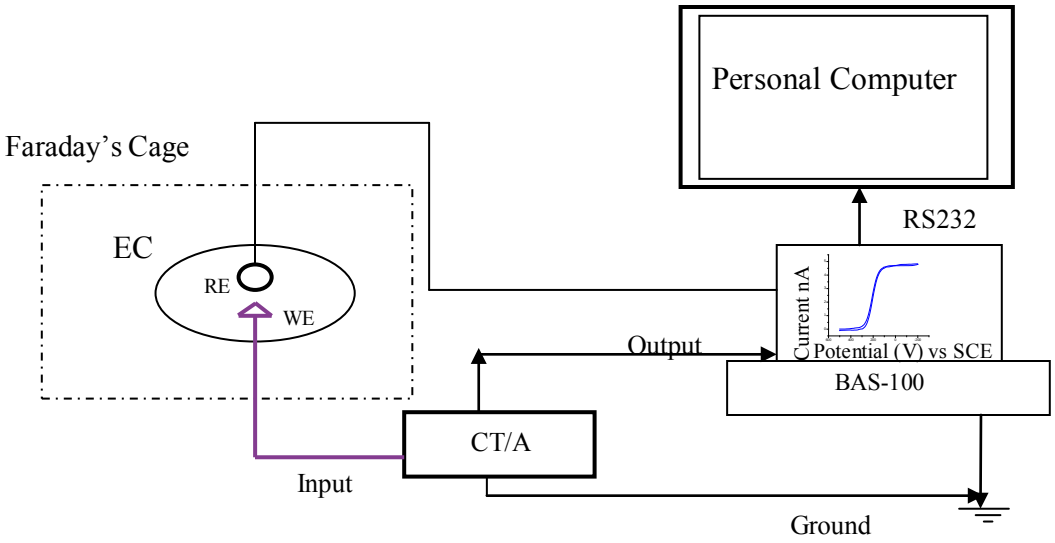

Figure 2-3. Schematic instrumental setup for N-CFS at slow scan rates upto 1 V s^{-1}. BAS-100 potentiostat, CT/A: current transducer/amplifier, WE: working electrode, RE: reference electrode which also functions as the counter electrode, EC: electrochemical cell, RS232: connection port between potentiostat and computer

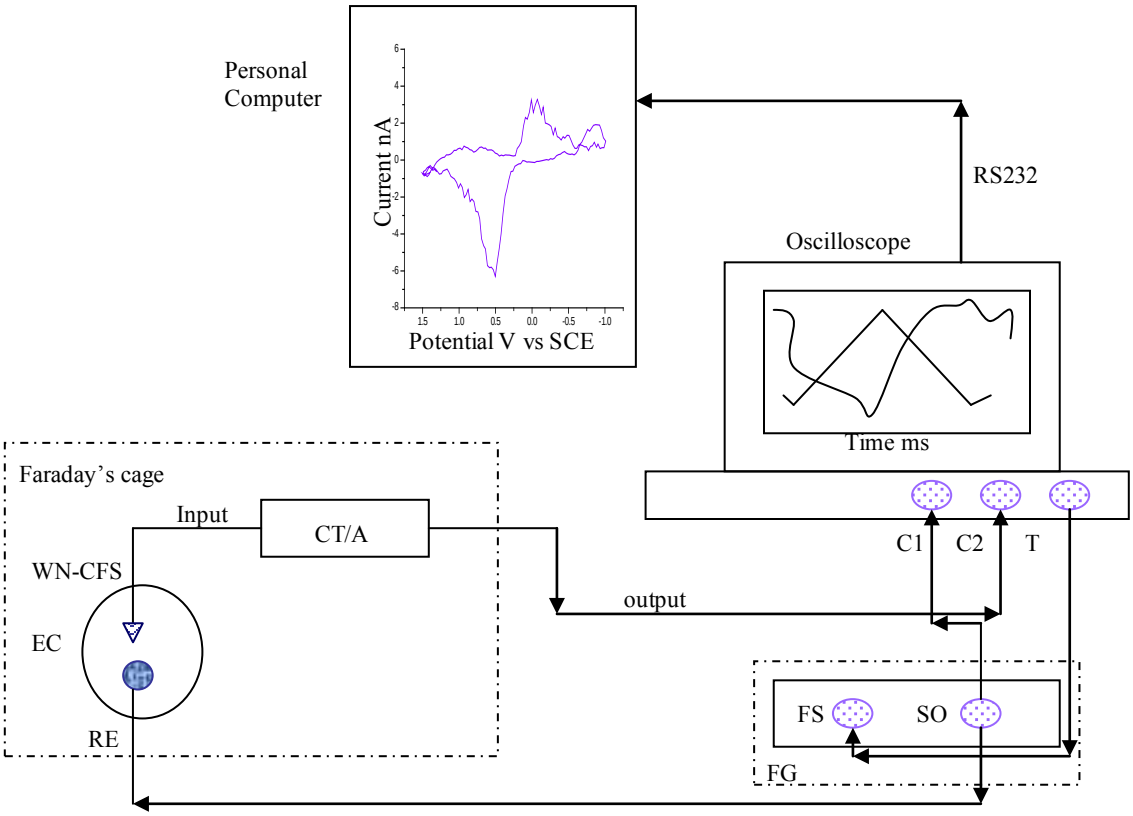

Figure 2-4. Schematic instrumental setup for N-CFS at fast scan rate of 1 V s^{-1} and higher; oscilloscope: C1: channel 1 to monitor applied waveform, C2: channel 2 to monitor response of electrode, T: trigger of oscilloscope to trigger the FG (function generator), FS: frame synchronizer of FG, SO: signal output of FG, CT/A: current transducer/ amplifier, WN-CFS: working nanostructured carbon fiber sensor, RE: reference electrode (SCE) which also works as the counter electrode, EC: electrochemical cell (80 µL volume), RS232: connection between oscilloscope and computer

CHAPTER 3
CARBON FIBER SENSOR FABRICATION FOR USE IN CELLULAR MEDIA

Introduction

Nanostructured carbon fiber sensors (N-CFS) used with fast scan cyclic voltammetry (FSV) are sensitive and selective toward metabolites such as Ado, XA and UA. The nanostructured surface of the sensor contributes significantly to these properties.[62, 71, 91, 93] The high sensitivity of the N-CFS is due to the highly active nanoporous surface structure, which has a large surface area, achieved by electrochemical fabrication. The nanostructured surface is obtained by initial mechanical polishing of the fiber on the polishing wheel for 2-3 s, followed by potential cycling in low ionic strength phosphate buffer between -1.0 to + 1.5 V at 10 V s^{-1} for 30 min. The continuous cycling between the positive and negative potentials, which is also performed during analytical signal acquisition, regenerates the surface and removes surface debris, and in the process it produces a stable background signal which is highly reproducible.[62, 73, 105, 106] During signal acquisition, the background signal is recorded for subsequent subtraction from the analyte signal. The background signal is obtained by signal averaging of 250 scans within the same potential window. In the case of limited sample availability, the stored background signal can be used for subtraction from multiple analyte runs.

Nanostructuring of the sensor surface is necessary to achieve a large electrode area, which facilitates charge transfer processes,[105, 106] and the electrochemical fabrication procedure can expose surface defects and reveal new sites for electron transfer.[107, 108] Finally, the electrochemical method produces oxide groups, such as phenol,[109] carboxyl, quinone and carbonyl at the nanostructured surface. High density of these groups may decrease the response of negatively charged analytes.[73] However, the oxide groups may allow preconcentration of positively charged analytes through adsorption. The high sensitivity of DA at carbon fiber

sensors in the presence of high concentrations of ascorbate may be explained in part by the interactions of surface oxide groups with the positively charged DA. However, UA, which is negatively charged, also exhibits high sensitivity, a result of the fast electron transfer kinetics of UA at the nanostructured surface.[93]

The combined effect of mechanical polishing and electrochemical fabrication creates a nanoporous electrode,[62] as evidenced by the massive capacitance of the sensor. However, the stable background current, which in spite of its large size can be efficiently subtracted from the analyte current, results in high sensitivity. In this work, FSV was employed in biological measurements because of the high sensitivity and the compatibility of N-CFS for the measurements of UA in physiological buffers, such as Krebs Henseleit, KCl, HBSS and phosphate.[63] In the buffers containing chloride the potential window during fabrication of the electrode and signal acquisition was reduced, to suppress the effect of the buffers.

FSV at electrochemically fabricated N-CFS has allowed measurements of XA in 2000-fold diluted xanthinuric urine with LOD of 400 nM which is described in chapter 4.[62] The selection criteria to obtain high quality N-CFS that were developed allowed considerable improvements in limits of detection.[62] Measurements of Hy, XA and UA in the presence of each other have been demonstrated at 10 V s^{-1}, with a limit of detection of 6 μM for XA in pH 7.4 phosphate buffer.[71]

Dulbecco's Modified Eagle Medium (DMEM) and Hank's Balanced Salt Solution (HBSS) are some of the most commonly used physiological buffers for maintaining cells in culture.[110-114] Preliminary work with FSV at N-CFS with UA and XA standards in HBSS and DMEM posed difficulties due to the high background signal in the case of HBSS, and from apparent passivation of the sensor surface in the case of DMEM. Earlier work from our laboratory, in the measurements of Ado in HBSS, demonstrated that the high concentrations of chloride ions in

HBSS, which leads to the evolution of chlorine at the positive potentials, can contribute to a large background current, hindering background subtraction and leading to high LODs.[91] Efforts to reduce the background signal to improve the LOD for Ado were futile.

For analytical purposes, compatibility of the N-CFS in the measurements of small metabolites in physiological buffers, which are used in the preparation of biological samples and to maintain cells in culture, is important. This chapter describes a method with FSV using N-CFS, which was developed for the measurement of purine metabolites in cell supernatants, containing DMEM or HBSS and its feasibility in the measurements of UA. We modified the fabrication and signal acquisition procedures to produce optimum sensitivity in physiological buffers without decreasing the potential window, maintaining the -1.0 to + 1.5 V window before and during analysis helps in cleaning the sensor surface.

Results and Discussion

Nanostructured Carbon Fiber Sensor Electrode (N-CFS) Background Current in Physiological Buffers

The surface of carbon electrodes (pyrolytic graphite, glassy carbon and carbon fiber) requires modifications to improve charge transfer properties, maintain a clean surface and ensure reproducible surface structure. This can be accomplished by various methods such as mechanical[115, 116] and/or electrochemical polishing,[63, 117] vacuum heat treatment,[118, 119] or laser activation.[120]

We have shown that a combination of mechanical and electrochemical carbon fiber fabrication procedures can produce an active nanostructured surface resulting in stable background, which can be efficiently subtracted. Surface fabrication by potential cycling for 3600 cycles at relatively slow scan rates of 10 V s^{-1} coupled with +1.5 V and -1.0 V potential window generates the nanoporous surface. Double layer charging and reactions of surface

functional groups and solution impurities give rise to high background current in FSV.[73] The current may be two orders of magnitude greater than that of the analyte signal. This requires stable background currents for efficient background subtraction. If the surface structure changes during signal acquisition, the background current is modified, and this will limit the LOD of analytical measurements. The surface fabrication and signal acquisition method that was developed for FSV measurements with the N-CFS allows regeneration of the surface structure, since surface oxides that are produced at positive potentials can be reduced at negative potentials and the process clears the surface. Application of potentials more negative than -1.0 V leads to an increase in background current.[121] In the determination of positively charged analytes, surface functional groups that have a negative charge may aid in the accumulation of the analyte at the surface, which facilitates charge transfer and enhance sensitivity.

(Figure 3-1) shows the background signal obtained before (solid) and after (dotted) the electrochemical fabrication of the nanostructured surface at pH 7.4 in (A) 31 mM phosphate buffer, (B) HBSS; and (C) DMEM. In phosphate buffer the background current is small before the electrochemical treatment but increases after 30 min of potential cycling and finally becomes stable. The features observed at 0.1 V after 30 min of surface fabrication are likely due to surface functional groups. Formation of surface groups is limited in phosphate presumably because of low ionic strength of the buffer and the presence of more reversible surface oxidation processes.

In HBSS the background signal is larger than in phosphate and the current at +1.5 V is higher before fabrication of the nanostructure. After 30 min of surface fabrication, the background current increases significantly above that in phosphate throughout the potential window (Figure 3-1B). The larger surface area in HBSS and more pronounced features at 0.1 V compared to phosphate suggests irreversible oxidation of the surface in HBSS. The larger

background current is due, in part, to the evolution of chlorine at positive potentials from the chloride present in HBSS. However, the current is stable and can be used in background subtraction. The larger background current at ca. 0.1 V contributes to higher LODs in HBSS compared to those in phosphate.

Throughout the potential window (Figure 3-1) the background current is smaller in DMEM than in phosphate. After fabrication of the nanostructure, there is a small increase in the background signal throughout the potential window and a new peak at around 0.9 V is visible (this peak is seen more clearly in (Figure 3-6 A and B), which may be due to the oxidation of tryptophan, which is present in this complex buffer.[122] However, the background current in DMEM is not stable. DMEM contains several amines, which are known to affect the background signal in cyclic voltammetry.[83] Also, the serine present in DMEM may adsorb at the N-CFS surface. The low background signal in this buffer may be due to irreversible adsorption of buffer components to form an inert film, which may prevent surface reactions. In DMEM continuous cycling between the potential of + 1.5 to -1.0 V does not appear to reverse the adsorption processes and may generate a new passivating film by oxidation of buffer components. Because of background fluctuations, the background current cannot be efficiently subtracted. The N-CFS does not respond to UA or XA in DMEM, possibly because of surface passivation.

The results shown in (Figure 3-1) confirm that the lowest and most stable background signal is obtained in phosphate buffer. However, cellular measurements that are of major interest to us and others require the use of physiological buffers, such as HBSS or DMEM. FSV measurements with the N-CFS are a challenge and require a sensor compatible with the measurements. We show that a low and stable background current similar to that obtained in

phosphate can be obtained in physiological media with good sensitivity towards the metabolites of interest.

Voltammetry of Ferricyanide at the Carbon Fiber Sensor Before and After Surface Fabrication

Potassium ferricyanide ($K_3Fe(CN)_6$) in 0.5 M KCl, pH 6.0 can be used as a test analyte to probe the change in electrode surface activity and structure during fabrication of the surface nanostructure. The geometric radius of the electrode can be determined from the limiting current to evaluate the sensors for further experiments.

(Figure 3-2) shows the voltammetric curves of $Fe(CN)_6^{3-}$ before (solid) and after (dotted) fabrication of the nanostructure at pH 7.4 in (A) 31 mM phosphate buffer, (B) HBSS and (C) DMEM. At first the limiting current is not well defined and increases slowly. Changes in the $Fe(CN)_6^{3-}$ response due to the variations in preparation and mechanical polishing are observed, but the fabrication of the nanostructure has a pronounced effect since a steep current rise and a well defined plateau are observed. The i-E response is a direct indication of the changes in the carbon fiber surface during fabrication. Thus different response after fabrication in phosphate, HBSS and DMEM for $Fe(CN)_6^{3-}$ indicates a different surface structure of the sensor after surface fabrication in these media.

At N-CFS fabricated in HBSS (Figure 3-2B), the response of $Fe(CN)_6^{3-}$ after the fabrication procedure shows an increase in capacitance, evidenced by the larger separation between the forward and reverse traces, but this does not justify the large background signal obtained at 10 V s^{-1} in HBSS at the N-CFS (Figure 3-1B). As mentioned earlier, this could be due to the extensive surface oxidation which will also repel the negatively charged $Fe(CN)_6^{3-}$ ions. Different responses were obtained for N-CFS fabricated in HBSS, in which the $Fe(CN)_6^{3-}$ limiting current was greater than that predicted by the theoretical radius by a factor of 2 or more.

Thus, in some cases the $Fe(CN)_6^{3-}$ response is in agreement with the observed increase in the background signal. The reason for this discrepancy requires further investigation. However, it could be possible that the evolution of chlorine causes the epoxy surrounding the fiber to be removed exposing the carbon fiber, leading to larger limiting currents because when the $Fe(CN)_6^{3-}$ ions have access to a larger surface area.

In (Figure 3-2C) the $Fe(CN)_6^{3-}$ response after the surface fabrication of the N-CFS in DMEM is reduced drastically. Also, the response for this electrode before the fabrication procedure represents an active electrode surface, which is known to reduce the $Fe(CN)_6^{3-}$ response after fabrication. But the decrease in current observed here is due to DMEM, which limits the access of $Fe(CN)_6^{3-}$ at the surface due to clogging and formation of an inert film. Therefore, in addition to providing the radius of the sensor, the response to $Fe(CN)_6^{3-}$ shown in (Figure 3-2 A, B and C) before and after the fabrication procedure strengthen the conclusion drawn from the background current measurements. The steady state voltammograms provide information regarding the quality of the sensor by measuring the radius and the activity of the surface.[73, 91] The sensors were chosen for further analysis based on their radius, surface activity and background current at +1.5 V at 10V s^{-1}.

Voltammetry of Uric Acid (UA) in Physiological Media

UA is the end product of purine metabolism and its measurements in cellular fluids would serve as an important marker of stress. UA has been measured in 2000-fold diluted urine, where its measurement serves as a disease marker. Since cellular matrices are more complex than urine, UA measurements should be more sensitive and selective to reduce or eliminate interferences in physiological media.

In HBSS and phosphate buffer, the effect of surface oxide on analyte measurement as shown in (Figure 3-1) and (Figure 3-2) can be seen more clearly in (Figure 3-3 A and B), which

illustrate the response of 32 and 38 μM UA at the sensor in 31 mM phosphate buffer and in HBSS respectively. A lower peak current of UA in HBSS compared to phosphate buffer is observed. Further, the background-current-subtracted voltammogram in HBSS shows additional peaks (0.10 and 0.35 V), attributed to the surface functional groups, which prevent the measurements of low concentrations of UA and also exhibit lower sensitivity at the N-CFS for UA. Also the peak potential of UA in HBSS is shifted to higher positive potentials of (0.75 ± 0.7) V compared to (0.51 ± 0.4) V in phosphate buffer, presumably due to the effect of the buffer on the sensor surface. As mentioned earlier, UA response could not be observed in DMEM due to the clogged surface.

N-CFS Fabrication for Use in Physiological Media

As described above, UA has low sensitivity at N-CFS fabricated in HBSS and cannot be detected at the N-CFS fabricated in DMEM. Since the cells are maintained in HBSS and DMEM, and the levels of the metabolites released from the endothelial cells were expected to be low, it was of utmost importance to modify the existing method of pretreatment and data acquisition in order to improve the sensitivity for UA at the N-CFS in these media.

Dilution of biological fluids is known to reduce matrix effects and also reduce the effect of other analytes that may interfere in the measurements. Phosphate buffer has been used to dilute biological fluids such as urine in the measurement of UA and XA. Therefore, we decided to dilute the physiological buffers with 31 mM phosphate buffer, pH 7.4. Phosphate buffer was used to dilute HBSS and DMEM due to the success of measurements in urine, and also because it gave the best limits of detection for UA and gave a stable background signal, which could be efficiently subtracted from the analyte signal.

HBSS and DMEM were diluted with 31 mM phosphate buffer, pH 7.4 in the ratio 1:5 and 1:10 and were used for the N-CFS fabrication. Comparing (Figures 3-1 and 3-4) it is observed that the background current obtained at the N-CFS with diluted HBSS before the fabrication procedure was lower throughout the potential window. The current at +1.5 V in 1:10 diluted HBSS decreased considerably compared to undiluted and 1:5 diluted HBSS, as seen in (Figure 3-4B).

The low background signal at the sensor in HBSS:phosphate (1:5) (Figure 3-4A) and HBSS:phosphate (1:10) (Figure 3-4B) enhanced the sensitivity for UA and resulted in lower LODs compared to undiluted HBSS, as shown in (Table 3-1). The sensitivities in both the diluted HBSS buffers were almost similar with the same LOD. The i-E curves for $Fe(CN)_6^{3-}$ at the sensor, as seen in (Figure 3-5 A and B), illustrate that the different dilutions of HBSS produce different features on the sensor surface. The surface created after fabrication in 1:10 diluted HBSS resembles the surface produced in phosphate buffer, whereas the surface produced in 1:5 diluted HBSS is similar to the surface produced in undiluted HBSS, but the capacitance increase is less pronounced.

(Figure 3-6A and B) show the background signal before and after surface fabrication in DMEM:phosphate (1:5) and DMEM:phosphate (1:10), respectively. From the increase in background signal, is can be inferred that, consistent with the decrease in DMEM concentration in the fabrication media, less blockage of the surface occurs. As a result, a stable background current is obtained compared to that observed in undiluted DMEM. This behavior can also be observed in the i-E curves as shown in (Figure 3-7A and B). The analyte signal and LOD obtained for UA in diluted DMEM are summarized in (Table 3-1). In summary, the buffer that is used for the fabrication of the nanostructure sensor surface should contain the smallest amounts

of the physiological buffers (HBSS and DMEM) in order to achieve good sensitivity for the analytes being measured.

Fabrication of the sensors with diluted buffers improved the sensitivity for UA compared to their undiluted counterparts, but the problems persisted with continued usage. The longevity of the sensor was compromised in DMEM, because the DMEM in the media would gradually clog the surface and limit the number of measurements. Diluted HBSS, on the other hand, leads to opening of the pores over time giving a larger than theoretical radius. These problems make the task of obtaining an ideal sensor extremely time consuming and difficult.

As mentioned in the Introduction, work was done in our laboratory to lower the background current due to HBSS in the measurements of Ado, where the sensor was fabricated using phosphate buffer and the analysis was carried out in HBSS, but this approach did not give the desired results. Now, since we have found experimentally that dilution of physiological buffers during signal acquisition is also required to obtain better results, we tried to use the diluted buffers for analysis at 500 V s^{-1} on sensors pretreated in 31 mM phosphate buffer, pH 7.4.

Different concentrations of UA were prepared in diluted HBSS and DMEM in the ratio 1:5 with pH 7.4 phosphate buffer. The 1:5 ratio was chosen, because the cell sample was limited to 2 mL, and for FSV the sample amount that is needed to perform at least 3-4 measurements would be approximately 10 mL. We could not use the 1: 10 ratio since the concentrations of the metabolites released from the cells were not known and the sensitivities in both the diluted HBSS buffers were similar. Also since, the concentrations of metabolites were expected to be very low the ratio of 1:5 was chosen. Further, we chose to cease work with DMEM, as it posed experimental difficulties, such as light sensitivity and more importantly passivation of the sensor surface. The sensors that were fabricated in phosphate buffer followed by analyte signal

acquisition in diluted HBSS showed an even better improvement in LOD as shown in (Table 3-1).

When the fabrication procedure was carried out in phosphate buffer, which is the ideal choice, it activated the sensor surface and enhanced its charge transfer properties. With either DMEM or HBSS in the fabricating media, the time of exposure (i.e. 30 min) during the fabrication procedure at slow scan rates of 10 V s^{-1} is very long and the surface becomes affected by the physiological buffers. During the 30 min period, the surface is passivated by DMEM and the chlorine gas from HBSS increases the background current leading to erroneous results for the radius from the $Fe(CN)_6^{3-}$ response. On the other hand, if the analysis is performed with the diluted buffer at 500 V s^{-1}, the time of exposure is decreased due to fast scan rates, thus limiting the effects of the physiological buffer on the N-CFS surface. With this new protocol of fabrication in phosphate buffer and signal acquisition in 1:5 diluted HBSS, we were able to measure 2 μM UA with ease and with a sensitivity of 0.45 nA/ μM.

The results obtained with undiluted HBSS in the fabricating media for background current and $Fe(CN)_6^{3-}$ response are in agreement with previously obtained results by Kholoud et al.[91, 92] Further, it was observed that HBSS and DMEM limited the analysis of UA due to high background signals as well as surface oxidation (HBSS) and clogging of the electrode surface (DMEM). However, decreasing the concentration of HBSS and DMEM in the fabricating media led to a less capacitive sensor with an active surface area, the major advantages being the low and stable background current and limited surface reactions which did not vary when the scan rate was changed or when the electrode came in contact with the diluted buffer. Regardless of the improvements observed for fabrication in diluted HBSS, sensor fabrication in 31 mM phosphate buffer, pH 7.4 offers several advantages: a) the background current does not increase as much as

with HBSS, nor does phosphate buffer clog the surface like DMEM; b) the surface becomes highly active and does not cause a great increase in capacitance; and finally c) use of 31 mM phosphate buffer lowers the detection limit and enhances the sensitivity compared to sensors fabricated in both diluted and undiluted HBSS and DMEM.

Based on these experimental observations, the protocol for N-CFS fabrication for all future experiments for cell sample analysis was fabrication of the sensor in 31 mM phosphate buffer followed by signal acquisition at 500 V s^{-1} in 1:5 diluted supernatant containing HBSS. The LOD of 2 μM for UA in diluted HBSS is high, but as we have observed in urine, the sensitivity for analytes (0.45 nA/μM) is greater than in the undiluted physiological buffers, due to possible effects of biological medium. Thus, the analysis of metabolites in cell samples with FSV may lead to enhancement of the sensitivity for the metabolites.

Conclusions

In this chapter, we have demonstrated that the N-CFS with a highly active surface along with defects or pores can be fabricated by mechanical polishing and electrochemical fabrication of the nanostructured surface by continuous potential cycling between -1.0 and +1.5 V at 10 V s^{-1} for 3600 cycles. The fabricated N-CFS has a highly stable background signal in phosphate buffer for repeated measurements. DMEM clogs the sensor surface and results in unstable background signals, while HBSS causes an increase in the background signal. However, for lower limits of detection and improved sensitivity in cellular samples, the pretreatment of the sensor in phosphate buffer is most feasible, followed by analyte determination in 1:5 diluted HBSS. The application of the sensor in measurement of UA in cellular media will be tested in the following chapters.

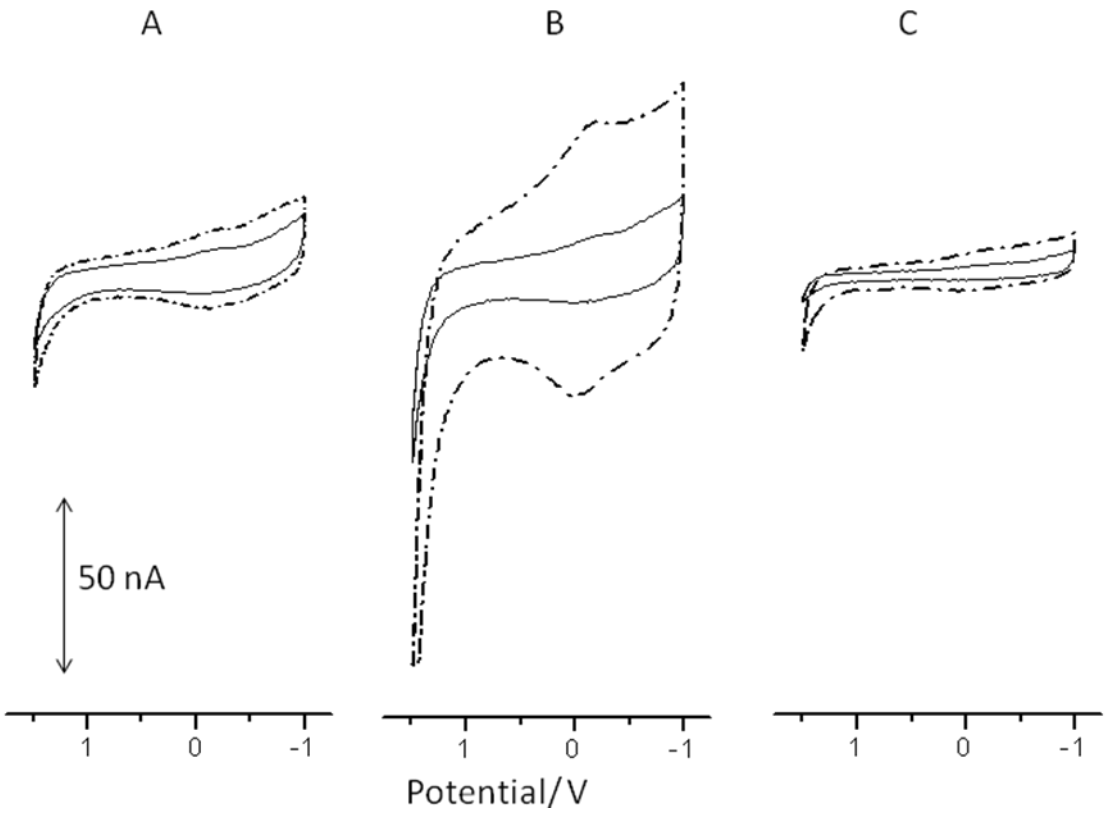

Figure 3-1. Background current at N-CFS ca. 7.5 μm diameter in pH 7.4 A) 31 mM phosphate buffer, B) HBSS and C) DMEM; before (solid line) and after (dotted line) surface fabrication by potential cycling at 10 V s^{-1}; 50 scans were signal averaged

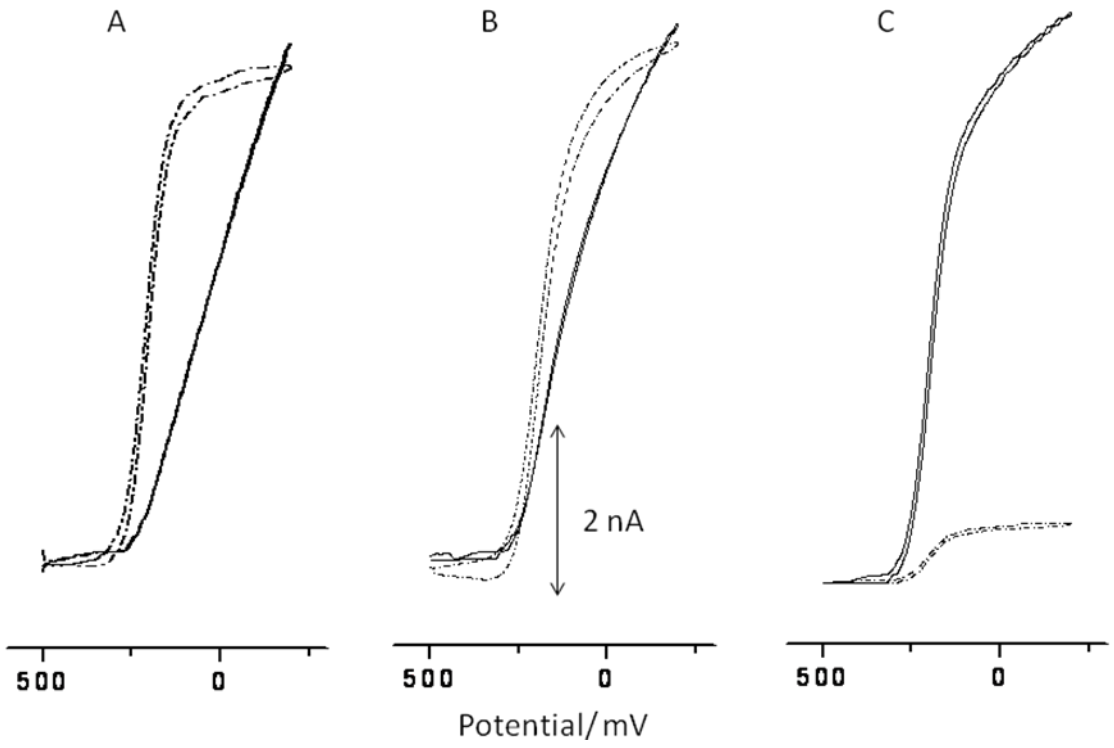

Figure 3-2. Cyclic Voltammetry of 5 mM $Fe(CN)_6^{3-}$ in 0.5 M KCl (pH 6.0) at carbon fiber sensor before (solid line) and after (dotted line) surface fabrication in A) 31 mM phosphate buffer, B) HBSS and C) DMEM. Scan rate 50 mV s^{-1}

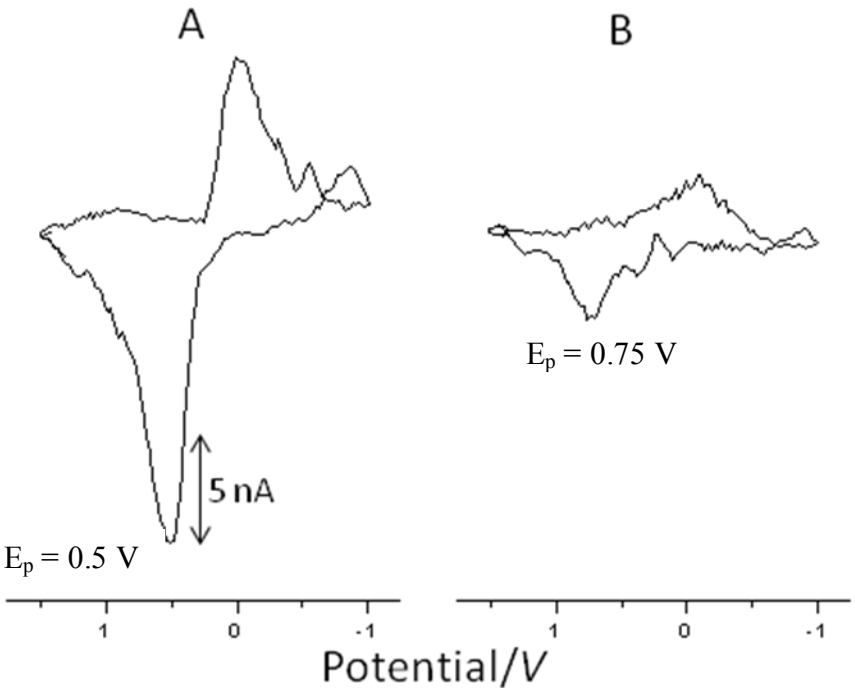

Figure 3-3. Fast scan voltammetry of uric acid at 500 V s^{-1} A) 32 μM in 31 mM phosphate buffer, and B) 38 μM in HBSS. 250 scans averaged, 500 V s^{-1}

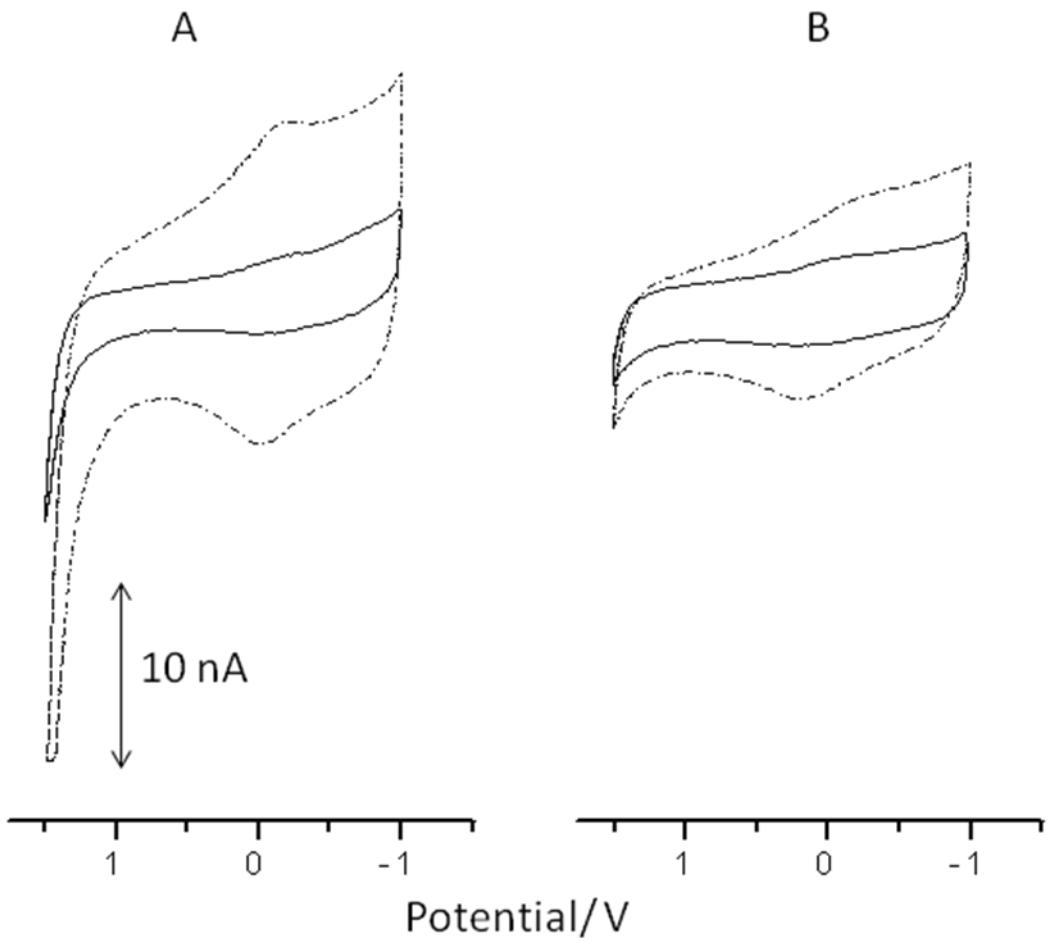

Figure 3-4. Background current at N-CFS ca. 7.5 μm diameter in pH 7.4 A) 1:5 phosphate diluted HBSS and B) 1:10 phosphate diluted HBSS, before (solid line) and after (dotted line) surface fabrication by potential cycling at 10 V s^{-1}; 50 scans averaged

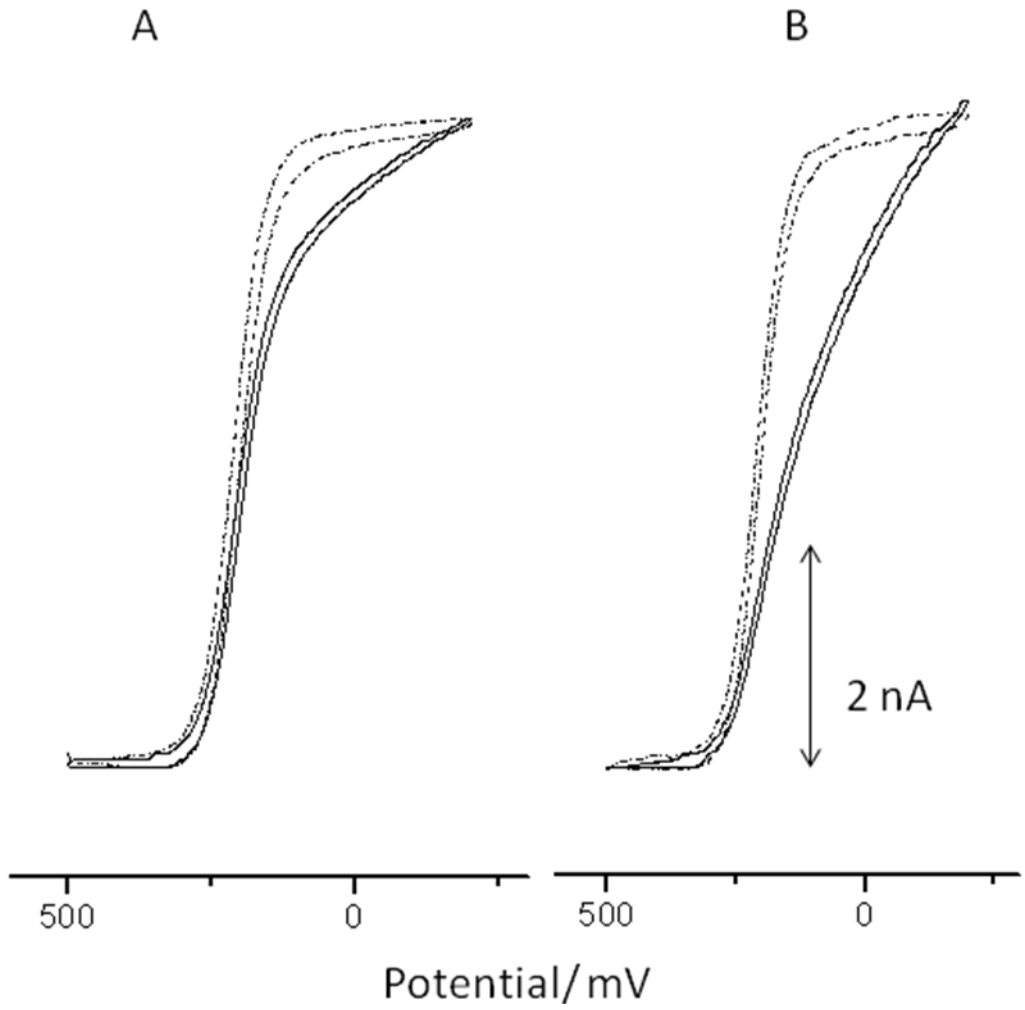

Figure 3-5. Cyclic Voltammetry of 5 mM $Fe(CN)_6^{3-}$ in 0.5 M KCl (pH 6.0) at carbon fiber sensor before (solid line) and after (dotted line) surface fabrication in A) 1:5 phosphate diluted HBSS and B) 1:10 phosphate diluted HBSS. Scan rate 50 mV s^{-1}

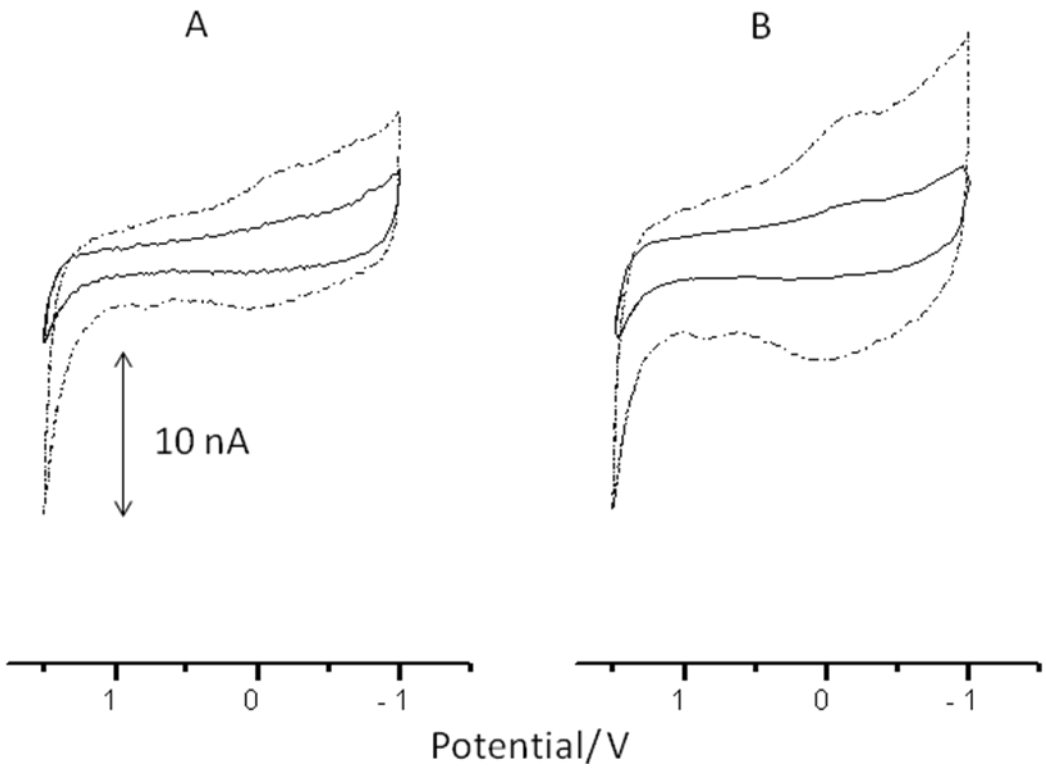

Figure 3-6. Background current at N-CFS ca. 7.5 μm diameter in pH 7.4 A) 1:5 phosphate diluted DMEM and B) 1:10 phosphate diluted DMEM, before (solid line) and after (dotted line) surface fabrication by potential cycling at 10 V s^{-1}; 50 scans averaged

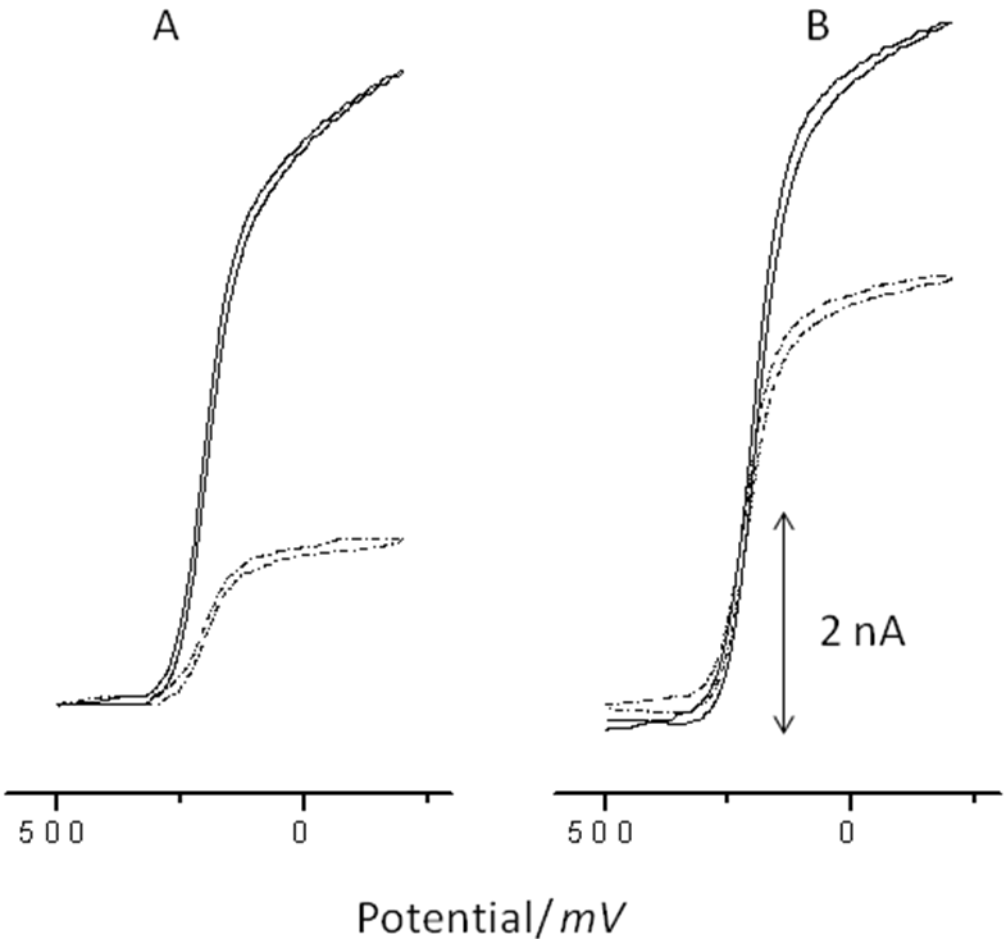

Figure 3-7. Cyclic Voltammetry of 5 mM $Fe(CN)_6^{3-}$ in 0.5 M KCl (pH 6.0) at carbon fiber sensor before (solid line) and after (dotted line) surface fabrication in A) 1:5 phosphate diluted DMEM and B) 1:10 phosphate diluted DMEM. Scan rate 50 mV s^{-1}

Table 3-1. Sensitivities and LOD for uric acid at the N-CFS with FSV in different physiological media which are either undiluted or diluted with phosphate buffer in the ratio 1:5 and 1:10

Medium, pH 7.4	Sensitivity[a]	LOD[b]
31 mM Phosphate[c]	0.99 ± 0.01 nA/μM	0.5 μM
HBSS[c]	0.14 ± 0.03 nA/ mM	10 μM
DMEM[c]	NA	NA
1:5 HBSS: 31 mM Phosphate[c]	0.27 ± 0.01 nA/μM	5.0 μM
1:10 HBSS: 31 mM Phosphate[c]	0.24 ± 0.01 nA/μM	5.0 μM
1:5 DMEM: 31 mM Phosphate[c]	0.14 ± 0.01 nA/μM	15 μM
1:10 DMEM: 31 mM Phosphate[c]	0.18 ± 0.01 nA/μM	2.8 μM
31 mM Phosphate buffer/ analysis in 1:5 HBSS:Phosphate[d]	0.45 ± 0.01 nA/ μM	2 μM

a = Uric acid (UA). Sensitivity from the slope of the calibration curve at 500 V s^{-1}. Atleast 3 points for each calibration curve and 4 determinations for each point were performed.

b = Limit of detection (LOD) when S/N =3. Peak-to-peak noise was used.

c = same buffer was used for surface modification and analysis of UA.

d = 31 mM phosphate buffer was used for surface modification followed by UA analysis in dilute HBSS.

CHAPTER 4
DIRECT MEASUREMENTS OF XANTHINE IN 2000-FOLD DILUTED XANTHINURIC URINE WITH A NANOPOROUS CARBON FIBER SENSOR

Introduction

Purines are key cellular building blocks and their synthesis and salvage are carefully regulated, as illustrated in (Figure 4-1).[123] Disruptions of the purine cycle by, for example, hypoxic stress, lead to the accumulation of purines in the brain,[124] heart and kidneys,[125, 126] and can lead to disease.[127] Diseases such as diabetes, arthritis, gout, and high blood pressure have been linked to high levels of UA in blood and urine.[126, 127] Screening for abnormal purine profiles, which requires measurements of UA and XA in biological fluids, has been recommended in the diagnosis of inborn metabolic disorders and diseases.[128, 129] XA, which is the metabolic precursor of UA, is the first indicator of an abnormal purine profile, and can serve as a marker of acute hypoxic stress.[130] Hy, the precursor of XA, can be recycled via a salvage pathway (Figure 4-1). Concentrations of UA in the normal human urine range from 2-8 mM;[67] XA between 41-161 μM;[64] Hy from 22-92 μM.[64]

HPLC and capillary electrophoresis (CE) with UV detection have been used in XA measurements in blood serum,[131, 132] urine[133] and saliva,[134] after separation from UA and quantification at different wavelengths.[9] CE with UV detection has the limits of detection (LOD) of 0.56 μM for XA;[132] the LOD by HPLC/UV is 0.5 μM. In electrochemical measurements, LOD's of XA in the nanomolar,[72] submicromolar[135] and micromolar[136] range have been reported.

Electrochemical sensors have major advantages in biological analysis;[92, 137] speed of measurements, portability, low cost and ease of miniaturization. Nanomaterials-based electrochemical sensor technology is particularly promising for biological analysis. The LODs

for XA that have been previously reported[72, 135, 136] indicate that sensitive electrochemical sensors can be fabricated for practical clinical analysis.

Since the sample volume is generally not an issue, a conventional graphite electrode, with a diameter in the millimeter range, can be used in urine analysis. Previous electrochemical measurements of XA, which achieved limits of detection in the nanomolar range, were performed with a conventional sized rough pyrolytic graphite (RPG) electrode by square wave voltammetry.[72] However, because of the problems with the reproducibility of the RPG surface in this method, the reproducibility of the measurements was low. Determinations of XA with a carbon fiber sensor have been reported, but the sensitivity and resolution were lower than required in biological measurements because of unstable background currents in the reported method.[71]

Carbon fiber sensors developed in our laboratory[73] have been shown to have high sensitivity in the measurements of small metabolites by fast scan voltammetry (FSV).[73, 121, 138] High sensitivity of the sensors is due to the high activity and stability of the nanostructured surface, and to the method of signal acquisition by FSV. A very large surface area is obtained by the method of fabrication of the nanostructure at the carbon fiber surface, and surface charge transport is facilitated without restricting mass transport.

Measurements of UA with the nanostructured carbon fiber sensor by FSV, directly in 1000-fold diluted urine, have been reported.[138] The results demonstrated the advantages of the electrochemical sensor for direct, rapid screening of urine samples. Determinations of purine metabolites in urine, after higher (2000-fold) dilution of urine samples, were tested in this work. It was expected that in more dilute samples, improved background subtraction of a more stable background will improve the S/N and increase the sensitivity in FSV measurements. Further, the

method of measurements of XA and UA in highly diluted samples can be applied to cellular samples. Finally, the results indicate that the high dilution benefits the determinations of XA, because it facilitates rapid oxidation of XA in FSV.

Sensors with a reproducible surface structure and dimensions have been difficult to fabricate, resulting in the need for frequent sensor calibration in biological measurements.[79, 121] This chapter describes improvements in the reproducibility of sensor fabrication and the development of the sensor selection criteria based on the measurement of sensor radius and activity. This procedure allowed pooling of the data obtained with different sensors and eliminated the need for frequent sensor calibration.

The sensor fabricated in phosphate buffer as described in chapter 3 and the new selection criteria were first used in the measurement of XA in urine of a xanthinuric patient, prior to application to cell samples. In addition, direct measurements of UA in 2000-fold diluted normal urine are shown. Xanthinuria is a rare autosomal disease that is marked by the deficiency of xanthine oxidase; it can also occur as a result of the treatment of gout and arthritis.[65, 66] The condition elevates XA levels, with little or no UA being produced, while the concentration of Hy is between 6- 50 μM[64] due to the up regulation of the salvage pathway.[68] Degradation of guanine nucleotides to XA bypasses the Hy salvage pathway, and may explain the predominance of XA in xanthinuria.

Results and Discussion

Background Current and Surface Structure of the Carbon Fiber Sensor

Carbon fibers have been successfully used for the past 20 years as materials for electrochemical sensors.[139] However, new materials are needed to improve the sensitivity and selectivity in biological analysis. Nanostructured electrochemical sensor materials have demonstrated advantages in biological analysis.[73, 137]

Sensitive and stable nanostructured PAN-based carbon fiber electrochemical sensors have been fabricated by electrochemical methods. Electrochemical oxidation, followed by reduction, between +1.5 and -1.0 V, by slow potential cycling in buffer, can expose and connect surface pores that are present in PAN fibers as a result of the manufacturing process, and a stable surface nanostructure can be obtained.

(Equations 4-1 to 4-5) summarize the reactions at the surface. Oxygen-containing surface functional groups,[140-142] formed at positive potentials (Equation 4-1), can be reduced at negative potentials, with the evolution of CO_2.[142] CO_2 and O_2 are produced at positive potentials and OH^- and H_2 are produced at negative potentials, as shown in (Equations 4-2 through 4-5) respectively (eq. 2-5). The evolution of CO_2 and H_2 contributes to the formation of surface pores,[140] together with the intercalation and deintercalation of electrolyte and water.[142]

$$C_x + 2H_2O \longrightarrow C_xO_2H_y + (4\text{-}y)\,H^+ + (4\text{-}y)e^- \qquad (4\text{-}1)$$

where x= 8-12 and y =1-2

$$C + 2H_2O \longrightarrow CO_2 + 4H^+ + 4e^- \qquad (4\text{-}2)$$

$$2H_2O \longrightarrow O_2 + 4H^+ + 4e^- \qquad (4\text{-}3)$$

$$2H_2O + O_2 + 4e^- \longrightarrow 4OH^- \qquad (4\text{-}4)$$

$$2H_2O + 2e^- \longrightarrow 4OH^- + H_2 \qquad (4\text{-}5)$$

Scanning electron microscope (SEM) images were obtained to gain insight into the surface structure of PAN carbon fiber sensors. Formation of pores at the surface has been postulated from previous observations of the increase in sensor surface area after the electrochemical oxidation and reduction of the surface, as described above. The experimental difficulties of imaging fiber surfaces of ca. 7.5 μm diameter, supported by epoxy and in plastic structures of much larger diameter were overcome here by insulating the sides of the fiber with a thin coating

of nail varnish, which unambiguously exposed the conducting fiber surface. When the SEM images were obtained, the thin coating of the insulator allowed easy location in the insulating layer of the conductive disk surface.

(Figure 4-2) shows the SEM images of the surfaces of the cleaved (electrochemically untreated) and of the electrochemically treated PAN carbon fibers. In agreement with previous reports, the structure of the cleaved surface shows visible defects and pores[143] and has a rough step-like (ladder-like) appearance.[144] The cleaved PAN fiber surface is highly irregular because of the nanofeatures at the surface; however, no major pores are visible on the surface. Along the entire length of the fiber, the fiber edge contains transverse ridges, but there are few apparent gaps between these ridges. After the electrochemical treatment, the most prominent change is the appearance of the exposed pores on the surface (Figure 4-2). (It is important to note the lower magnification in (Figure 4-2B) which clearly shows the pores.) An additional important change in the surface structure after the surface fabrication is the appearance of the cracks perpendicular to the transverse ridges and nodules visible in some regions of the surface.

Charging of the fiber surface is observed as evident by the bright spots in (Figure 4-2A), consistent with the relatively high porosity of PAN fibers.[145] After the electrochemical oxidation and reduction the surface contains salt deposits from the buffer electrolyte, which is not completely washed off after the electrochemical treatment of the surface. SEM shows that the pores on the surface are better defined, in agreement with the higher background current after the electrochemical oxidation and reduction of the surface. (Figure 4-3A) illustrates the background current of the nanostructured PAN sensor before and after fabrication by the procedure described in chapter 2. Of interest is the magnitude of the background current at +1.5 V, which is an indication of the extent of the over-oxidation of the surface.[73, 78] A small current at +1.5 V, such

as in (Figure 4-3A), indicates a limited over-oxidation of the surface.[73] The increase in surface area by the nanostructure can be determined from the current at + 0.75 V, which is mostly capacitive.[63]

Voltammetry of Ferricyanide

Steady state response from slow scan voltammetry at 50 mVs^{-1} of 5 mM ferricyanide can be used to select sensors without major defects.[73, 146] (Figure 4-3B) (dotted line) represents the response of a sensor for which the geometric disk radius determined from the limiting current[146] is in good agreement with the manufacturer's value. The radius determined from the limiting current which is greater than 4.0 μm, larger than the value provided by the manufacturer (3.75 μm), is likely due to geometry other than the disk. The electrochemical activity of the sensors was confirmed from the slope of ~60 mV of the E vs log $(i_L-i)/i$ plot,[146] which is the value expected for active sensors; only active sensors were used in analysis. The increase in the sensor surface area by the nanostructure is not evident from slow scan voltammetry of ferricyanide. The diffusion limited current in slow scan voltammetry at 50 mVs^{-1} cannot be used to diagnose the presence of scratches or pores of nanometer dimensions, smaller than the average diffusion length of 28 μm, which were identified by SEM (Figure 4-2B). The experiments with 5 mM ferricyanide at slow scan rates were conducted for the purpose of verifying the surface radius and of identifying active sensors for the measurements.

Voltammetry of Xanthine

The XA oxidation peak in FSV is half the height of UA oxidation peak, as shown in (Figure 2-2C). UA forms in the electrochemical oxidation of XA, as shown in (Figure 2-2C) peaks 1 and 2. Because UA has a lower oxidation potential than XA, UA is oxidized at the potentials of XA oxidation in a fast 2e, $2H^+$ reaction (peak 2). The reduction peak of the UA

oxidation product, the diimine (peak 3), is smaller than the UA oxidation peak, because the diimine is easily hydrolyzed.

(Scheme 4-1) shows the proposed oxidation pathway of XA. The results of FSV are consistent with fast 1e- oxidation of XA[147, 148] to XA radicals (I). Further oxidation of the radicals to UA, following H^+ loss, which can be slow, competes at high XA concentrations with the disproportionation of the radicals.[149] Broadening of the XA oxidation peak at high concentrations of XA is a result of the chemical reactions which follow the FSV oxidation of XA.

The formation of XA radical intermediates, which decay by disproportionation to XA, has been proposed from ESR studies of XA oxidation with sulphate and hydroxyl radicals.[147, 148] From these studies the distribution of XA oxidation products was found to be concentration dependent.[149] (Scheme 4-1) parallels the pathways observed by pulse radiolysis.[148]

Oxidation peak potential of XA of 0.83 ± 0.06 V (pH 7.4) vs SCE in FSV is more positive than 0.62 V (vs SCE) predicted at pH 7 from slow scan voltammetry[150] and $E^{0'}$= 0.35 V vs SCE (pH 13) from pulse radiolysis and EPR measurements. From slow scan voltammetry, the oxidation peak potential of 0.36 V vs SCE is predicted at pH 12.[150] Xanthine pK_a's are 0.8, 7.44 and 11.12.[151] The positive peak shift in FSV in XA oxidation is due in part to the high iR drop in FSV.[152] The reaction pathway may also be different in FSV; the pathway is different at low XA concentrations, where the competing subsequent chemical reactions do not interfere with the oxidation.

Sensitivity in Fast Scan Voltammetry of Xanthine

In slow scan voltammetry of XA using PAN carbon fiber sensors at 10 Vs^{-1}, the LOD is 6 μM, and there is low resolution of the XA and UA peaks.[71] A stable background current at 0.83

± 0.06 V, the potential corresponding to the XA oxidation peak, is needed for good S/N. The stable background is difficult to achieve during voltammetric measurements because the surface reactions such as the reactions described above can change the surface structure of the sensor, which can change the background current. At potentials more positive than 0.83 V (oxidation potential of XA) the contribution of surface reactions to the background current is expected to increase. However, at +0.75V at 500 Vs^{-1} the background current that was measured was only 35 times higher than at 10 Vs^{-1} (Figure 2-2B) or lower than expected from the direct dependence of the charging (background) current on scan rate. At 10 Vs^{-1} the oxidation reactions of/at the sensor surface can contribute to the background current, but appear to be limited at 500 Vs^{-1}, possibly due to slow kinetics. The lower background and signal averaging can improve the S/N at 500 Vs^{-1}.

In FSV at 500 Vs^{-1} of XA (10 μM), the peak current is (3.2 ± 0.2) nA, compared to the theoretical current of 3.6 x 10^{-2} nA. Thus, the observed peak current is 88 times higher than the calculated value for an irreversible reaction.[146] At 10 Vs^{-1}, the XA oxidation peak current is (0.30± 0.02) nA (radius 3.6 μm), ca. 60 times higher than the theoretical current. XA and UA oxidation peaks are well-resolved in FSV at 500 Vs^{-1} (Figure 2-2C). Similarly, at 500 Vs^{-1} the peak current of UA is 100 times greater than the theoretical current. The improved sensitivity, LOD and resolution of the measurements is attributed to the nanostructure of the sensor, with the large surface area of low volume surface pores as well as the FSV method of signal acquisition, which limits contributions to the response of slower reactions, such as the oxidation reactions at/of the surface. Higher sensitivity at 500 Vs^{-1} verifies that the pores are exposed and that the larger surface area is available to the analyte as the diffusion layer shrinks. The diffusion layer

thickness at 500 Vs^{-1} of ~230 nm approaches the diameter of the pores visible in SEM images (Figure 4-2B).

The sensitivity to XA in buffer using FSV at 500 Vs^{-1} (3.5 ± 0.4 μm radius), is 0.40 ± 0.02 nA/μM (R^2 = 0.995) in the concentration range of 0.5 to 6 μM, and the LOD is 1.0 μM, based on the conservative estimate of S/N =3. At 10 Vs^{-1} the sensitivity is 0.038 nA/μM.[71] FSV of 400 nM XA shows resolved XA and UA peaks, although the S/N is low. The LOD for XA in FSV is similar to that in CE and HPLC. However, the speed of analysis is improved in FSV with the nanostructured sensor.

Xanthine and Uric Acid in Xanthinuric and Normal Urine

In FSV measurements in 2000-fold diluted xanthinuric urine, XA and UA oxidation peaks are well defined as shown in (Figure 4-4A). In 2000-fold diluted normal urine only the UA peak is observed (Figure4-4B). The reverse reduction peaks are not well developed in urine samples.[138] Based on the known levels of XA in xanthinuric urine, the 2000-fold dilution was expected to result in ~1 μM concentration of XA in the diluted sample.

(Figure 4-5) shows the standard additions plot for XA using two (380 and 760 μL) additions of 52.6 μM standard XA corresponding to final concentrations of 2 and 4 μM in total 10 mL, respectively. The sensitivity of XA measurements in 2000-fold diluted xanthinuric urine by FSV at 500 Vs^{-1} by standard addition is (0.80 ± 0.04) nA/μM (R^2 = 0.992). The XA concentration is (1.6 ± 0.2) μM or (3.2 ± 0.4) mM in the undiluted sample (Figure 4-5). The concentration is near the 1 μM LOD of the method. Good signal-to- noise allows the measurements of XA concentrations in the vicinity of the LOD. From HPLC the concentration of XA is (1.45 ± 0.07) μM or (2.90 ± 0.14) mM in the undiluted sample. The standard deviations overlap, showing that the concentrations of XA from HPLC and FSV are in agreement. From the

standard addition, the concentration of UA in 2000-fold diluted normal urine is (3.80 ± 0.08) μM (sensitivity = 0.99 nA/ μM, R^2 = 0.999) or (7.60 ± 0.16) mM in the undiluted urine, in agreement with the concentration determined by HPLC (7.65 ± 0.05) mM.

Direct Determinations of Metabolite Concentrations in Urine

Advanced calibration of the sensor in buffer speeds up analysis compared to the standard additions method. For XA, the sensitivity in buffer is (0.40 ± 0.02) nA/μM (3.5 ± 0.4 μm radius) compared to (0.80 ± 0.04) nA/μM (3.5 ± 0.4 μm radius) from standard addition (Figure 4-5). The higher sensitivity measured by standard addition is attributed to lower and more stable background current in 2000-fold diluted urine at the oxidation peak potential of XA, compared to the background measured at the same potential in buffer (Figure 2-2C) and (Figure 4-3A). Further investigations are necessary to understand the exact source of the higher sensitivity in XA measurements in the urine samples diluted with buffer. After the correction for the 2:1 sensitivity ratio, calibration curves obtained in buffer, prior to the measurements in urine samples, can be used to determine XA concentration in the diluted urine samples. The sensitivity of UA is (0.99 ± 0.01) nA/μM (0.998), (3.5 ± 0.4) μm radius, in buffer in the concentration range of 0.5 to 4.5 μM and is the same as that obtained from standard additions to urine samples.

The stability of the sensors was evaluated after the measurements of UA in the diluted urine sample, after the initial calibration of the sensor in buffer. For a 4 μM UA standard, the oxidation peak current was (3.91 ± 0.06) nA, before and after the measurements in urine samples (Figure 4-6). UA concentration of (3.95 ± 0.06) μM was determined from the calibration curve in buffer, in good agreement with 4 μM concentration of the standard.

Conclusions

High sensitivity of the nanostructured PAN carbon fiber sensors, with FSV as the signal acquisition method, is demonstrated in the measurements of two major purine metabolites, XA and UA, in highly diluted urine. For XA, low LOD is due to the low and stable background current of the sensor at the positive potentials of XA oxidation peak. It appears that in the 2000-fold diluted urine samples sensor background is lowered, which stabilizes the background current. In addition, high dilution of urine samples reduces matrix effects and reduces the interference from electroactive sample components in the measurements of XA and UA with the sensor.

The stability and reproducibility of fabrication of the sensors, which was verified from the measurements of sensor radius and the electrochemical activity of the sensors in ferricyanide solution, allowed pooling of data from different analyses and for different sensors. The geometric disk radius of the sensors that were used for analysis of (3.5 ± 0.4) μm, verified tight packing of the sealing resin and verified the absence of gaps in seals around the fiber.

The pathway of XA oxidation in FSV likely involves an initial $1e^-$ oxidation, which is followed by chemical reactions, and by $1e^-$ oxidation of the intermediates. High resolution of XA and UA peaks is achieved in FSV at 500 Vs^{-1} at low concentrations of XA when the following chemical reactions do not distort the XA oxidation peak.

XA and UA concentrations determined with the nanostructured PAN carbon fiber sensor and FSV and by HPLC are in good agreement. Pre- or post-calibration of the sensor in buffer can be used in the determinations of XA and UA concentrations in urine to save time. The sensors are stable and can be used for repeated measurements. The method of determination of low concentrations of XA and UA that was developed in chapters 3 and 4 will enable measurements of purine metabolites in cellular samples.

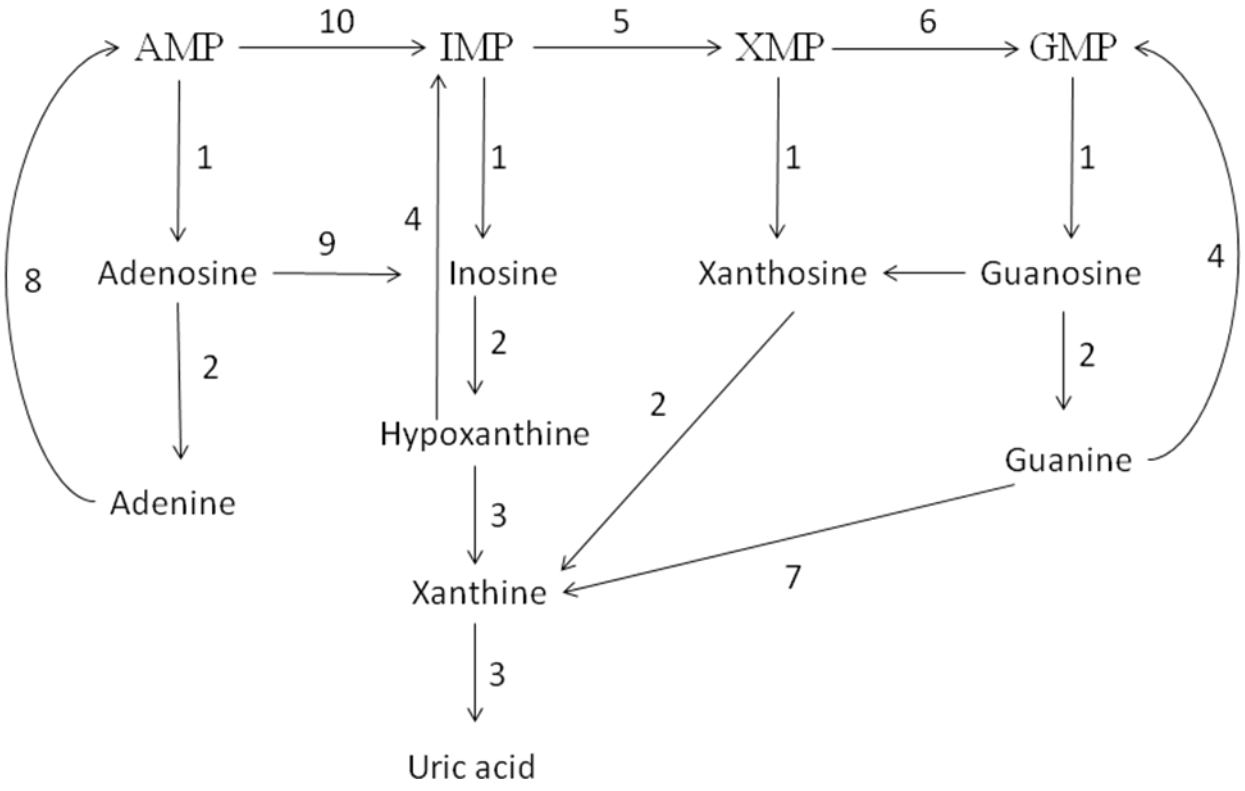

Figure 4-1. Metabolic pathway of purines in humans. (Adapted from Ref. 123) 1 = 5'-nucleotidase, 2 = Purine nucleoside phosphorylase, 3 = Xanthine oxidase, 4 = Hypoxanthine-guanine phosphoribosyl transferase, 5 = Inosine-5' –monophosphate dehydrogenase, 6 = Guanine monophosphate synthetase, 7 = Guanine deaminase, 8 = Adenine phosphoribosyl transferase, 9 = Adenosine deaminase and 10 = AMP deaminase. AMP = Adenosine monophosphate, IMP = Inosine monophosphate, XMP = Xanthosine monophosphate and GMP = Guanosine monophosphate

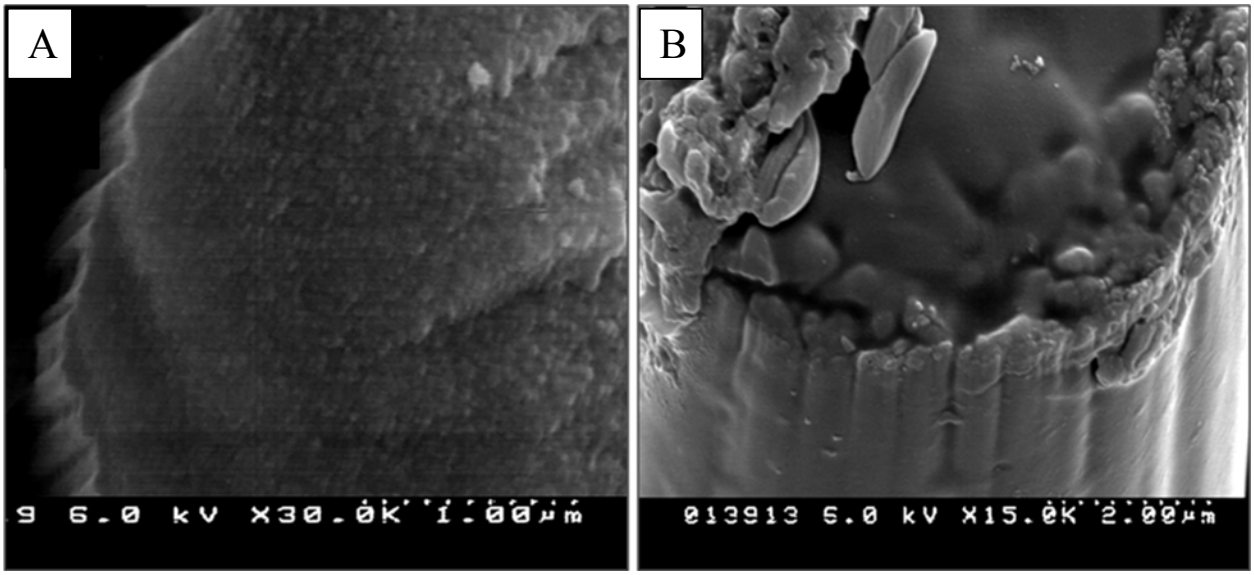

Figure 4-2. SEM images of the carbon fiber before (A) and after (B) electrochemical treatment. The increase in the width of the edge dimensions from 140 nm to 200 nm and the appearance of pores can be seen in (B)

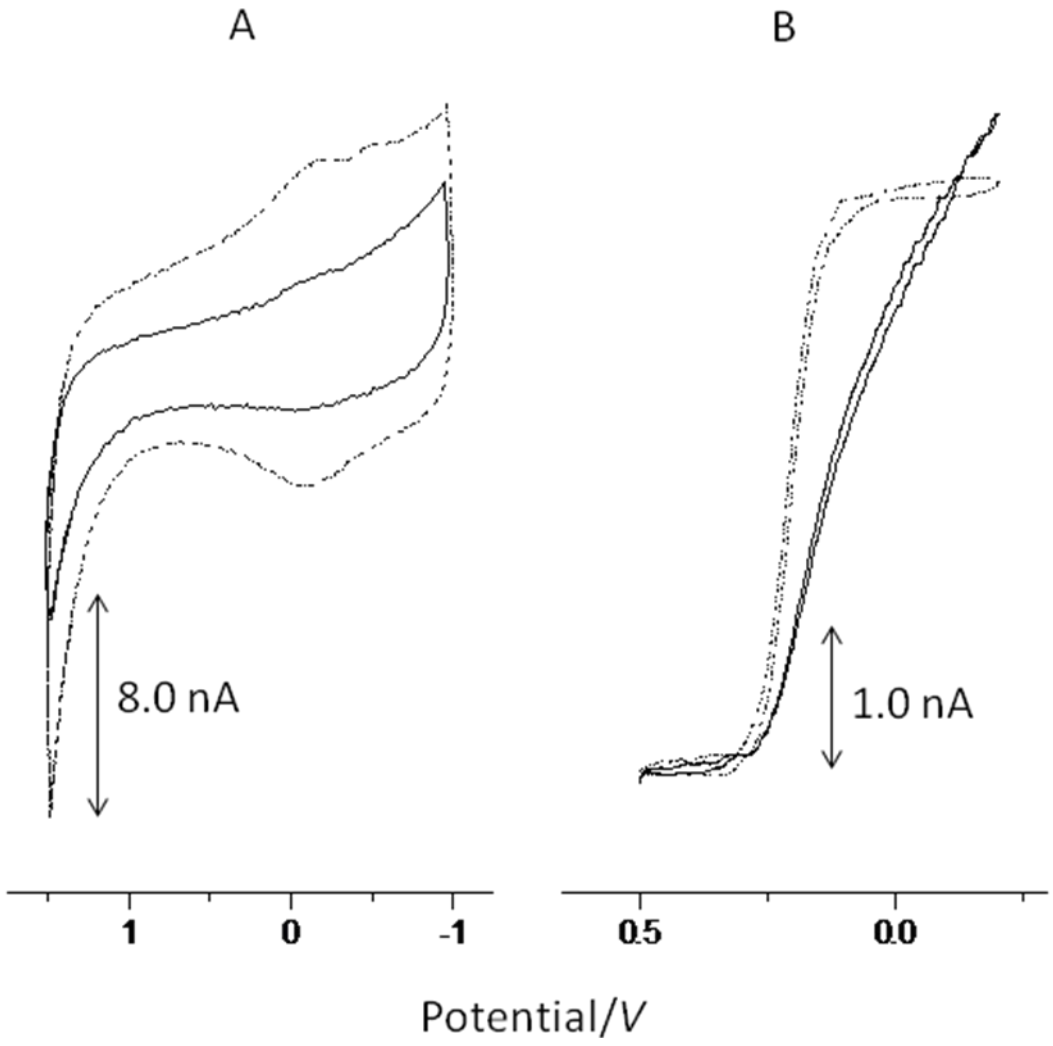

Figure 4-3. Characterization of the sensor by slow scan voltammetry before (solid) and after (dash) electrochemical treatment: A) background current at 10 V s^{-1} in buffer; 50 cycles averaged; B) 5 mM $K_3Fe(CN)_6$ in 0.5 M KCl, pH 6.0, at 50 mV s^{-1}

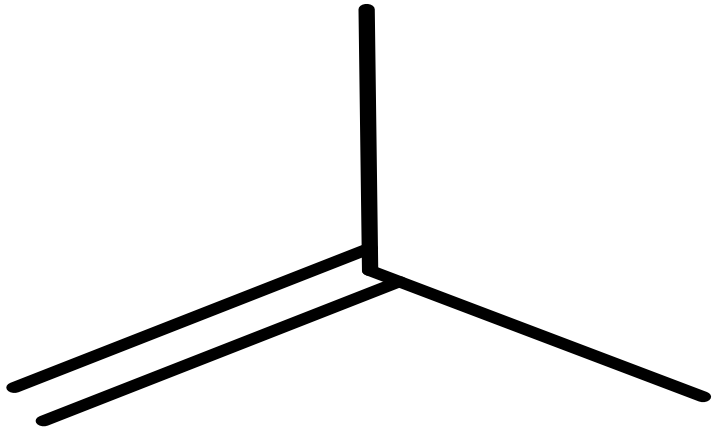

Scheme 4-1. Proposed electrochemical oxidation pathway of xanthine at the N-CFS

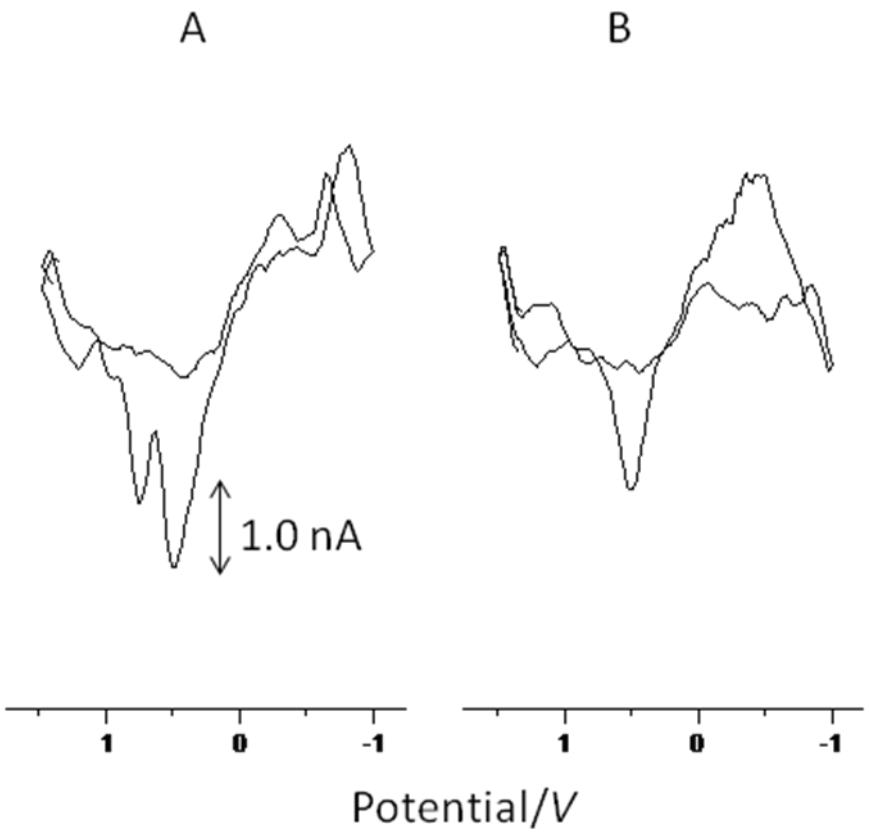

Figure 4-4. Fast scan voltammetry in 2000-fold diluted urine: A) xanthinuric and B) normal; 500 V s^{-1}; 250 scans averaged; background subtracted with buffer background; sensor radius (A) 3.4 μm and (B) 3.1 μm

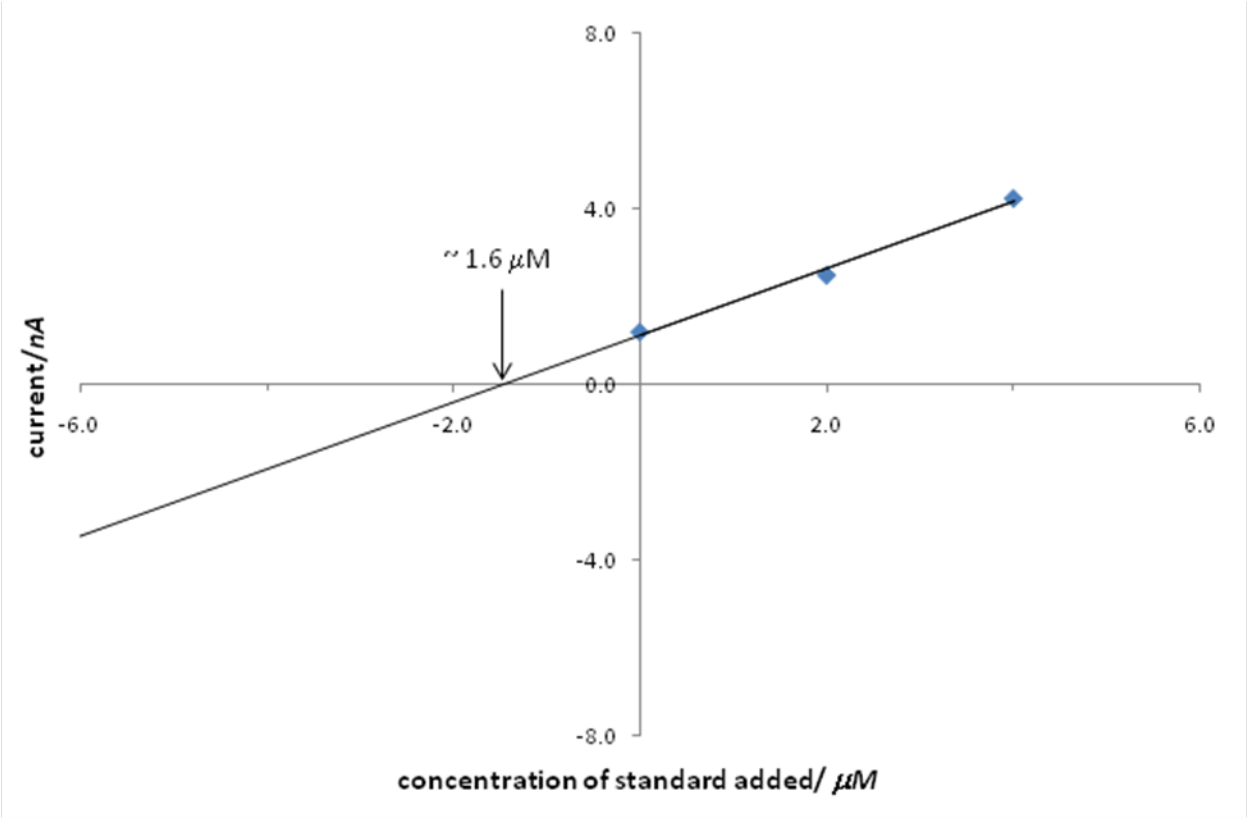

Figure 4-5. Standard additions plot for xanthine concentration in 2000-fold diluted xanthinuric urine. Experimental conditions as in (Figure 4-4); sensor radius 3.4 µm

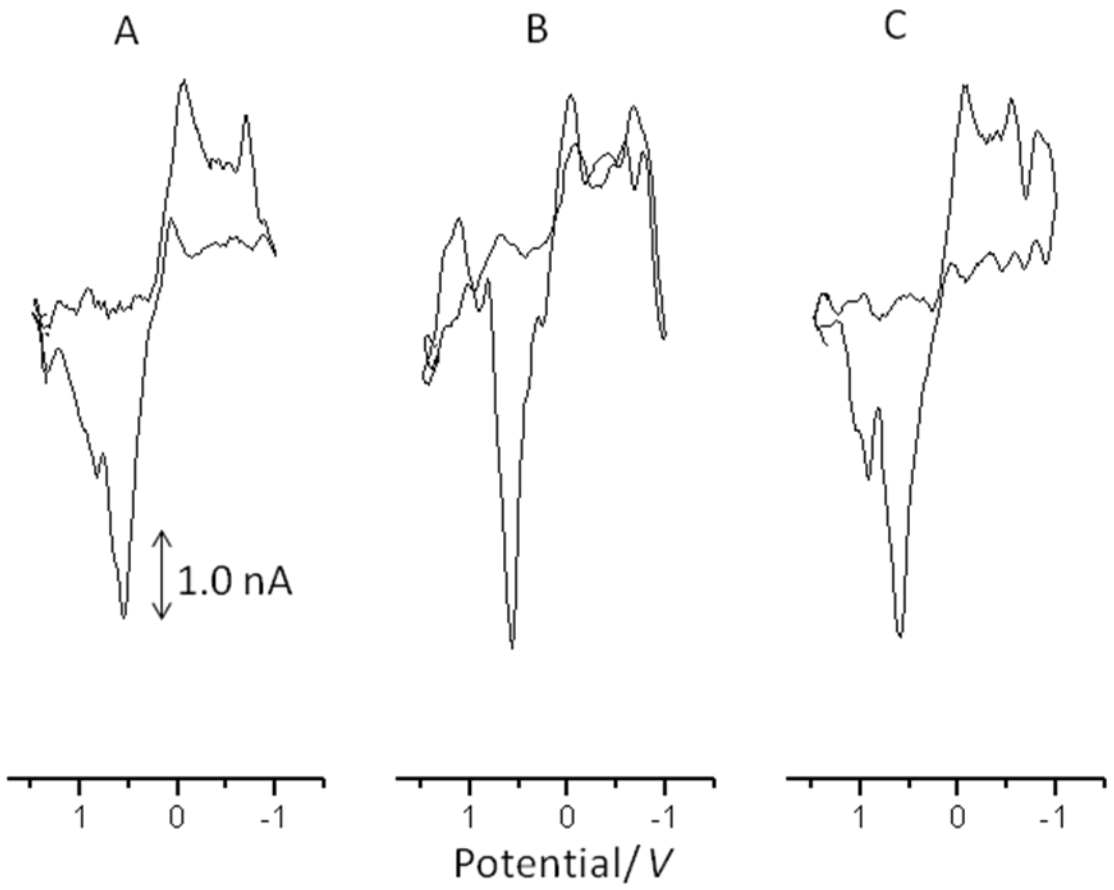

Figure 4-6. Stability of the carbon fiber sensor in fast scan voltammetry measurements in urine: A) 4 μM uric acid in buffer before the measurement in urine sample; B) sensor response in 2000-fold diluted normal urine after the measurement in (A); C) 4 μM uric acid in buffer measured after the experiment in (B); experimental conditions as in (Figure 4-5); sensor radius 3.4 μm

CHAPTER 5
HPLC-UV MEASUREMENTS OF CHANGES IN METABOLITE CONCENTRATIONS IN THE SUPERNATANT OF ENDOTHELIAL CELLS EXPOSED TO OXIDATIVE STRESS

Introduction

Endothelial cells serve as a barrier between blood and tissues and are thus the first to experience composition changes in the extracellular environment associated with stress and disease, such as changes in normal levels of glucose and in oxygen pressure.[23] Under physiological conditions pulmonary artery endothelial cells (PAECs) are exposed to low oxygen pressures of 3-5%,[24] since the artery carries deoxygenated blood from the heart to the lungs for purification. Consequently, PAECs are highly tolerant to these low oxygen pressures, which in other cells are associated with hypoxic stress. The tolerance to low oxygen pressure in PAECs is likely due to the cellular processes which preserve ATP by increasing glycolytic metabolism for the production of nucleotides.[25, 26] Thus, oxygen pressures in excess of 5% are considered hyperoxic for PAECs. On the other hand, aortic endothelial cells (AECs), which line the aorta, are exposed to normal oxygen pressures of around 14-20% and oxygen pressures below 14% are considered hypoxic for AECs.

Cells can adapt to oxidative stress by up- or down-regulation of metabolism, while extended stress can lead to cell injury through damage to lipids, proteins, RNA, and finally DNA. This may eventually lead to cell death triggered by apoptosis (programmed cell death) or necrosis (cell death due to traumatic injury).

Recent analysis of glucose deprivation at AECs showed an increase in the levels of purine metabolites in the cell supernatant. During glucose deprivation, the cells can use triglycerides as the energy source to upregulate purine *de novo* synthesis.[27] Studies have shown that ^{14}C from [^{14}C]formate was incorporated at position 8 of the purine ring.[27, 28] Normal conditions in the cells are marked by purine and pyrimidine catabolism and salvage pathways occurring in conjunction,

since the energy cost of synthesizing a nucleotide *de novo* is higher in ATP equivalents than that of reutilizing an intact purine or pyrimidine ring.

After 24 -48 hr of hypoxia in rat brain, levels of UA increase, while the levels of XA and Hy decrease, indicating activity of xanthine oxidase during hypoxia.[29-31, 153] In contrast, in PAECs supernatant the ratio of Hy to XA increases 5 fold after exposure to 3% oxygen for 24 hr, while the levels of UA remain unchanged.[32] However, UA and Ur measured by HPLC-UV and confirmed by MS have been found to increase during energy stress due to vasoconstriction of smooth muscle tissue.[34] Similarly, in the lungs the levels of UA have found to increase after 24 hr of hypoxic exposure.[33] The activity of xanthine oxidase observed by the production of UA upon addition of XA, NAD^+ or allopurinol decreases under hyperoxia in rat PAECs and in human umbilical vein endothelial cells (HUVECs).[32, 154] Thus hypoxia and hyperoxia can cause disruptions in the normal purine and pyrimidine cycle and can lead to changes in the levels of purines and pyrimidines from normal, associated with decreased use and/or increased degradation.[60] These metabolites are susceptible to further oxidation by reactive oxygen species (ROS).[155, 156]

Hypoxia and hyperoxia can cause an increase in the production of ROS and reactive nitrogen species (RNS), forming superoxide ($O_2^{\bullet-}$), hydrogen peroxide (H_2O_2), hydroxyl radicals ($OH^{\bullet}$) and nitric oxide ($NO^{\bullet}$).[35] Sources of ROS are the electron transport chain in the mitochondria and metabolic pathways, such as NADPH oxidase and xanthine oxidase/dehydrogenase systems.[4, 36, 37] Under hypoxia, endothelial nitrogen oxide synthase (eNOS), which is located in the Golgi complex and the cell membrane,[38] is activated by Ca^{2+} influx and generates $NO^{\bullet}$ above basal levels. Hyperoxia in ovine-PAECs causes a 2.7-fold increase in the expression of eNOS.[39] In addition, eNOS cofactor tetrahydrobiopterin (BH_4) is

susceptible to oxidation and degrades to 7,8-dihydrobiopterin which, together with lower intracellular levels of the eNOS substrate L-arginine,[40] can cause reduction of heme in eNOS. This leads to uncoupling of the enzyme and production of $O_2^{\bullet-}$ and $NO^{\bullet}$ in the case of partial uncoupling, the levels of $NO^{\bullet}$ decrease.[41, 42, 157] The reaction of $O_2^{\bullet-}$ and $NO^{\bullet}$ at diffusion-limited rates forms $ONOO^-$, and causes the levels of $NO^{\bullet}$ to drop further.[43] Reduced levels of L-arginine may be due to argininosuccinate synthetase deficiency, while the absence of the BH_4 cofactor can be due to the defects in its synthesis and/or regeneration. It has been proposed that Ca^{2+} increases mitochondrial ROS production by a) stimulation of the tricarboxylic acid (TCA) cycle and enhancement of electron flow into the respiratory chain, b) stimulation of $NO^{\bullet}$ production from eNOS, resulting in inhibition of complex IV, where most molecular oxygen is reduced to water, c) dissociation of cytochrome c, an antioxidant, possibly resulting in increased ROS levels.[158] It has been proposed that in a hypoxic environment, feedback inhibition of the electron transport chain may occur leading to ROS production particularly in complex III. Under hypoxia there is increased inhibition of complex IV by $NO^{\bullet}$ leading to ROS production.[159] In the case of hyperoxia, ROS production is stimulated from complex III in human umbilical vein endothelial cells (HUVECs).[160]

Under normal conditions there is a balance between ROS production and the levels of cellular radical scavengers, such as superoxide dismutase, catalase and glutathione peroxidase.[44, 45] An imbalance between ROS production and antioxidant levels induces oxidative stress. It has been suggested that UA can scavenge $O_2^{\bullet-}$, $ONOO^-$, and $NO^{\bullet}$ to form allantoin, triuret and 6-aminouracil, respectively, in urine.[46] However, since $ONOO^-$ is formed at diffusion-limited rates, the formation of 6-aminouracil and allantoin should be limited.[46, 47] In γ-irradiated plasma, UA has been suggested as a scavenger of nitrogen dioxide radical ($NO^{\bullet}_2$) formed from $ONOO^-$.[48, 49]

Extended exposure to oxidative stress can cause DNA damage by fragmentation, hydroxylation and strand cleavage, leading to base degradation.[6, 7, 56] Since RNA is more abundant in cells than DNA, it is damaged more easily by ROS, causing subsequent errors in protein synthesis.[57] This is however, less lethal than the mutations in the genome of the cell, and the cells can tolerate higher levels of damage to RNA than DNA. RNA degradation is the major mechanism of removal of damaged RNA,[58] with Ur and XA as the final degradation products. Ur is formed due to the degradation of the pyrimidines (Ur and cytosine) and XA is formed due to the degradation of the purines (Ade and guanine).[59]

Different methods have been developed for the measurements of purine and pyrimidine metabolites. CE has been used in the analysis with LOD's ranging from 0.9 fmol for cAMP to 30 fmol for Ado.[61] Electrochemical sensors show good sensitivity and selectivity towards purine metabolites in urine samples.[62, 138] The most widely used method for the measurements is gradient elution HPLC with UV-detection, with limits of detection in the nanomolar range for purines and pyrimidines.[27]

During oxidative stress, the chain of events summarized above and depicted in (Figure 1-1) is expected to lead to changes in the concentrations of the metabolites, many of which can be released into the cell supernatant. Purine and pyrimidine metabolites are expected to be released in the cell supernatant due to the presence of transporters such as nucleobase transporters[161] and also due to the degradation of extracellular ATP and UTP.[52, 162] Further, as part of normal metabolism, the cells release these metabolites. Because the cell supernatant is a complex matrix, before the N-CFS developed for use in biological fluids in chapters 3 and 4 could be applied to cell supernatants, we used HPLC-UV to separate the metabolites released in the supernatant of PAECs and AECs exposed to oxygen pressures representing physiological and stressed

conditions. Furthermore, the feasibility of measuring changes in the concentrations of the metabolites in the cell supernatant of PAECs and AECs as markers of oxidative stress/damage due to changes in oxygen pressure from normal was also tested. Based on previous work, final metabolites of the purine and pyrimidine cycle released in the cell supernatant were expected to change after exposure to stress.[12, 27] Isocratic elution with HPLC-UV was used, since it limits sample losses and allows good separation of purines, pyrimidines and their oxidation products.[100] The results indicate that concentration changes of the metabolites detected can be used to provide insight into the survival techniques adapted by the cells to delay death under oxidative stress.

Results and Discussion

Measurements of Metabolites in Cell Supernatant

Hank's Balanced Salt Solution (HBSS), a common physiological buffer used for maintaining cells in culture, can be used in FSV measurements with N-CFS.[91, 163, 164] The relatively low and stable background currents in HBSS buffer result in low LOD's. In this work HBSS was diluted with phosphate buffer to further reduce the background signal, and FSV at the N-CFS was used for the validation of metabolite concentrations in cell supernatants. The advantages of FSV at N-CFS for rapid screening for metabolites of interest in biological media have been demonstrated in the measurements of small purine metabolites such as UA and XA in diluted urine as shown in chapter 4.[62, 91] HPLC-UV, which allowed measurements of metabolite concentrations without sample dilution, is slower compared to FSV.

Gradient[9, 27, 165, 166] and isocratic[34, 167] elution reversed phase HPLC-UV have been used to measure purine metabolites in biological fluids. A linear gradient of 10 mM KH_2PO_4, pH 4.55 and 10 mM KH_2PO_4 in 50% (v/v) methanol/water was used to separate UA with retention times (6.89 ± 0.03) min, Hy (8.11 ± 0.02) min, XA (10.34 ± 0.02) min, Ado (24.51 ± 0.01) min and Ino (20.10 ± 0.01) min[9] In a related method, samples were diluted with 0.01% sodium azide to

prevent bacterial degradation, and purines were separated using a 100 mM KH_2PO_4/ methanol gradient.[168] In another method, a gradient of 67% methanol-33% water- ammonium acetate (26 mM, pH 5) was used.[7] In this work isocratic reversed phase HPLC[100] was used with a low ionic strength 20 mM KH_2PO_4 buffer, pH 5.1. This allowed separation of neutral forms of structurally similar purine and pyrimidine metabolites Hy (pK_a 8.8),[169] XA (7.44),[151] UA (5.8),[170] Ur (9.5)[171] and Ade (3.6)[172] from their oxidation products. Longer retention times and higher capacity factors in isocratic elution favor separation of structurally similar metabolites such as 2,8-DHA and UA, and Hy and XA. Some variations in retention times were observed, which may be due to changes in the pH of cell supernatants. Consequently, standards and enzyme assays were used to confirm metabolite identity.

Ado and Ino (13.5 ± 0.2) min were not detected in cell supernatants. Breakdown of Ado to Hy is very rapid in endothelial cells, due in part to the high activity of purine nucleoside phosphorylase.[173] This suggests that ATP breakdown products are released from cells, while some may be formed by the degradation of exogenous ATP. Ado may be transported back into the cell to form Hy, XA and UA, which are then released.[167]

The tolerance and adaptation to changes in oxygen pressures from normal is crucial to the survival of endothelial cells and tissues, as well as the blood vessels they line. However, the response of PAECs and AECs to oxidative stress induced by hyperoxia and hypoxia, respectively, is different due to the differences in their physiological environment. *In vivo*, low oxygen pressures are normal at PAECs, but are considered hypoxic at other cell. PAECs area dapted to this environment and they preserve plasma membrane integrity and ATP. In hypoxic PAECs, metabolic arrest may occur, and could be responsible for the tolerance, although the cellular mechanisms responsible for the maintenance of high energy phosphates are unknown.

Aortic endothelial cells (AECs), on the other hand, are exposed to normal oxygen pressures of 14%, but are known to tolerate hypoxia for up to 18 hr by up-regulating glucose transporter mRNA, glucose utilization, and protein levels. Augmented utilization of phosphocreatine may also be responsible for AECs tolerance to hypoxia.[174] Phosphocreatine is an important energy store and is used under hypoxia to generate ATP from ADP and creatine. AECs are sensitive to oxidative stress induced by the addition of H_2O_2, where cell injury was observed from changes in % viability and lactate dehydrogenase (LDH) activity.[175] Cells cultured in Dulbecco's modified eagle medium (DMEM) were less injured at any given time compared to cells in M199 medium, which contains Hanks salts.[175] The difference in these media is the lack of vitamins and lower amounts of glucose in M199.

In this chapter, changes in the composition of the metabolites in cell supernatant and the concentration changes of these metabolites with time were determined for cells exposed to physiological oxygen pressures, PAECs (3%) and AECs (20%), and oxygen pressures which would induce oxidative stress, PAECs (20%) and AECs (3%), after 24 and 48 hr in HBSS media (without vitamins and amino acids). Gradual changes in metabolite concentrations were expected when normal oxygen pressures were resumed for these cells.

Metabolite Identification in Cell Supernatant by HPLC-UV

(Figure 5-1) shows typical chromatograms (at 293 and 254 nm) of cell supernatants using hyperoxic oxygen pressures at PAECs, with 5 peaks (1-5) of Ur (6.8 ± 0.1) min, UA (8.4 ± 0.2) min, 2,8-DHA (10.7 ± 0.4) min, Hy (12.6 ± 0.1) min and XA (14.6 ± 0.1) min, which were identified using standards and enzyme assays. Peak 3 at (10.7 ± 0.4) min was assigned to 2,8-DHA based on the retention time of 2,8-DHA standard. The highest peak 3 intensity was observed at 293 nm, consistent with the 2,8-DHA λ_{max} at 305 nm.

The concentrations of the metabolites that were identified vs time in the media are plotted in (Figure 5-2) and are summarized in the first two rows (Table 5-1) and (Table 5-2). The concentrations of all metabolites determined are high. The concentration of 2,8-DHA is the highest among the metabolites that were detected and are higher in PAECs than in AECs. Furthermore, the concentration of 2,8-DHA increases by 45.5 % at PAECs between 24 and 48 hr in the media, while the increase at AECs is 9% at their respective physiological oxygen pressures, indicating different activities of the metabolic processes which generate 2,8-DHA in these cells. 2,8-DHA has been identified previously only in urine under conditions of 2,8-dihydroxyadenine nephrolithiasis.[176]

As shown in (Figure 5-2) concentrations of Ur, which increase with time at both the cells are higher at PAECs than in AECs. However, the increase with time is greater at AECs (49%) than at PAECs (36%). These observations are consistent with the different activity of Ur pathways in the two cell types and the cellular pathways generating Ur, which are different from those forming 2,8-DHA. The concentrations of Ur in cell supernatants are higher than the values of 0.15 to 1.2 μM reported for the same number of AECs maintained in phosphate buffer saline (PBS) for 2 hr with or without glucose.[27]

The concentrations of final purine metabolites Hy, XA and UA are shown more clearly in (Figure 5-3). Unlike the observations for 2,8-DHA and Ur, purine metabolite concentrations are higher at AECs than of PAECs after the first 24 hr in HBSS media. The concentrations of Hy are high (Figure 5-2) and (Figure 5-3) compared to the value of 0.3 μM reported in the supernatant of AECs with glucose (no stress) in PBS.[27] At physiological oxygen pressures, UA values are lower than 5 μM UA as reported by Hassoun et al at bovine pulmonary artery endothelial cells (BAECs) in serum free RPMI-1640 medium. The discrepancy in UA concentrations could be

due to differences in the media and, more importantly the animal source. However in Hassoun et al's work, the chromatogram showed an unidentified peak at 11.3 min between UA and Hy peaks. Furthermore, the XA peak was not visible, even though drastic changes were reported in the Hy to XA ratio, and the chromatograms showed inconsistencies in the peak intensities of Hy based on the reported concentrations at its λ_{max} 254 nm.[12]

If, as proposed, the main source of purines is the degradation of ATP,[167] then it is reasonable to propose that the extent of degradation of ATP is greater at AECs than at PAECs. At AECs the concentrations decrease between 24 and 48 hr, but increase at PAECs. It is possible that ATP degradation in AECs is reduced as the cell viability is compromised with time, while ATP degradation increases at PAECs, as they respond to stress. The results confirm the differences in the responses of PAECs and AECs. Although physiological oxygen pressures should not alter cellular metabolism over short time periods, the changes in metabolite concentration with time illustrated in (Figures 5-4 and 5-5) may be due to stress caused by the changes in cellular metabolism by unsupplemented HBSS media.

Oxidative Stress

Oxidative stress induced by changes in oxygen pressure triggers a chain of events (Figure 1-1), which reduces metabolite salvage, and thus increases formation of final degradation products.[59] Cellular processes triggered by hypoxia and hyperoxia lead to the release of signaling molecules which are metabolized to Ado and Ur by the action of surface enzymes, whose activities have also been found to increase under hypoxia.[34, 52, 162, 177-179] Based on previous reports, hypoxia at AECs and hyperoxia at PAECs was expected to cause changes in the concentration of final purine and pyrimidine metabolites.[27] Purine and pyrimidine metabolites were expected to be released in the cell supernatant and the concentrations may be enhanced by

the degradation of extracellular ATP and UTP.[52, 162] Furthermore, as part of normal metabolism the cells release these metabolites.

Purines and pyrimidines are transported via concentrative nucleoside transporters (CNT1 and CNT2) into the extracellular fluid, while equilibrative nucleoside transporter (ENT) families of transporters, which are concentration gradient dependent, mediate influx and efflux of nucleosides and nucleobases.[161] Further changes in membrane potential and cell pH can alter metabolite flux.[180] Other researchers have suggested that purines permeate cellular membranes via carrier-mediated transporters and diffuse passively through the interendothelial clefts.[181]

Effect of Hyperoxia on Adaptation of PAECs

(Figure 5-4) illustrates changes in metabolite concentrations at PAECs after exposures of cells to hyperoxia (20% O_2) and the results are summarized in the lower two rows of (Table 5-1). After 24 hr hyperoxia, metabolite concentrations are lower than the concentrations of the same metabolites in the media under physiological oxygen pressures, except for XA concentration, which is the same. Similar to what is observed with time under normal oxygen pressures, extended hyperoxia (48 hr) causes the concentration of the metabolites to increase, but the levels attained after 48 hr of hyperoxia are lower than after 48 hr at normal oxygen pressures, except for Ur whose concentrations are higher by 10% after 48 hr hyperoxia. The change in Ur concentration is greater than that of 2,8-DHA, a reflection of the pathways that generate these metabolites. After hyperoxia, the levels of 2,8-DHA in the extracellular fluid at PAECs are the highest among the measured metabolites.

The ratio of Hy to XA in the extracellular fluid reduces from (3.4 ± 0.3) to (0.6 ± 0.4) after 48 hr of hyperoxia at PAECs.[12] However, in this work there is no significant change in the values of the ratios. Further, XA values reported from microdialysis studies in animal heart (80 μM)[9]

and human brain (58 μM)[182] under hypoxia are higher than those reported here. Similarly UA concentrations are lower than the values reported in the heart (12 μM)[9] and the brain (12- 15 μM) microdialysates,[153] and in BAECs supernatant (5 μM) exposed to hyperoxia. It is important to note the higher concentrations of Hy compared to XA at PAECs after 48 hr of hyperoxia compared to 48 hr of physiological oxygen pressure. At physiological oxygen pressures the concentration of Hy is greater than that of XA after 24 hr in the medium, suggesting reduced metabolism of ATP.

The lower concentrations of the metabolites at PAECs exposed to hyperoxia (24 hr) may indicate that these cells are suppressing metabolism during the 24 hr of hyperoxia. The activity of xanthine oxidase has been reported to decrease in PAECs after 18 hr of hyperoxia, where the cells may be under hibernation to conserve energy.[32] This condition is also referred to as cellular relaxation, which is reversible as the cells return to normal metabolism when physiological oxygen pressures are restored.[183] When PAECs were exposed to anoxic conditions of 0% oxygen for 18 hr, the measured levels of ATP were higher compared to the levels under hyperoxic oxygen pressures, an indication of down-regulation of cellular metabolism under oxidative stress induced by hyperoxia.[24] Because PAECs are exposed to low oxygen pressures *in vivo* of 3-5 %, they adapt to 0% oxygen pressures with ease and do not downregulate their cellular metabolism.

Hypoxia at AECs

(Figure 5-5) and the bottom two rows of (Table 5-2) show the concentrations of metabolites vs. time under hypoxia in AECs supernatant. Unlike hyperoxia at PAECs, hypoxia at AECs results in an overall decrease in the concentrations of the metabolites with time, which is in contrast to the behavior at PAECs where the concentrations of the metabolites increase over time. However, after the first 24 hr of hypoxia there is an increase in the concentrations of Ur

and 2,8-DHA. The changes in the concentrations of purines can be seen more clearly in (Figure 5-3), where UA concentrations remain unchanged and Hy and XA concentrations decrease after 24 hr compared to the concentrations at 24 hr normoxia and are very similar to the concentrations at 48 hr normoxia. Again this is different than the behavior observed in PAECs. As shown in (Table 5-2), extended hypoxia (48 hr) at AECs sees a significant decline in the concentrations of Ur (118%), 2,8-DHA (57%), UA (83%), Hy (165%) and XA (161%). The concentrations of metabolites after 48 hr hypoxia are the lowest observed during any conditions at AECs, except for Ur. This is again in contrast to the behavior of PAECs, where the levels of all metabolites increased after 48 hr of hyperoxia (20% O_2).

The concentrations of 2,8-DHA in the extracellular fluid of AECs are the highest among the measured metabolites. However, the concentrations of 2,8-DHA are lower in the supernatant of AECs than at PAECs. From the observed changes in the metabolite levels at AECs, it is reasonable to propose that the cells in HBSS can adapt to oxidative stress of hypoxia for 24 hr, and may do so by increasing the activities of pathways that lead to the production of 2,8-DHA and Ur. The pathways leading to final purine metabolites are less active. AECs, however, cannot survive extended hypoxia, which is shown by the low levels of metabolites after 48 hr of hypoxia. This likely marks cell death, as lower cell viability was also observed.

Observations of the Effects of Oxidative Stress

The differences in the concentrations of the metabolites in the supernatants of AECs and PAECs reflect different adaptation of cells to oxidative stress induced. They may also indicate differences in cellular response to hypoxia and hyperoxia. The effects of hyperoxia on AECs and of anoxia on PAECs were studied. The results showed the sensitivity of AECs to hyperoxia, where a significant decrease in DNA synthesis after 48 hr was measured along with a decrease in the thymidine kinase (a salvage enzyme in the DNA synthesis pathway) activity after 12 hr of

hyperoxia,[184] as well as the resistance of PAECs to anoxia, where exposure of PAECs to 0 % oxygen for 18 hr did not alter the profile of Ado and guanine nucleotides.[24] It was also observed that human lung epithelial cells died only after 6-8 days of hyperoxic stress.[185]

Changes in the concentrations of the metabolites that were identified in the extracellular fluid of AECs and PAECs show clear differences in cellular response to hypoxia and hyperoxia. The details of the cellular processes that contribute to these changes will require further investigations. However, the results indicate that new insights into cellular adaptation can be obtained from the investigation of the effects of oxidative stress of hypoxia and hyperoxia at endothelial cells and that a combination of multiple precesses involved in cellular functioning lead to changes in the levels of the metabolites in the cell supernatant of PAECs and AECs exposed to varying oxygen pressures with time.

The highest concentrations were measured for 2,8-DHA, and it was also interesting that the concentrations of 2,8-DHA changed not only with oxidative stress of hyperoxia (20% O_2) at PAECs and hypoxia (3% O_2) at AECs with time, but also at physiological oxygen pressures with time. Furthermore, the pattern for changes in concentrations of 2,8-DHA and Ur were the same for a particular cell type. Previously, 2,8-DHA has not been measured in cellular fluid, except in urine. However in the 1970's, it was described as the product of adenosine phosphorybosyl transferase (APRT) deficiency. As a result, 2,8-dihydroxyadenine nephrolithiasis was misdiagnosed as uric acid lithiasis due to the identical reactivity of 2,8-DHA and UA in the tests routinely used, such as the murexide test, colorimetric reactions and thermogravimetric analysis,[70] and also due to the similar absorption maxima of 2,8-DHA (305 nm) and UA (293 nm).

The polyamines (spermine, spermidine and putrescine) are involved in the expression of genes which encode the antioxidant defense enzymes.[186] Polyamines are also known to scavenge ROS in PAECs under hyperoxia[187] and in smooth muscle cells under hypoxia,[188] where the polyamines protect the cells against DNA damage. The mechanism by which the polyamines exert their antioxidant effect or scavenge the ROS is still under debate. However, it is proposed that the polyamines can act by reaction with nucleic acids and DNA to change the DNA structure making it less susceptible to ROS damage, or by scavenging the free radicals to prevent DNA from oxidative damage.[189-191] The adducts of polyamines with ROS were determined by NMR spectroscopy, and their structures were verified with high resolution mass spectrometry.[190] Polyamines are also known to retard the auto-oxidation of Fe^{2+} (by forming a ternary complex with iron), which generates free radicals[192-194] and are also known to moderate the toxicity of paraquat, a source of superoxide anion, as suggested by the decrease in the uptake of paraquat in the presence of polyamines in cell media.[195] The complexation of spermine with Fe^{2+} was measured indirectly via the reduction of cytochrome c. Uncomplexed Fe^{2+} was reduced by cytochrome c, but spermine-Fe^{2+} halted this reaction.[196] At physiological pH, polyamines are fully protonated and polycationic, and it has been suggested that they achieve their physiological effects by associating with the negative charges on the nucleic acids and phospholipids.[197]

Based on our results and the functions of polyamines, it is reasonable to propose that the high levels of 2,8-DHA in the cell supernatants may reflect changes in the polyamine synthesis pathway along with the reduced salvage of Ade, as shown in (Figure 5-6). The byproduct (5'-methythioadenosine) of the polyamine synthesis pathway is converted to Ade via the enzyme 5'-methylthioadenosine transferase (MTAP). Under normal conditions, Ade is salvaged to AMP, but under diseased conditions, Ade is oxidized to 2,8-DHA via the enzyme xanthine oxidase.

(Figure 5-6) shows the purine degradation pathway and the *de novo* synthesis pathway. Ade accumulation may be due to a) reduced salvage to conserve energy, b) halt in ATP production, so AMP is also not required in an effort to conserve energy or c) enhancement of Ade production as a result of upregulation of the polyamine synthesis pathway. Furthermore, in the coronary endothelium the major catabolite of cardiac adenine nucleotides and Ado under normoxia and ischemia was found to be UA. This was confirmed by inhibition of xanthine oxidase activity by allopurinol.[167, 198] Xanthine oxidase is the same enzyme responsible for the conversion of Ade to 2,8-DHA. UA was also found to be the major catabolite in smooth muscle cells.[167] It may be possible that the major metabolite, as we have observed in this work was 2,8-DHA in the coronary endothelium and in smooth muscle cells, but the compound was mistakenly identified as UA, as in the diseased urine in the early 70's.

As mentioned earlier, ROS production increases under oxidative stress induced by either hypoxia or hyperoxia, and ROS may also be responsible for the oxidation of Ade to 2,8-DHA. Furthermore, the reaction of xanthine oxidase with Ade can also lead to 2,8-DHA due to the deficiency of the salvage enzyme APRT as seen *in vivo* in 2,8-dihydroxyadenine nephrolithiasis, an inherited disease. The enzyme deficiency leads to high levels of 2,8-DHA in urine, with no change in Hy, XA and UA levels.[199] Thus, the higher levels of 2,8-DHA in the cell supernatants may be possible without drastic changes in the levels of Hy, XA and UA. The highest concentrations of 2,8-DHA are observed at PAECs for physiological oxygen pressures of 3% for 48 hr, the next highest 2,8-DHA concentrations are observed after exposure to 3% for 24 hr, and the same result as 24 hr of physiological oxygen pressure was observed after 48 hr hyperoxia at these cells. Thus, it is possible that, since these cells are exposed to low oxygen pressures *in vivo*, they need to have the most efficient system to survive under reduced oxygen, where their cellular

pathways generate more of the polyamines to regulate cell turnover, protect the DNA, scavenge ROS, and survive.

Uridine triphosphate (UTP) and cytidine triphosphate (CTP) are precursors in the synthesis of RNA and also play an important role in the biosynthesis of phospholipids (CTP) and glycogen (UTP). UTP is released during cardiac ischemia and is proposed to exert a protective effect against myocardial damage.[200, 201] UTP metabolism was also proposed to increase during energy stress of smooth muscles, due to the elevated levels of Ur measured.[34] Like ATP, UTP is an extracellular signaling molecule which activates the purinergic receptors.[162] Extracellular UTP stimulates vasodilation and has been suggested to be very important in cardiac regulation. Plasma UTP levels have been found to increase after hypoxia and hyperoxia, indicating the protective effect of UTP. The possible sources of UTP released in the plasma were identified as cardiac myocytes, endothelial cells and platelets.[200] The mechanisms proposed for ATP release from endothelial cells such as hemi-channels may also apply to UTP.[202] Concentrations of Ur, a metabolite of UTP, may increase as a result of hypoxia and prolonged hyperoxia resulting in the hydrolysis of UTP by the surface bound ecto-enzymes.[179] In addition, high levels of Ur have been associated with RNA degradation[59] and degradation of extracellular CTP via the ectonucleotidases.[167] Protein synthesis is the major energy consuming process[203] and is down regulated under glucose deprivation, which can lead to RNA degradation. Ur levels in PAECs and AECs supernatant in HBSS under physiological conditions may most likely be due to UTP and CTP degradation, rather than RNA degradation, since the levels of Ur are higher after stress at PAECs (20% O_2) and AECs (3% O_2). This provides evidence for the protective effects of UTP (increased metabolism), followed by hydrolysis to Ur and rapid degradation of CTP, which is also a high energy molecule. Further, since the salvage of the pyrimidine nucleosides requires

ATP as the phosphate donor, it is likely that salvage is stopped to conserve energy, thus leading to accumulation of Ur.

Changes in the concentrations of purines (Hy, XA and UA) in the cell supernatants are indicative of changes in ATP degradation and *de novo* synthesis of purines. Purine metabolism increases after 48 hr of physiological conditions (3% O_2) at PAECs in HBSS. This could be due to possible up-regulation of purine *de novo* synthesis. Further, the increased xanthine oxidase activity in PAECs after 48 hr of low oxygen pressures[35] may also enhance purine metabolism. Thus, physiological conditions (3% O_2) at PAECs in HBSS show enhanced purine metabolism or reduced salvage with time. Enhanced purine metabolism in cells is indicative of either mechanical work done by cells or continuous formation and turnover of cells.[167] A decrease in purine metabolism at PAECs after 24 hr of hyperoxic exposure may be indicative of relaxed cells or reduction in mechanical work done by the cells (as under stress to conserve energy). The increase in the concentrations of the metabolites after 48 hr has been proposed to be due to the reaction of UA with free radicals to form new oxidation products,[46] and thus UA must be continuously produced via oxidation of Hy and XA.[48]

Furthermore, it has been observed that under hyperoxia (20% O_2) the activity of xanthine oxidase decreases in PAECs.[32, 204, 205] This decreased activity of the enzyme would also explain the drop in the concentrations of XA and UA. As mentioned above, Elsayed proposed that the decreased UA concentration may be due to its antioxidant properties.[204]However, the decreased levels of 2,8-DHA measured after hyperoxic (20% O_2) conditions suggest otherwise. Since Ade is also a substrate for xanthine oxidase, the levels of 2,8-DHA should have increased if the enzyme activity was enhanced to produce UA to function as an antioxidant. Furthermore, toxic ROS generated by xanthine oxidase have been implicated in both hypoxia and hyperoxia

mediated endothelial cell injury. ATP metabolism leading to increased substrates for the enzyme and elevated levels of superoxide and hydrogen peroxide have been proposed to contribute to the damage. The H_2O_2 and $O_2^{\bullet-}$ combine to form the more toxic $OH^{\bullet}$ radical.[206] Therefore, decreased xanthine oxidase activity under hyperoxia may deactivate this potentially destructive enzyme at a time when the cells are already oxidatively stressed. A 48 hr period of hyperoxia (20% O_2) exerts stress on these cells and thus purine metabolism increases. Similar results were obtained by Mei et al when hypoxia was followed by continued reperfusion.[9]

Production of $NO^{\bullet}$ is dependent on the levels of oxygen; the production of $NO^{\bullet}$ is low at high oxygen pressures and is high at low oxygen pressures.[207] Thus, at physiological oxygen pressures (3% O_2) after 48 hr at PAECs the concentrations of $NO^{\bullet}$ and $ONOO^-$ radicals will be high compared to their levels in PAECs after hyperoxia (20% O_2) for 48 hr. Xanthine oxidase can reduce nitrite to produce $NO^{\bullet}$, which will further elevate the levels of $NO^{\bullet}$.[208] The elevated levels of ROS will cause an influx of Ca^{2+} and an efflux of ATP and UTP, which in turn will activate purine receptors and kinases, and finally be degraded to their metabolites by the surface enzymes. The polyamine synthesis pathway will also be upregulated and produce 2,8-DHA as a secondary byproduct, due to Ade accumulation followed by oxidation. The activity of xanthine oxidase combined with the formation of ROS causes the levels of metabolites to increase after extended periods at physiological conditions (48 hr) in PAECs due to extracellular ATP and UTP degradation or due to increased cell metabolism and purine *de novo* synthesis.

At AECs, purine metabolism is the highest under physiological conditions (20% O_2 for 24 hr, an indication that these cells are stressed in HBSS even at 24 hr and that there is higher activity of xanthine oxidase in AECs compared to PAECs. After 48 hr physiological oxygen pressures at AECs, the purine metabolism decreases slightly. Similar levels are attained after 24

hr of oxidative stress induced by hypoxia (3% O_2), and these levels drop to very low values after 48 hr.

As mentioned earlier, xanthine oxidase activity increases under hypoxia/glucose stress and may lead to elevated levels of UA and 2,8-DHA. Measurement of 2,8-DHA (Ade oxidation product) in high concentrations, reinforces enhancement of xanthine oxidase activity (for which Ade is a substrate). The elevated levels of 2,8-DHA in PAECs compared to AECS suggest increased oxidation of Ade by ROS, since the purine metabolites suggest higher activity of xanthine oxidase in AECs.

Enhanced $NO^{\bullet}$ and $ONOO^{-}$ production, (which suppresses respiration)[209] could in turn lead to cell death and a major decline in the concentrations of the metabolites as is seen in AECs exposed to hypoxia (3% O_2) for 48 hr. As mentioned earlier, our results indicate that a combination of multiple processes involved in cellular functioning lead to the observed changes in the cell supernatants.

The results obtained in our experiments for PAECs are similar to those obtained earlier by Terada et al, Hassoun et al and Elsayed et al in terms of xanthine oxidase activity.[33, 204, 205] Further, our results for AECs support the work of Schrader and Mei.[9, 27] In the experiments performed by Schrader et al, glucose deprivation in AECs caused an increase in the levels of the metabolites (Hy, Ino, Ado, guanine, guanosine, uridine, Ur and cytidine). Ur levels remained elevated, while Hy showed an initial increase in concentration with glucose stress followed by a steady decline.[27] Mei et al showed that high levels of purine metabolites (Ado 6 μM, Ino 290 μM, Hy 180 μM, XA 60 μM and UA 12 μM) help in blood regulation by local decreases in sympathetic tone, closure of calcium channels or opening of ATP-sensitive potassium channels

in smooth muscle and in myocardial cells. Thus these metabolites may exert some cardio protection against ischemia by myocardial preconditioning.[9]

Conclusions

In this chapter we have demonstrated a simple reversed phase HPLC-UV method with isocratic elution for the measurement of purine and pyrimidine metabolites released in the supernatants of PAECs and AECs exposed to oxidative stress induced by hyperoxia and hypoxia. It was observed that the cellular media which contained HBSS may stress the cells resulting in changes in metabolite concentrations after return to physiological oxygen pressures.

PAECs appear to be more robust and may adapt to hyperoxia by cellular relaxation and by regulating the polyamine synthesis pathway and purine metabolism, which in turn decreases metabolite concentrations. The changes in the concentration of the metabolites in the extracellular fluid could serve as stress markers. Longer exposure of PAECs to hyperoxia increases metabolite concentrations, likely by upregulation of the polyamine pathway and purine metabolism. The changes in the levels of Ur are attributed mainly to increased UTP, CTP and RNA degradation.

AECs on the other hand seem to tolerate hypoxia for 24h hr by maintaining purine metabolism, enzyme activity and polyamine synthesis, while down-regulating the salvage pathways. The changes in the levels of metabolites at AECs that result could serve as stress markers. We can conclude that AECs cannot survive extended hypoxia (48 hr), as evident by the drastic drop in metabolite concentration, presumably from oxidative damage to RNA and DNA, leading to cell death.

An important finding of this work is the measurement and identification of a new stress marker, 2,8-DHA, whose accumulation is proposed to be a result of reduced Ade salvage and the upregulation of the polyamine synthesis pathway. Presumably when cells require polyamines for

cell turnover and DNA protection, they also generate Ade as a secondary byproduct, which can be oxidized to 2,8-DHA by xanthine oxidase or ROS.

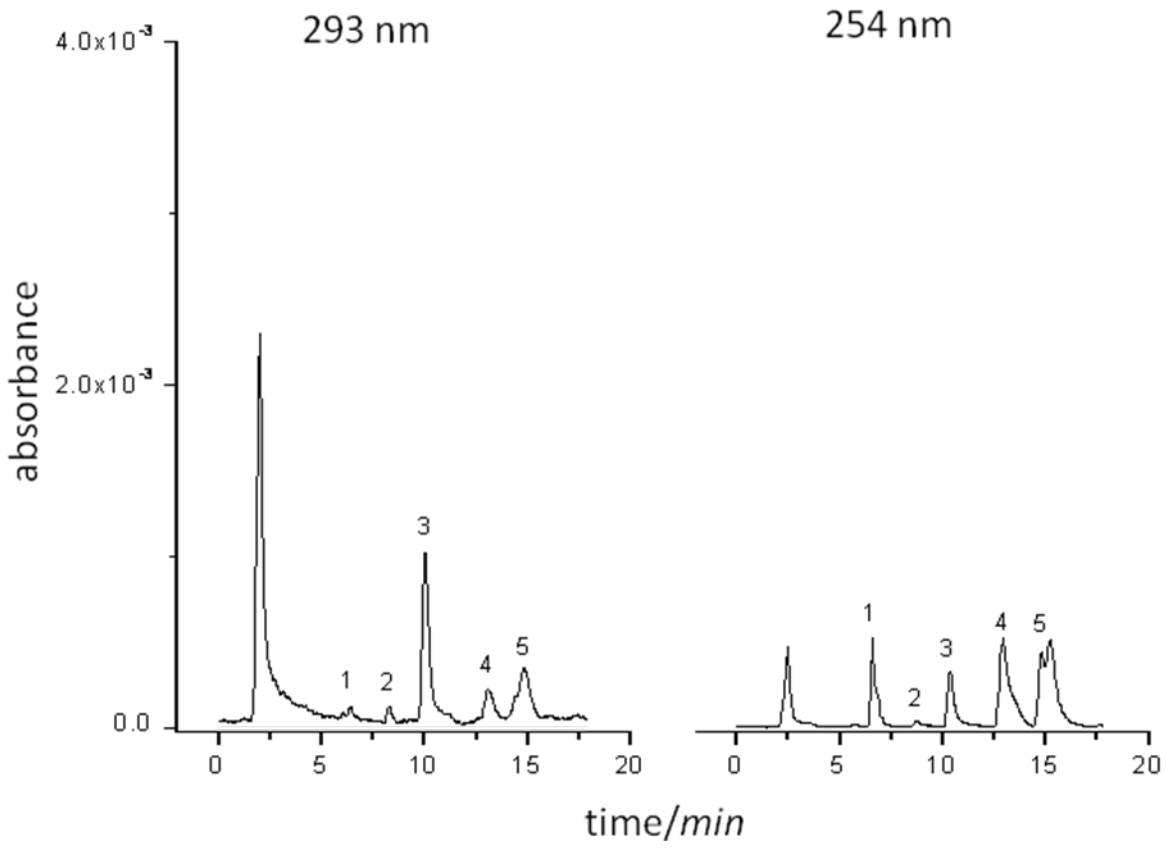

Figure 5-1. Chromatogram of PAECs supernatant for cells exposed to hyperoxia for 48hr. Peak 1= Ur, 2= UA, 3= 2,8-DHA, 4= Hy and 5= XA. HPLC conditions: 20 mM KH_2PO_4, pH 5.1, flow rate = 1 mL/min, 20 μL supernatant

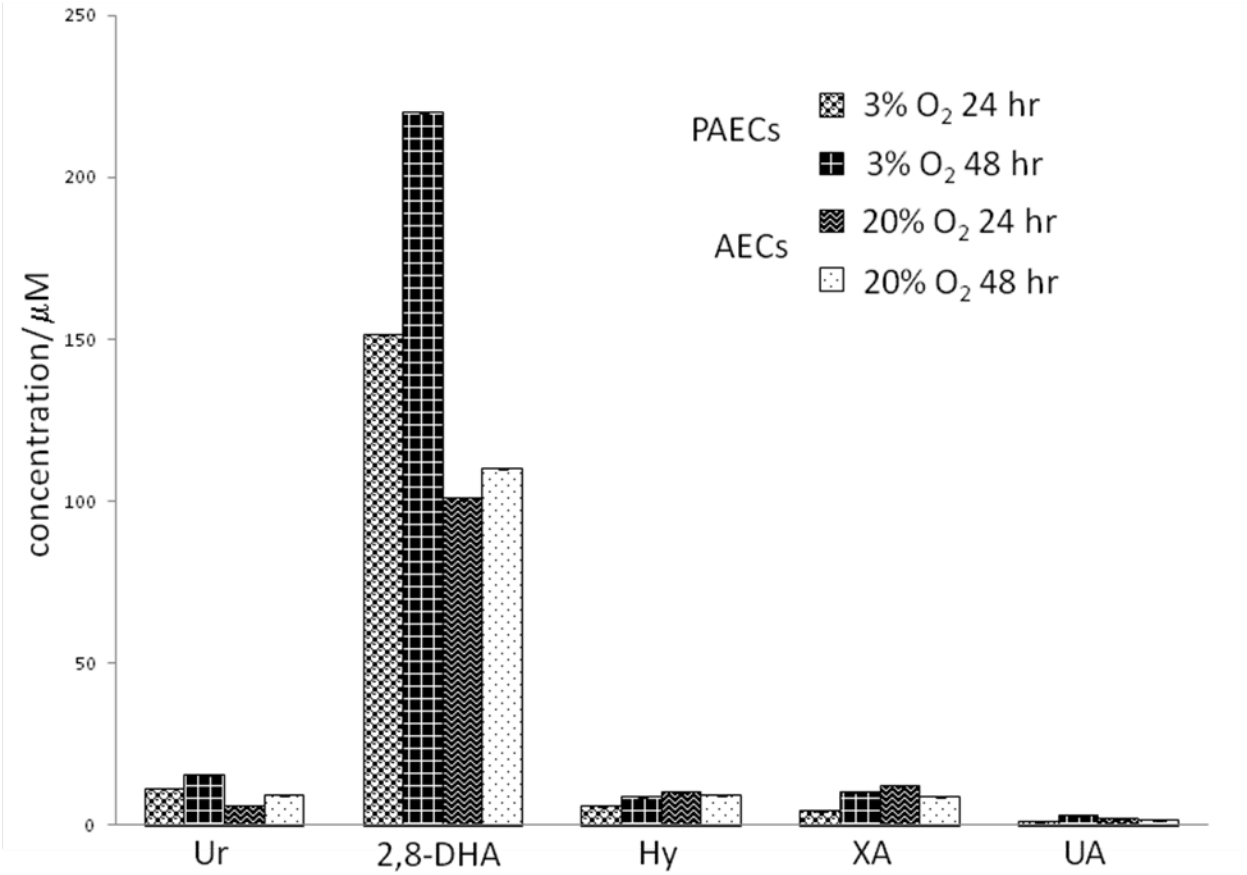

Figure 5-2. Metabolite concentrations in PAECs and AECs supernatants under physiological oxygen pressures with time. HPLC conditions as in (Figure 5-1)

Table 5-1. Concentration of metabolites detected in cell supernatant of PAECs with time and change in oxygen pressure. Data are expressed as mean ± SD, (n =3)

PAECs	Uracil (μM)	Uric acid (μM)	2,8- DHA (μM)	Hypoxanthine (μM)	Xanthine (μM)
3% O_2 24hr	11.4±0.1	1.2±0.1	151.3±0.3	6.0±0.1	4.6±0.1
3% O_2 48hr	15.5±0.2	3.0±0.1	220.0±0.1	8.8±0.1	10.1±0.1
20% O_2 24hr	3.1±0.1	0.5±0.1	100.8±0.1	4.3±0.1	4.8±0.1
20% O_2 48hr	17.0±0.1	1.8±0.1	151.3±0.1	9.5±0.1	8.0±0.1

Table 5-2. Concentration of metabolites detected in cell supernatant of AECs with time and change in oxygen pressure. Data are expressed as mean ± SD, (n =3)

AECs	Uracil (μM)	Uric acid (μM)	2,8-DHA (μM)	Hypoxanthine (μM)	Xanthine (μM)
20% O_2 24hr	6.1±0.1	2.2±0.1	100.8±0.3	10.1±0.1	12.0±0.1
20% O 48hr	9.1±0.1	1.7±0.1	110.0±0.1	9.2±0.1	8.7±0.1
3% O_2 24hr	13.3±0.1	2.3±0.1	119.2±0.5	8.8±0.1	9.3±0.1
3% O_2 48hr	6.1±0.1	1.2±0.1	64.2±0.1	3.8±0.1	4.6±0.1

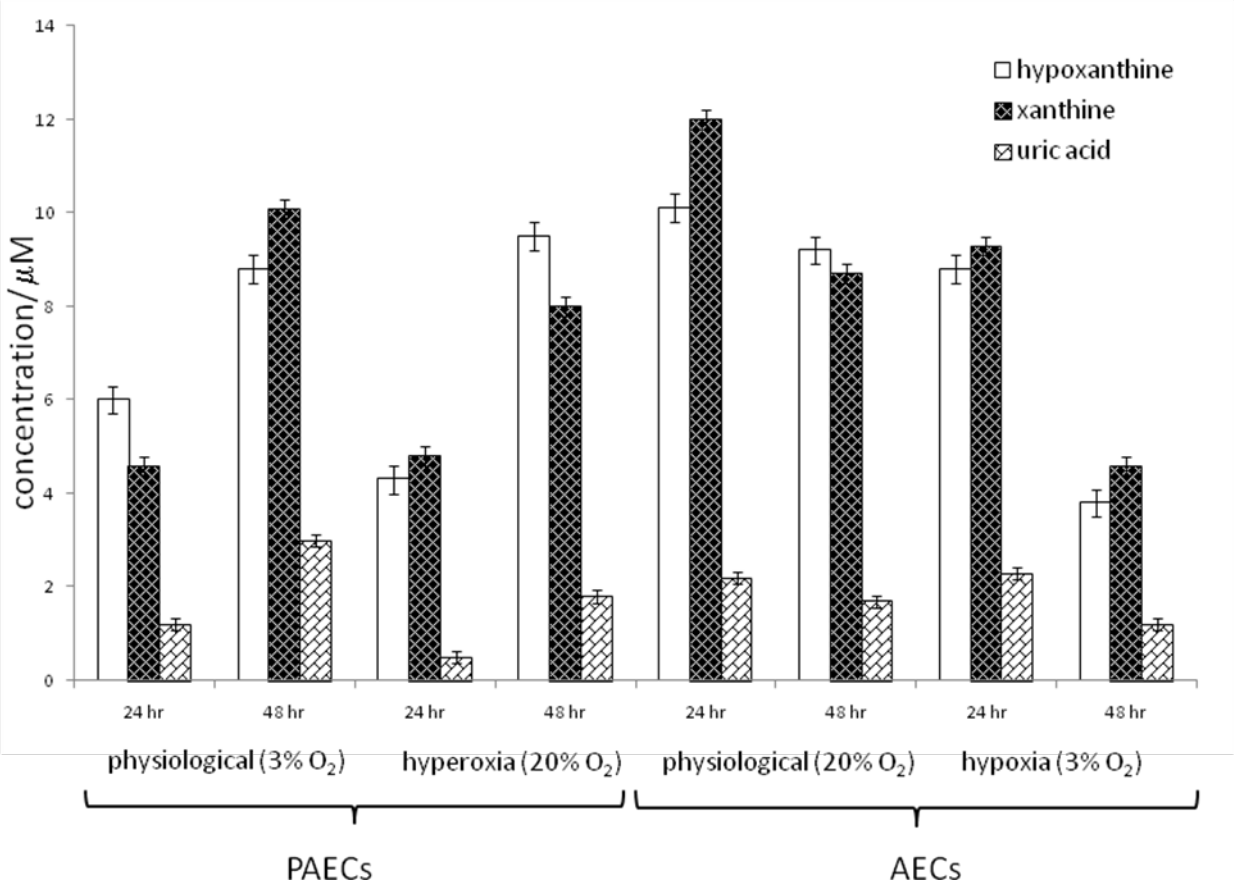

Figure 5-3. Purine metabolites (Hy, XA and UA) concentrations in PAECs and AECs supernatant under stress and under physiological oxygen pressure with time. HPLC conditions as in (Figure 5-1)

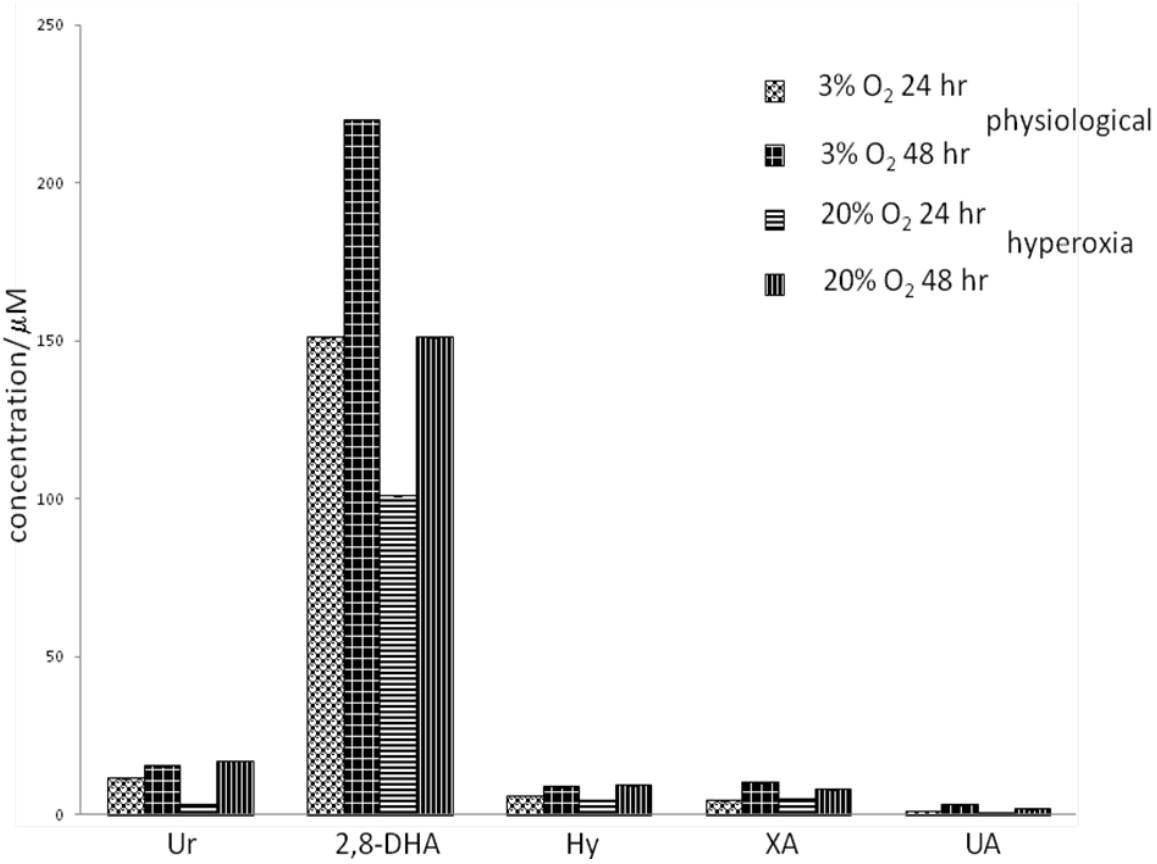

Figure 5-4. Metabolite concentrations in PAECs supernatant at physiological and hyperoxic oxygen pressures with time. HPLC conditions as in (Figure5-1)

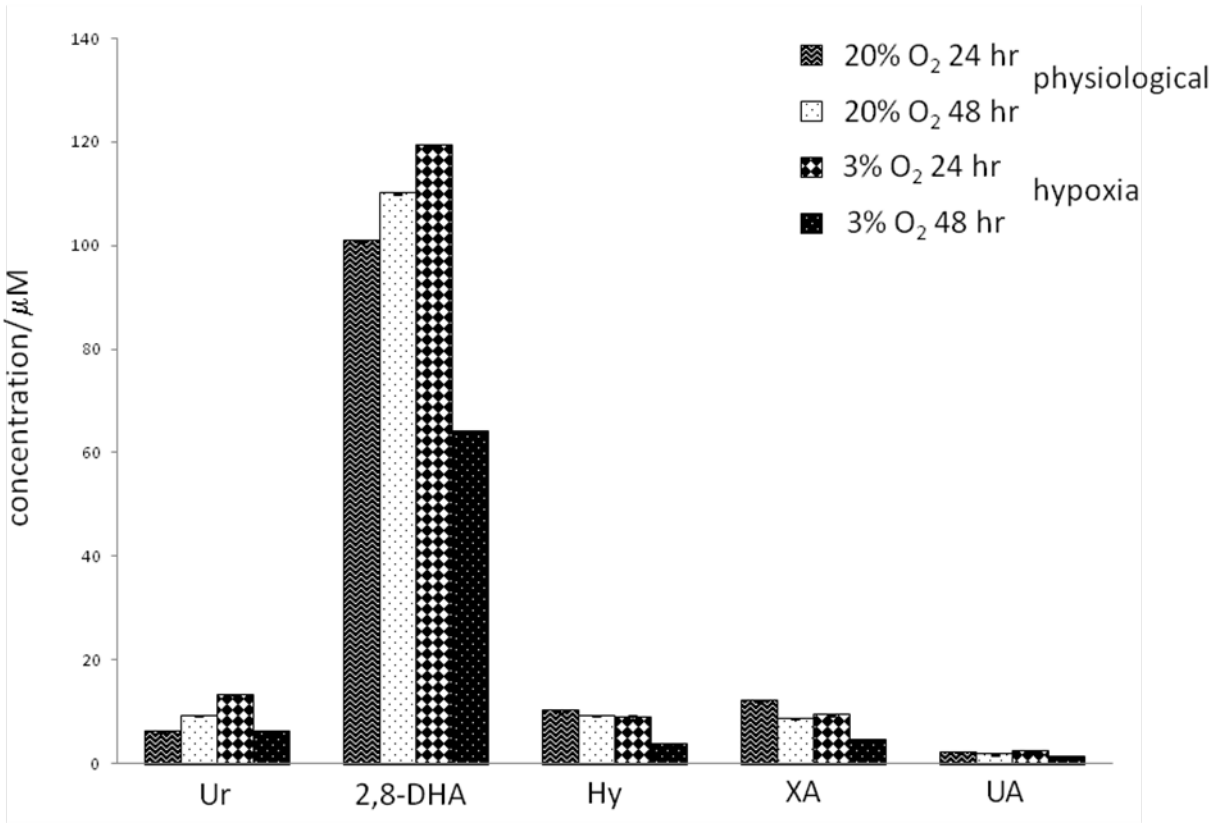

Figure 5-5. Metabolite concentrations in AECs supernatant at physiological and hypoxic oxygen pressures with time. HPLC conditions as in (Figure 5-1)

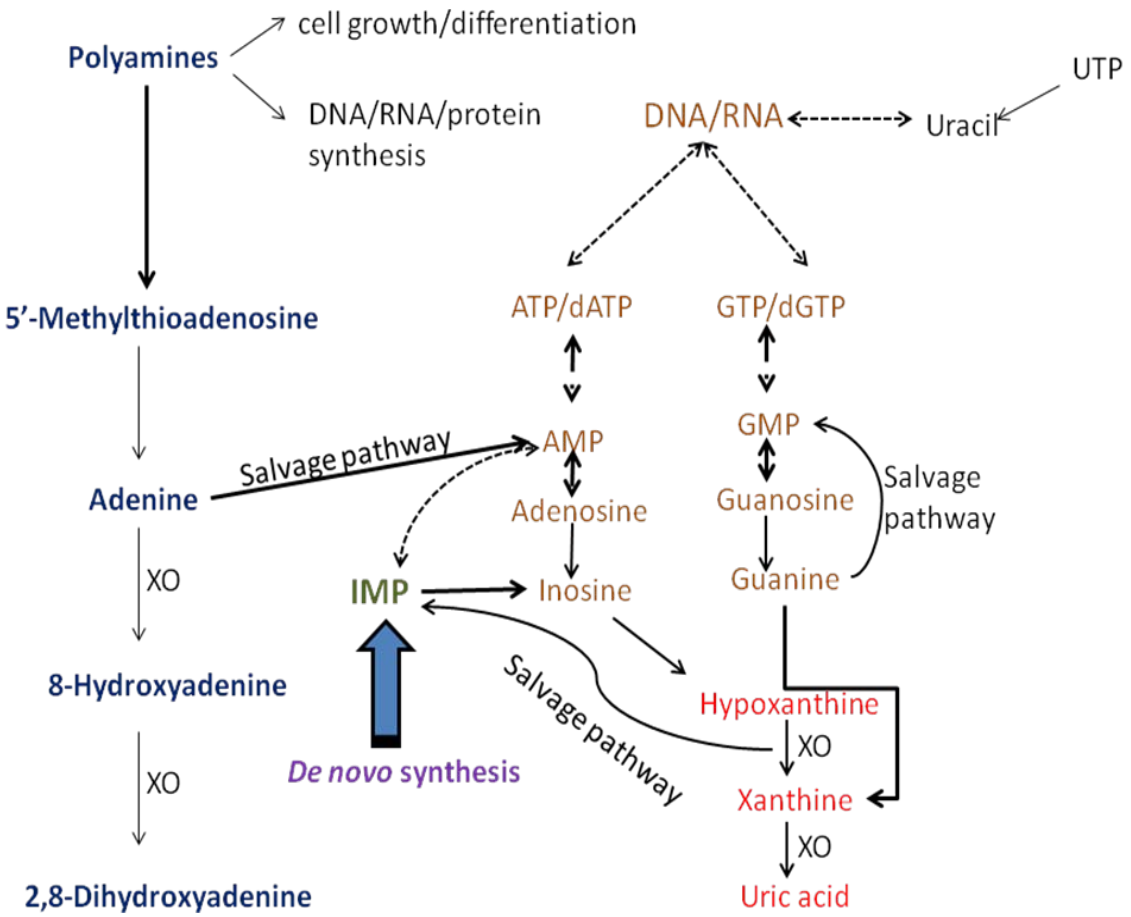

Figure 5-6. Purine metabolism pathway and polyamine synthesis pathway as the source of adenine. 5'-methylthioadenosine which is a byproduct of polyamine synthesis is converted to adenine by methylthioadenosine phosphorylase (MTAP). Adenine is salvaged to AMP via adenine phosphoribosyl transferase (APRT) under normal conditions. However under oxidative stress, the salvage pathway may not be effective leading to the accumulation of adenine. The accumulated adenine may be oxidized to 2,8-DHA. Alternatively, the polyamine synthesis pathway which is up-regulated in PAECs exposed to oxidative stress can cause adenine concentrations to increase. APRT deficiency leads to high levels of 2,8-DHA in urine, with no change in Hy, XA and UA levels. Thus higher levels of 2,8-DHA in the cell supernatants may be possible without drastic changes in the levels of Hy, XA and UA

CHAPTER 6
RAPID MEASUREMENT OF 2,8-DIHYDROXYADENINE WITH FAST SCAN CYCLIC VOLTAMMETRY AT A NANOSTRUCTURED CARBON FIBER SENSOR IN 5-FOLD DILUTED ENDOTHELIAL CELL SUPERNATANTS EXPOSED TO OXYGEN STRESS

Introduction

Chapter 5 described the HPLC-UV analysis of the endothelial cell supernatants, which showed 2,8-DHA (6-amino-1H-purine-2,8-dione) to be the major metabolite present in these samples. This chapter focuses on the application of FSV method with N-CFS that was developed in chapters 3 and 4 for rapid and direct measurements of 2,8-DHA metabolite in cell supernatant of endothelial cells. Advantages of FSV measurements with a N-CFS in rapid screening of biological fluids for small metabolites have been demonstrated in chapter 4 and in previous work.[62, 73, 91] In FSV, chemical reactions which occur during analysis, can be outrun to reduce passivation and improve sensitivity of sensors. The method developed for the measurements of metabolites was designed to prolong sensor lifetime by continuous cycling of the potential between -1.0 to +1.5 V vs. SCE during signal acquisition to regenerate the sensor surface.[93]

The electrochemically produced porous nanostructure of the N-CFS facilitates charge transport without restricting mass transport, resulting in high sensitivity in analytical measurements, as shown in the measurements of XA and UA in urine in chapter 4. The method of surface fabrication that was developed stabilizes the background signal of the sensor for efficient background subtraction, which is necessary because of the large background current produced in FSV.[73] Signal averaging capabilities of FSV improve the S/N ratio and contribute to low LOD's;[74] while kinetic filtering at scan rates of 500 V s^{-1} improves selectivity.[93] In addition, the N-CFS background signal increases less than expected at high scan rates, presumably because of reduced contribution of surface reactions to the background. Due to the high sensitivity of FSV with the N-CFS, dilution of biological samples such as urine is possible.

The FSV method was optimized for 2,8-DHA measurements in supernatants of aortic (AECs) and pulmonary artery endothelial cells (PAECs) exposed to hypoxia and hyperoxia. *In vivo*, endothelial cells form a barrier between blood and tissue and are the first line of defense against changes in oxygen pressure and changes in glucose levels. They are known to tolerate local environmental changes,[24, 27] but oxidative stress can trigger a chain of events leading to the production of reactive oxygen species (ROS) and can bring about changes in metabolic and salvage pathways, as the cells attempt to conserve energy or to compensate for depletion of metabolites.

The results presented in chapter 5 demonstrated that concentrations of purine and pyrimidine metabolites, including 2,8-DHA, change in supernatants of endothelial cells exposed to stress. The high measured concentrations of 2,8-DHA suggested that 2,8-DHA may be useful as a marker of oxidative stress. In endothelial cells during normal cellular work, 5'-methylthioadenosine (MTA), which is a byproduct of polyamine synthesis pathway (Figure 6-1), is degraded to Ade by 5'-methylthioadenosine phosphorylase (MTAP).[210] This pathway is the main source of endogenous Ade, which under normal conditions is efficiently salvaged via adenine phosphoribosyl transferase (APRT) to adenosine monophosphate (AMP)[211] (Figure 6-1). Accumulation of Ade can occur during oxidative stress, when the salvage pathways are significantly down-regulated and activity of MTAP is enhanced.[60] Ade is susceptible to oxidation by xanthine oxidase, which can produce 2,8-DHA as the final oxidation product via the formation of 8-hydroxyadenine.[212] A similar pathway is observed during electrochemical oxidation of Ade.[213, 214] Electrochemical oxidation of 2,8-DHA has been proposed to generate a diimine, which yields allantoin and parabanic acid (pH 7.5), or alloxan and urea (pH 3.0) as the final products.[215] Ade oxidation is known to occur *in vivo* in a rare autosomal recessive disorder

of APRT deficiency,[216] 2,8 dihydroxyadenine urolithiasis, which results in the inability to salvage Ade for purine synthesis. Levels of 2,8-DHA (34 mmol/L) have been detected in urine of APRT deficient patients by CE-UV[217] and by HPLC-UV[218, 219] with LOD's of 5 μM and 2 nmol, respectively. This chapter describes a new FSV method for measuring 2,8-DHA using N-CFS.

Results and Discussion

FSV of 2,8-DHA in pH 7.4 Phosphate Buffer at N-CFS

Limitations of slow scan cyclic voltammetry at large graphite electrodes have been identified in the detection of 2,8-DHA,[214, 215] as observed for other purine metabolites.[97] FVS measurements of 2,8-DHA at N-CFS were investigated in this work because of the high sensitivity of this method in the measurements of small metabolites.[71]

The 2,8-DHA concentrations were measured first in pH 7.4 phosphate buffer because of the observed high sensitivity in this buffer as observed in chapter 3 and previously reported.[63] For 1 μM 2,8-DHA, two oxidation peaks (IIa and IIIa) and three small reduction peaks (IIc, IIIc and Vc) were observed at 500 V s^{-1} (Figure 6-2A and B). A broad composite oxidation peak composed of 5 smaller peaks (Ia through Va), and a single reduction peak (Vc) were observed at higher concentrations (Figure 6-2B). The sensitivity determined at the potential of peak Ia, (0.61 ± 0.02) V, was (0.36 ± 0.01) nA/μM (R^2 = 0.98) in the concentration range of 2-15 μM. This sensitivity is lower than that of UA, (0.65 ± 0.01) nA/μM (2-16 μM range), but is similar to that of XA, of (0.31 ± 0.02) nA/μM (1-19 μM range). Peak Ia was chosen for 2,8-DHA measurements, because this peak is well defined in the concentration range expected to be biologically relevant. The expected peak Ia current is 0.36 nA for 1 μM 2,8-DHA based on the calibration curve sensitivity, (0.36 ± 0.01), nA/μM but the peak is not observed at that potential in phosphate buffer. However, a well developed peak is seen at more positive potentials; for 30

μM 2,8-DHA peak Ia (0.61 V) is a shoulder on the broad oxidation peak. The measured peak Ia current for 30 μM 2,8-DHA is (6.2 ± 0.3) nA, lower than expected from the calibration curve and consistent with adsorption of 2,8-DHA.

The electrochemical behavior of 2,8-DHA has been studied at glassy carbon electrodes (GCE, d = 1.5 mm) at pH 1-13 in 0.2 M acetate buffer by cyclic voltammetry, differential pulse voltammetry, and square wave voltammetry, at scan rates of 5 mV s^{-1} to 10 V s^{-1}, and by cyclic voltammetry at pyrolytic graphite electrodes (PGE) (d = 1.3 mm) in 0.5 M phosphate buffer at pH of 3-11.2 at 150 mV s^{-1}. The investigation of the effect of scan rate on the oxidation process showed strong adsorption of 2,8-DHA on graphite.[215]

The behavior of 2,8-DHA in FSV at N-CFS at 500 V s^{-1} in (Figure 6-2) parallels the behavior observed for 2,8-DHA at GCE and PGE. The oxidation process at peak Ia is likely that observed at 0.35 V at GCE and at 0.25 V at PGE,[215] which has been proposed to be due to the formation of a diimine by a $2e^-$, $2H^+$ oxidation of 2,8-DHA. The more positive value of the oxidation peak at N-CFS can be attributed to the high scan rates in FSV. Similar peak potential shifts were observed in FSV of UA.[73]

Fast scan cyclic voltammetry (FSV) at the N-CFS allowed detection of lower concentrations of 2,8-DHA (1 μM) than reported previously[214] and allowed resolution of the complex oxidation processes. These oxidation processes, attributed to 2,8-DHA dimer oxidation, were observed previously but were not well resolved.[214] It has been proposed that the increase in scan rate should allow detection of the dimers due to their short lifetimes.[214] Dimer formation is well documented in the oxidation of Ade and guanine.[214, 220, 221] (Scheme 6-1) shows a possible dimer formation pathway.

At low concentrations of 1 μM, 2,8-DHA two small reduction peaks at 0.69 V (IIc) and 0.89 V (IIIc) may correspond to the reduction of the oxidation products formed in the reactions at 0.76 V (IIa) and 1.04 V (IIIa), respectively (Figure 6-2A). Peak potentials for the forward and reverse processes are close, which suggests adsorption of 2,8-DHA, as observed at GCE and PGE.[214] High sensitivity allows detection of the peaks at pH 7.4 which is otherwise difficult.[214]

FSV of 2,8-DHA at N-CFS in Physiological Buffers

The primary goal of this work was the development of an analytical method for 2,8-DHA measurements in physiological buffers that are used to maintain cells in culture. The final aim was to evaluate the feasibility of 2,8-DHA measurements as a marker of oxidative stress in cell supernatants which contain physiological buffers. Common media used to maintain cells in culture, including during exposure of cells to hypoxia and hyperoxia, are Dulbecco's Modified Eagle Medium (DMEM) and HBSS.[110-114] As described in chapter 3, HBSS was chosen for cellular measurements because background current in this medium was relatively low and stable. In DMEM, the N-CFS was easily passivated and the signal of the metabolites was detected only when the concentration was greater than 10 μM.

Despite the larger background current in HBSS compared to phosphate buffer, due to the greater surface area in HBSS, the current is stable and can be efficiently subtracted. However, even small changes in the background current during signal acquisition limit accuracy of background subtraction and prevent measurements of low concentrations of 2,8-DHA. In phosphate buffer, the LOD for UA is 0.5 μM and 0.4 μM for XA, compared to 0.5 μM for 2,8-DHA.

In earlier attempts,[91] to reduce the background signal in physiological buffers, the fabrication of the N-CFS surface was performed in phosphate and was followed by signal

acquisition in a physiological buffer. However, this procedure did not improve the LOD significantly.[91] In this work, the nanostructure of the sensor was fabricated in phosphate as before, but in order to optimize the LOD in HBSS containing samples, the samples were diluted with phosphate in the ratio of 1:5 or 1:10 for the acquisition of analyte signal as in chapter 3. Consequently, the time spent in HBSS during 30 min of surface fabrication was eliminated, and furthermore, during the short time of signal acquisition by FSV, the sensor was in contact only with dilute HBSS.

Chapter 5 showed that UA and XA have been identified as stress markers in the supernatants of endothelial cells exposed to non-physiological oxygen pressures and their concentrations were measured first by FSV at N-CFS in diluted HBSS. High sensitivity in the measurement of these metabolites by FSV at N-CFS in 2000-fold diluted normal and diseased urine is shown in chapter 4.[62] The sensitivity to UA (5-15 μM) was (0.45 ± 0.01) nA/μM in 1:5 diluted HBSS and (0.44 ±0.02) nA/μM in 1:10 diluted HBSS. Both of these values are lower than the sensitivity in phosphate (0.65 ± 0.01 nA/μM). Similarly, XA sensitivity in the 4-17 and 6-17 μM concentration ranges was (0.22 ± 0.02) nA/μM and (0.17 ± 0.02) nA/μM in 1:5 and 1:10 diluted HBSS, respectively. Although, the sensitivity to XA is lower than that of UA, the XA sensitivity decreased less in HBSS. The lower sensitivity in HBSS is due to the effect of the medium on the background current. When the background signal was monitored, it stabilized after the initial changes in the background current, possibly because of the effect of the components of HBSS, since this behavior was not observed in other physiological buffers. The 1:5 and 1:10 dilution resulted in similar low LOD's for UA and XA. The lowest measurable concentration in undiluted HBSS for UA was 10 μM and 15 μM for XA. These decreased to 2

and 5 μM, respectively, after the dilution. Considering that a similar pattern will be observed for 2,8-DHA in cell supernatants, in all further work 1:5 dilution was used.

The electrochemical behavior of 2,8-DHA in 1:5 diluted HBSS shows a complex oxidation behavior similar to that in phosphate (Figure 6-2 C and D). At higher concentrations (30 μM) there is a broad oxidation peak centered at (0.65 ± 0.06) V composed of 6 oxidation peaks shown as an inset in (Figure 6-2). The change in response compared to that in phosphate reflects changes in sensor background. In phosphate buffer, oxidation peaks of 2,8-DHA are better resolved from the background, in part because of lower current of surface reactions,[141, 142] which are pronounced in HBSS. In spite of this, in the concentration range of 2-15 μM, the peak (Ia) (0.65 ± 0.06 V) current is linear (R^2 = 0.99). The sensitivity, (0.34 ± 0.01) nA/μM is the same as that in phosphate, but the LOD is 1 μM compared to 0.5 μM in phosphate buffer. A positive shift of peak Ia to (0.65 ± 0.06) V and higher error bars in the oxidation peak potential indicate background current changes.

Measurement of 2,8-DHA in PAECs and AECs Supernatant

Physiological oxygen pressures *in vivo* are different at PAECs (3 % O_2) and AECs (20 % O_2), and therefore, the response of these cells to changes in oxygen pressure differs. Oxidative stress at endothelial cells leads to a series of events which can increase the formation of cellular degradation products.[52, 167] Thus, during oxidative stress, the composition and the concentration of metabolites released into cell supernatant depends on the duration and the type of stress. Ur, 2,8-DHA, Hy, XA and UA were identified in the supernatants of endothelial cells with 2,8-DHA as the major metabolite. In addition, the results in chapter 5 established that HBSS, which was used to maintain cells in culture, contributed to cell stress, which was likely due to the absence of vitamins and amino acids in the medium. The concentrations of Ur (6.1 ± 0.1) μM, UA (1.2 μM),

Hy (3.8 μM), and XA (4.6 μM) were determined for AECs by HPLC-UV in chapter 5. The results indicated that 5-fold dilution of the supernatant can eliminate interferences in FSV analyses, because the concentrations of electroactive metabolites in the diluted samples would be below the LOD by FSV, 6 μM for Hy[71] and 0.5 μM for UA. XA signal (LOD 0.4 μM) could interfere but would not be measured when 2,8-DHA is present at high concentrations.

(Figure 6-3) illustrates the results that were obtained in cell supernatants of AECs and PAECs subjected to oxidative stress. In AEC supernatant (Figure 6-3A), in agreement with the results obtained for 2,8-DHA standards in HBSS, multiple oxidation peaks are observed with a poorly developed reduction peak, as expected for low concentrations of 2,8-DHA. Higher pH (above 7) does not permit detection of a well developed reduction peak;[215] poorly developed reduction peaks were observed in diluted urine samples possibly due to the presence of biological sample components, as shown in chapter 4. Oxidation and reduction peaks are larger in PAECs supernatant (Figure 6-3B) because of higher concentrations of 2,8-DHA. Response different from that of standards (in buffer), is likely due to matrix effects which change the background signal.

The concentration of 2,8-DHA at AECs determined at peak Ia from calibration curve sensitivity (obtained in 1:5 diluted HBSS) as shown in (Figure 6-4) is (13.2 ± 0.01) μM or (66.0 ± 0.5) μM in the original undiluted sample, compared to (64.2 ± 0.1) μM from HPLC-UV. Previous work with 2000-fold diluted urine described in chapter 4 has shown that calibration curve obtained in buffer can be used for quantitation of analytes (UA and XA) in biological fluids. At PAECs the concentration of 2,8-DHA is (26.4 ± 0.2) μM or (132.2 ± 1.0) μM in the undiluted sample and is (151.3 ± 0.1) μM from HPLC-UV. The results are summarized in (Table 6-1) and (Figure 6-5). The complex electrochemical response of 2,8-DHA may contribute to

lower concentrations that were determined by FSV compared to HPLC-UV when the concentration of 2,8-DHA increased. However, the effect of the matrix on sensor signal cannot be excluded. Standard additions of UA to cell supernatant resulted in higher sensitivity for UA, (0.80 ± 0.02) nA/ μM than the value observed in HBSS. Peak current of UA that was measured at (0.52 ± 0.08) V overlapped with the peak of 2,8-DHA but a linear increase in peak current with the concentration of UA was measured in the standard additions plot. Low solubility of 2,8-DHA limited the use of standard additions method for the determination of 2,8-DHA.

The relative concentration changes of 2,8-DHA determined by HPLC-UV and FSV, with changes in oxygen pressure and time, are the same ((Figure 6-5). At PAECs, at physiological oxygen pressures, 2,8-DHA concentration increases with time and it decreases after initial hyperoxia (Figure 6-5). Prolonged hyperoxia causes 2,8-DHA concentration to increase. In AECs at physiological oxygen pressures, 2,8-DHA concentration increases with time, and increases further after initial hypoxia, but prolonged hypoxia causes the concentration to decease significantly, coinciding with the decrease in cell viability.

Ade concentration can increase during stress as a result of up-regulation of polyamine synthesis, high MTAP activity, and reduced salvage;[12, 27] and Ade can be oxidized by xanthine oxidase[70] and/or ROS to 2,8-DHA. Hyperoxia decreases xanthine oxidase activity in PAECs,[32] and the concentrations of 2,8-DHA decreases initially as expected (Figure 6-5). However, PAECs appear to increase their metabolism, since 2,8-DHA concentration increases during extended hyperoxia, although not to the levels observed at physiological oxygen pressures. This points to the tolerance of PAECs to hyperoxia; the cells are known to survive under hyperoxic conditions for up to 6-8 days.[185] At AECs up-regulation of xanthine oxidase activity and purine

metabolism has been indicated during hypoxia, as observed.[10, 222] The results in (Figure 6-5) show that AECs are not tolerant to extended hypoxia.

Conclusions

High sensitivity of 2,8-DHA measurements with FSV at N-CFS has been demonstrated in physiological media (HBSS). To limit the effect of matrix components and electroactive interferences on 2,8-DHA signal, endothelial cell supernatants were diluted 5-fold with phosphate buffer prior to FSV measurement. The high sensitivity of the FSV method with N-CFS allowed the dilution of cell supernatants. Most of the concentrations of 2,8-DHA in the cell supernatants determined by FSV at the N-CFS are in agreement with those obtained from HPLC-UV. The complex electrochemical reaction pathway of 2,8-DHA which contributes to the complex response in FSV at N-CFS may involve dimer formation. The results support previously demonstrated tolerance of PAECs to hyperoxia and the low tolerance of AECs to hypoxia. Thus, 2,8-DHA appears to be a useful extracellular marker of oxidative stress in endothelial cells. The cellular pathways responsible for the formation of this marker have been proposed. The results demonstrate a route to sensor development for monitoring oxidative cell stress.

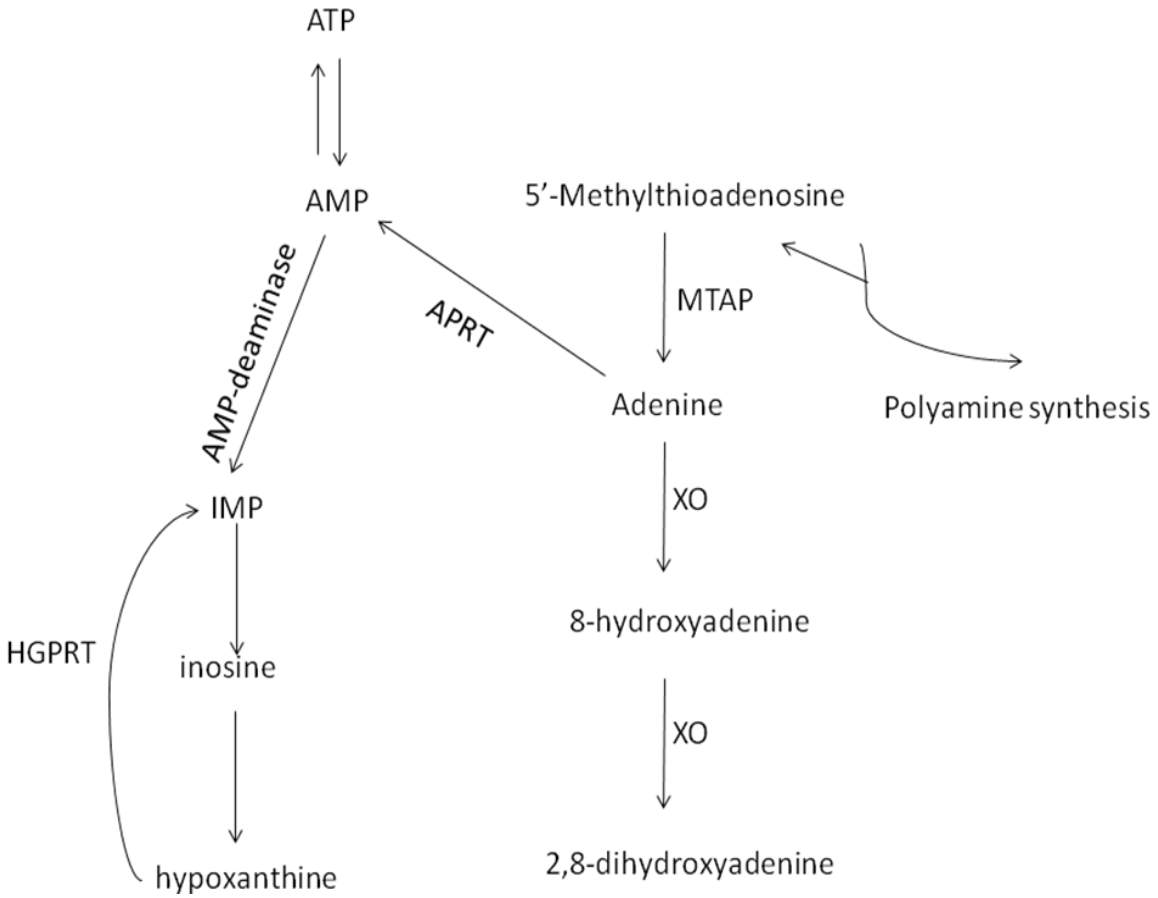

Figure 6-1. Polyamine synthesis pathway showing the source of adenine as a byproduct of 5'-methythioadenosine reaction with 5'methylthioadenosine phosphorylase (MTAP). Adenine is oxidized by xanthine oxidase to 2,8-dihydroxyadenine (2,8-DHA). Adenosine monophosphate (AMP) is converted to inosine monophosphate (IMP) via AMP-deaminase. IMP is converted to inosine, and then to Hy. Under normal conditions Hy is salvaged to IMP via hypoxanthine-guanine phosphoribosyl transferase (HGPRT)

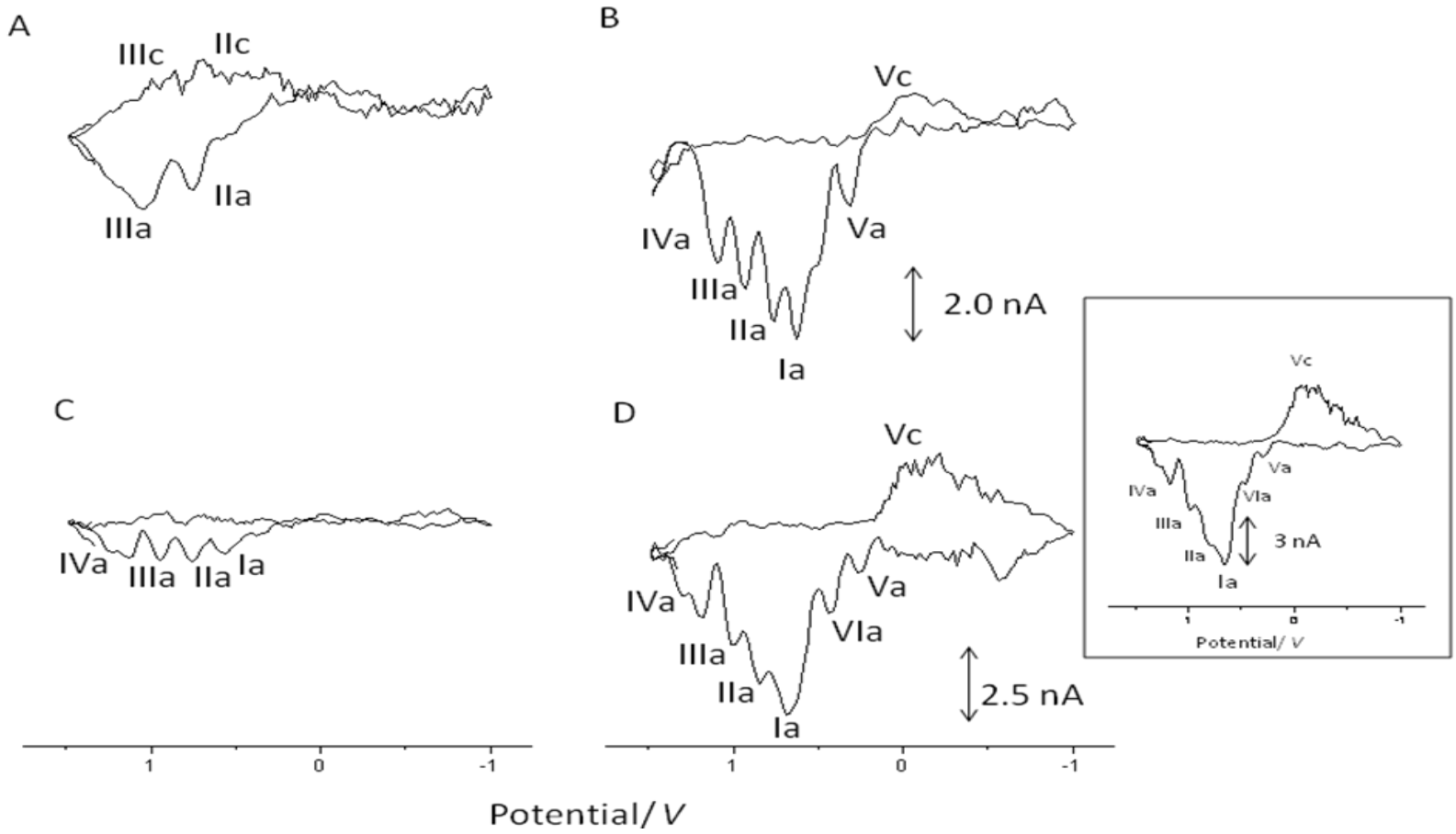

Figure 6-2. Fast scan cyclic voltammograms of: A) 1 μM and B) 15 μM 2,8-DHA in 31 mM phosphate buffer, pH 7.4 and C) 1 μM and D) 15 μM 2,8-DHA in 1:5 HBSS: phosphate buffer, pH 7.4. Inset shows voltammogram of 30 μM 2,8-DHA in 1:5 HBSS: phosphate buffer. Scan rate 500 V s^{-1}, electrode radius = 3.6 μM

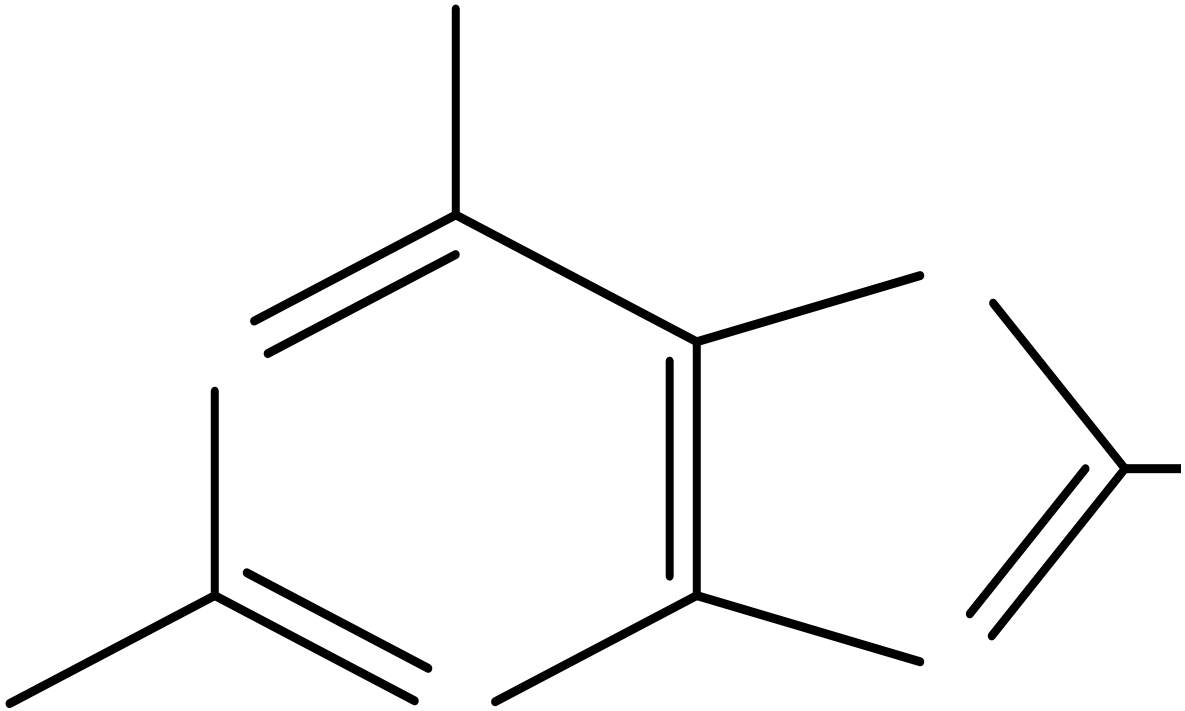

Scheme 6-1. Proposed electrochemical oxidation pathway of 2,8-DHA showing several possibilities for dimer formation

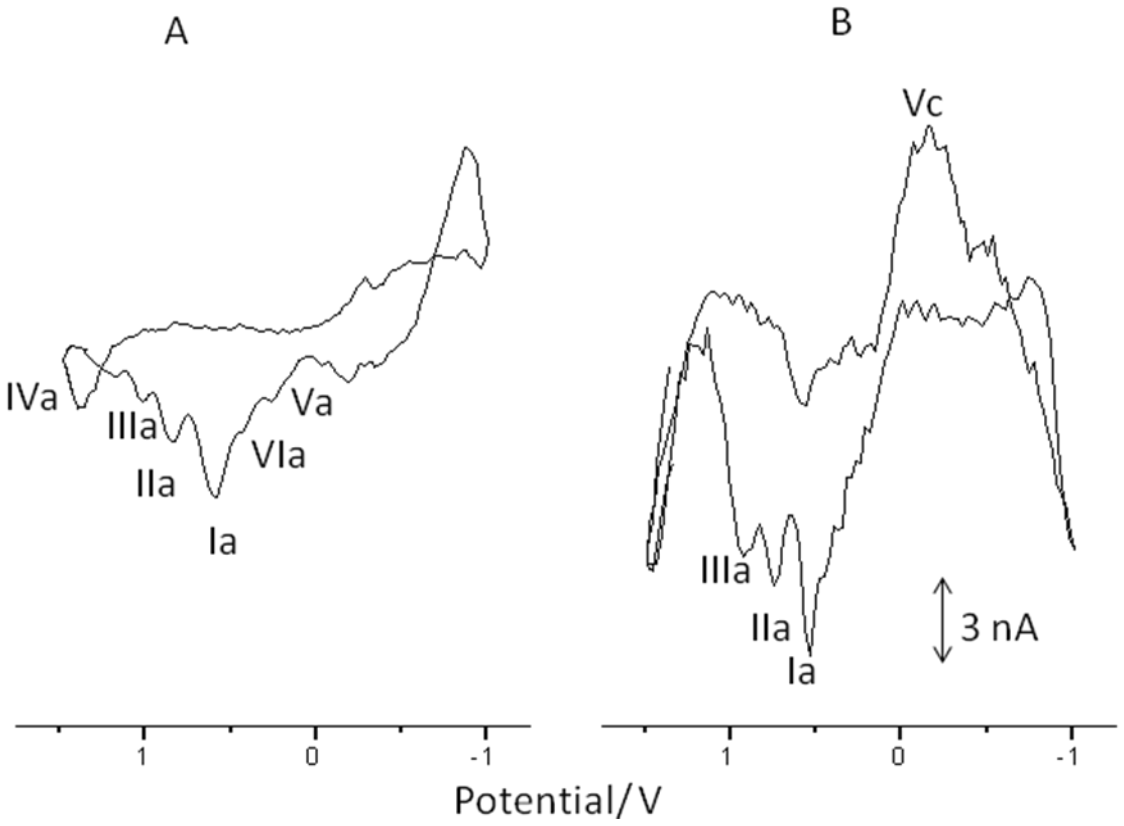

Figure 6-3. Fast scan cyclic voltammograms of: A) AECs supernatant after 48 hr of hypoxia and b) PAECs supernatant after 48 hr of hyperoxia. Other conditions as in (Figure 6-2C and D)

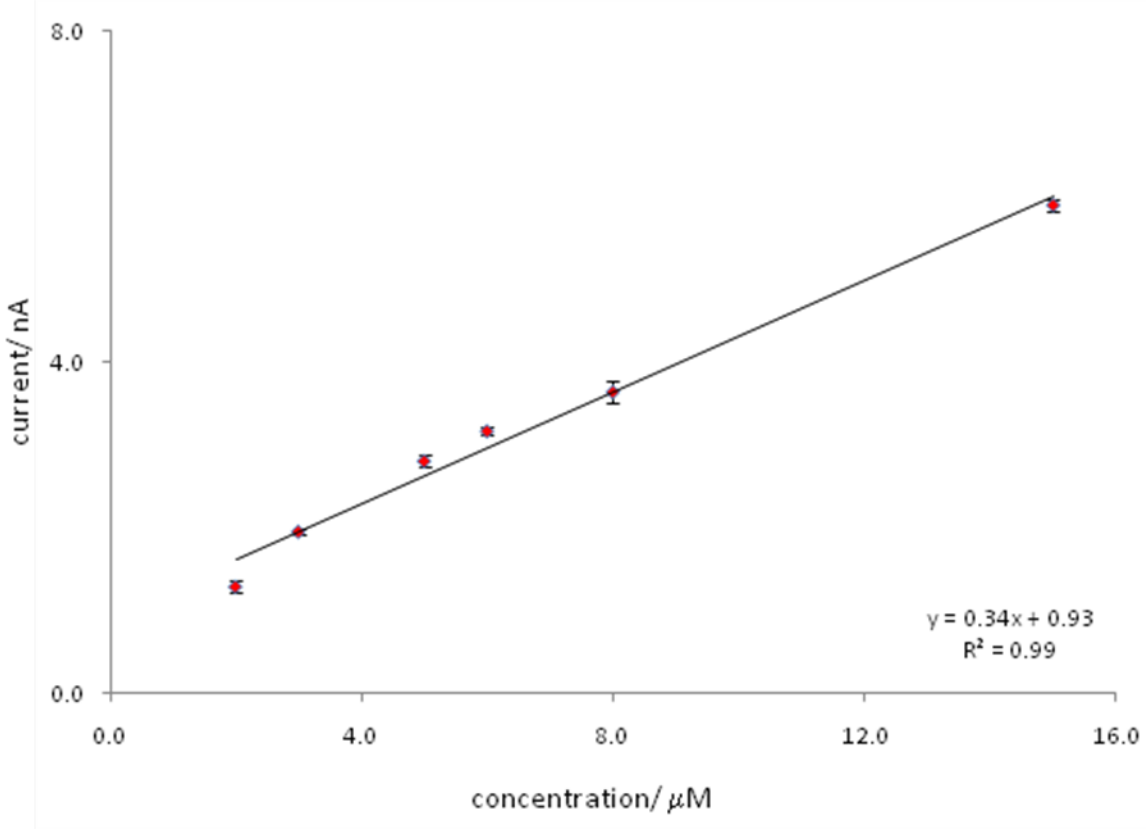

Figure 6-4. Calibration curve of 2,8-DHA in 1:5 HBSS: phosphate buffer, pH 7.4. Data are expressed as mean ± SD, (n =3)

Table 6-1. Concentrations of 2,8-DHA at endothelial cells with oxygen pressure and time by FSV at N-CFS and HPLC-UV

Cells	FSV at N-CFS (μM)	HPLC-UV (μM)
PAECs 3% O_2 24 hr	105.9 ± 0.6	151.3 ±0.3
PAECs 3% O_2 48 hr	161.8 ± 0.8	220 ± 0.1
PAECs 20% O_2 24 hr	86.6 ± 0.6	100.8 ± 0.1
PAECs 20% O_2 48 hr	132.2 ± 1.0	151.3 ± 0.1
AECs 20% O_2 24 hr	88.2 ± 0.2	100.8 ± 0.3
AECs 20% O_2 48 hr	95.6 ± 0.4	110.0 ± 0.1
AECs 3% O_2 24 hr	116.2 ± 0.8	119.2 ± 0.5
AECs 3% O_2 48 hr	66.0 ± 0.5	64.2 ± 0.1

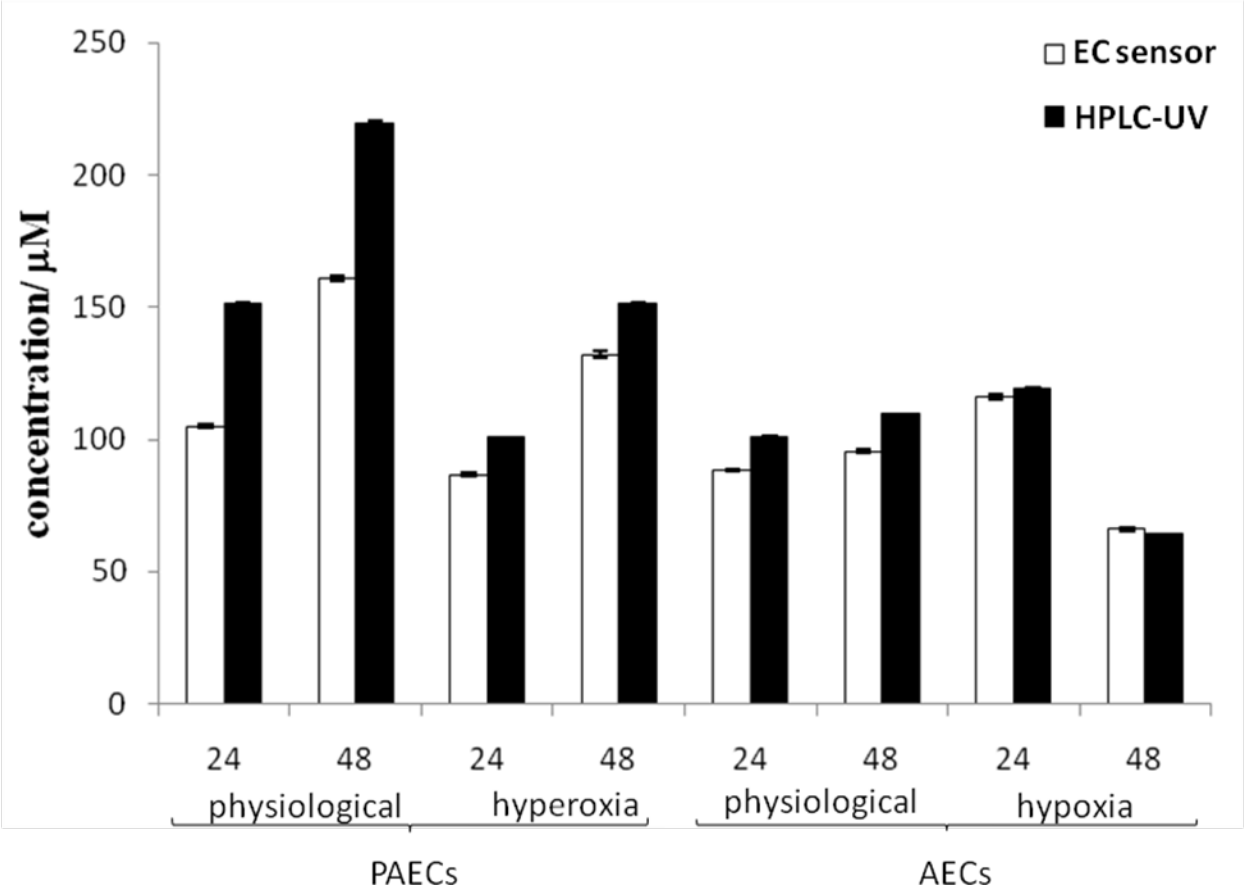

Figure 6-5. 2,8-DHA concentrations at PAECs and AECs with oxygen pressure and time measured by FSV at N-CFS and HPLC-UV

CHAPTER 7
CONCLUSIONS

Research to develop a N-CFS for measurement of purine metabolites in physiological media has led to several accomplishments. First, N-CFS with a highly active surface containing defects or pores were fabricated by a combination of mechanical polishing and electrochemical fabrication. Continuous potential cycling between -1.0 and +1.5 V at 10 V s^{-1} for 3600 cycles allowed moderate oxidation of the sensor surface, followed by reduction. When fabricated in phosphate buffer, the N-CFS have a highly stable background signal for repeated measurements. However fabrication of the N-CFS in the physiological buffer DMEM clogs the sensor surface and results in unstable background signals, while fabrication in HBSS causes an increase in the background signal. Therfore, in order to decrease the limits of detection and improve the sensitivity for cellular measurements, the fabrication of the sensor surface in phosphate buffer is most feasible, followed by analyte determination in 1:5 diluted HBSS as described in chapter 3.

Second, in chapter 4 the high sensitivity of the N-CFS with FSV as the signal acquisition method is demonstrated in the measurements of XA and UA in 2000-fold diluted urine. For XA, high sensitivity at the N-CFS is attributed to the low and stable background current at the sensor, especially at the oxidation potentials of XA.

The stability and reproducibility of fabrication of the sensors, which was verified from the measurements of sensor radius and the electrochemical activity of the sensors in ferricyanide solution, allowed pooling of data from different analyses and for different sensors. The geometric disk radius of the sensors that were used for analysis of (3.5 ± 0.4) µm, verified tight packing of the sealing resin and verified the absence of gaps in seals around the fiber.

The pathway of XA oxidation in FSV at the N-CFS is proposed, and it likely involves an initial $1e^-$ oxidation, which is followed by chemical reactions, and by $1e^-$ oxidation of the

intermediates. High resolution of XA and UA peaks is achieved in FSV at 500 Vs^{-1} at low concentrations of XA, at which the chemical reactions following the initial 1e- oxidation do not distort the XA oxidation peak. XA and UA concentrations, determined with the nanostructured PAN carbon fiber sensor and FSVare in good agreement with those obtained by HPLC-UV. Pre- or post-calibration of the sensor in buffer can be used in the determinations of XA and UA concentrations in urine to save time.

Third, in chapter 5 cell supernatants were first analyzed with a simple reversed phase HPLC-UV method with isocratic elution for the measurement of purine and pyrimidine metabolites released as a result of oxidative stress induced by hyperoxia and hypoxia. It was observed that the cellular media which contained HBSS may stress the cells resulting in changes in metabolite concentrations at physiological oxygen pressures with time.

PAECs appeared to be more robust and adaptive to hyperoxia by cellular relaxation and by regulation of both their polyamine synthesis pathway and purine metabolism, which in turn decrease the metabolite concentrations. The changes in the concentration of the metabolites in the extracellular fluid could serve as stress markers. Longer exposure of PAECs to hyperoxia increases metabolite concentrations, most likely by up-regulation of the polyamine pathway and purine metabolism. The changes in the levels of Ur are attributed mainly to increased UTP, CTP and RNA degradation.

AECs on the other hand seem to tolerate hypoxia for 24h hr by maintaing purine metabolism, enzyme activity and polyamine synthesis, as well as by reducing their salvage pathways. The resulting changes in the levels of metabolites at AECs could serve as stress markers. However, AECs cannot survive extended hypoxia (48 hr), as evident by the drastic drop

in metabolite concentrations, presumably from oxidative damage to RNA and DNA leading to cell death.

An important finding of this work is the measurement and identification of a new stress marker, 2,8-DHA, whose accumulation is proposed to be a result of reduced Ade salvage and the up-regulation of the polyamine synthesis pathway. Presumably when cells require polyamines for cell turnover and DNA protection, Ade is generated as a secondary byproduct which can be oxidized to 2,8-DHA by xanthine oxidase or ROS.

Finally, in chapter 6, the method developed for the N-CFS use in physiological media was applied to achieve high sensitivity in the determination of 2,8-DHA. The effect of matrix components and electroactive interferences on 2,8-DHA signal were limited by diluting the endothelial cell supernatants prior to FSV measurement. The high sensitivity of FSV method with N-CFS allowed the dilution of cell supernatants. Even though the concentrations of 2,8-DHA in the cell supernatants determined by FSV at the N-CFS are not in agreement with those obtained from HPLC-UV, the data obtained by FSV at N-CFS for 2,8-DHA support HPLC-UV results and demonstrate the tolerance of PAECs to hyperoxia and the low tolerance of AECs to hypoxia. 2,8-DHA appears to be a useful extracellular marker of oxidative stress in endothelial cells. The results demonstrate a route to sensor development for monitoring cell stress. The electrochemical reaction pathway of 2,8-DHA is proposed and helps explain the complex response in FSV at N-CFS and may involve dimer formation.

Future work could include mass spectrometry of the cell sample to verify the results obtained in this work. Also, standard addition to the cell supernatant using standard 2,8-DHA may be performed if the solubility issue of 2,8-DHA is solved in standard buffers. In HPLC-UV analysis, use of advanced stationary phases, such as Hilic, may allow separation of the

hydrophilic components in the cell supernatant and allow analysis of additional stress markers. Gradient elution could also be explored for additional information.

LIST OF REFERENCES

1 F. Q. Schafer and G. R. Buettner, *Free Radic. Biol. Med.,* 2001, **30**, 1191-1212.

2 M. C. Meyer and J. McHowat, *Am. J. Physiol.-Cell Physiol.,* 2007, **292**, C251-C258.

3 D. M. Rhoads, A. L. Umbach, C. C. Subbaiah and J. N. Siedow, *Plant Physiol.,* 2006, **141**, 357-366.

4 C. Y. Li and R. M. Jackson, *Am. J. Physiol. -Cell Physiol.,* 2002, **282**, C227-C241.

5 M. S. Lewis, R. E. Whatley, P. Cain, T. M. McIntyre, S. M. Prescott and G. A. Zimmerman, *J. Clin. Invest.,* 1988, **82**, 2045-2055.

6 S. W. Ballinger, C. Patterson, C. N. Yan, R. Doan, D. L. Burow, C. G. Young, F. M. Yakes, B. Van Houten, C. A. Ballinger, B. A. Freeman and M. S. Runge, *Circ. Res.,* 2000, **86**, 960-966.

7 E. S. Henle, R. Roots, W. R. Holley and A. Chatterjee, *Radiat. Res.,* 1995, **143**, 144-150.

8 A. Gorlach, *Circ. Res.,* 2005, **97**, 1-3.

9 D. A. Mei, G. J. Gross and K. Nithipatikom, *Anal. Biochem.,* 1996, **238**, 34-39.

10 W. B. Poss, T. P. Hueckstead, P. C. Panus, B. A. Freeman and J. R. Hoidal, *Am. J. Physiol.-Lung Cell. Molec. Physiol.,* 1996, **270**, L941-L946.

11 H. Kanemitsu, A. Tamura, T. Kirino, S. Karasawa, K. Sano, T. Iwamoto, M. Yoshiura and K. Iriyama, *J. Neurochem.,* 1988, **51**, 1882-1885.

12 P. M. Hassoun, A. L. Shedd, J. J. Lanzillo, V. Thappa, M. J. Landman and B. L. Fanburg, *Am. J. Respir. Cell Mol. Biol.,* 1992, **6**, 617-624.

13 G. Ermak and K. J. A. Davies, *Mol. Immunol.,* 2002, **38**, 713-721.

14 T. Kristian and B. K. Siesjo, *Life Sci.,* 1996, **59**, 357-367.

15 B. A. Freeman and J. D. Crapo, *J. Biol. Chem.,* 1981, **256**, 10986-10992.

16 H. Zenri, K. Rodriquez-Capote, L. McCaig, L. J. Yao, A. Brackenbury, F. Possmayer, R. Veldhuizen and J. Lewis, *Crit. Care Med.,* 2004, **32**, 1155-1160.

17 R. M. Jackson, *Chest,* 1985, **88**, 900-905.

18 H. Y. Kim, A. B. Singhal and E. H. Lo, *Ann. Neurol.,* 2005, **57**, 571-575.

19 A. B. Singhal, E. H. Lo, T. Dalkara and M. A. Moskowitz, *Neuroimaging Clin. N. Am.,* 2005, **15**, 697-720.

20 S. Papaiahgari, S. R. Kleeberger, H. Y. Cho, D. V. Kalvakolanu and S. P. Reddy, *J. Biol. Chem.,* 2004, **279**, 42302-42312.

21 D. R. Prows, A. P. Hafertepen, W. J. Gibbons Jr, A. V. Winterberg and T. G. Nick, *Physiol. Genomics,* 2007, **30**, 262-270.

22 D. R. Prows, A. P. Hafertepen, A. V. Winterberg, W. J. Gibbons Jr, C. Liu and T. G. Nick, *Physiol. Genomics,* 2007, **30**, 271-281.

23 A. C. Dudley, D. Thomas, J. Best and A. Jenkins, *Biochem. J.,* 2005, **390**, 427-436.

24 A. V. Tretyakov and H. W. Farber, *J. Clin. Invest.,* 1995, **95**, 738-744.

25 S. Mertens, T. Noll, R. Spahr, A. Krutzfeldt and H. M. Piper, *Am. J. Physiol.,* 1990, **258**, H689-H694.

26 J. Brett, D. Stern, S. Ogawa, S. C. Silverstein and J. D. Loike, *J. Cell Biol.,* 1989, **109**, 312A.

27 O. Culic, U. K. M. Decking and J. Schrader, *Am. J. Physiol. -Cell Physiol.,* 1999, **276**, C1061-C1068.

28 E. W. Nester and J. Spizizen, *J. Bacteriol.,* 1961, **82**, 867-874.

29 H. Kanemitsu, A. Tamura, K. Sano, T. Iwamoto, M. Yoshiura and K. Iriyama, *J. Neurochem.,* 1986, **46**, 851-853.

30 H. Kanemitsu, S. Karasawa, H. Nihei, N. Tomukai, A. Tamura, K. Sano, T. Iwamoto, M. Yoshiura and K. Iriyama, *Brain and Nerve (Tokyo),* 1989, **41**, 157-163.

31 H. Nihei, H. Kanemitsu, A. Tamura, H. Oka and K. Sano, *Neurosurgery,* 1989, **25**, 613-617.

32 P. M. Hassoun, F. S. Yu, A. L. Shedd, J. J. Zulueta, V. J. Thannickal, J. J. Lanzillo and B. L. Fanburg, *Am. J. Physiol.,* 1994, **266**, L163-L171.

33 P. M. Hassoun, F. S. Yu, C. G. Cote, J. J. Zulueta, R. Sawhney, K. A. Skinner, H. B. Skinner, D. A. Parks and J. J. Lanzillo, *Am. J. Respir. Crit. Care Med.,* 1998, **158**, 299-305.

34 M. G. Clark, S. M. Richards, M. Hettiarachchi, J. M. Ye, G. J. Appleby, S. Rattigan and E. Q. Colquhoun, *Biochem. J.,* 1990, **266**, 765-770.

35 A. T. Demiryurek and R. M. Wadsworth, *Pharmacol. Ther.,* 1999, **84**, 355-365.

36 G. Loschen and A. Azzi, *Hoppe-Seylers Zeitschrift Fur Physiologische Chemie,* 1974, **355**, 1226-1226.

37 S.Spiekermann, U. Landmesser, S. Dikalov, M. Bredt, G. Gamez, H. Tatge, N. Reepschlager, B. Hornig, H. Drexler and D. G. Harrison, *Circulation,* 2003, **107**, 1383-1389.

38 D. Jagnandan, W. C. Sessa and D. Fulton, *Am. J. Physiol. -Cell Physiol.,* 2005, **289**, C1024-C1033.

39 A. J. North, K. S. Lau, T. S. Brannon, L. J. C. Wu, L. B. Wells, Z. German and P. W. Shaul, *Am. J. Physiol. -Lung Cell. Mol. Physiol.,* 1996, **270**, L643-L649.

40 E. R. Block, H. Herrera and M. Couch, *Am. J. Physiol. -Lung Cell. Mol. Physiol.,* 1995, **269**, L574-L580.

41 R. Siekmeier, T. Grammer and W. Marz, *J. Cardiovasc. Pharmacol. Ther.,* 2008, **13**, 279-297.

42 Y. Xia, A. L. Tsai, V. Berka and J. L. Zweier, *J. Biol. Chem.,* 1998, **273**, 25804-25808.

43 K. A. Skinner, C. R. White, R. Patel, S. Tan, S. Barnes, M. Kirk, V. Darley-Usmar and D. A. Parks, *J. Biol. Chem.,* 1998, **273**, 24491-24497.

44 N. S. Dhalla, R. M. Temsah and T. Netticadan, *J. Hypertens.,* 2000, **18**, 655-673.

45 S. R. Thomas, K. Chen and J. F. Keaney, *Antioxid. Redox Signal.,* 2003, **5**, 181-194.

46 K. M. Kim, G. N. Henderson, R. F. Frye, C. D. Galloway, N. J. Brown, M. S. Segal, W. Imaram, A. Angerhofer and R. J. Johnson, *J. Chromatogr. B,* 2009, **877**, 65-70.

47 I. F. F. Benzie, W. Y. Chung and B. Tomlinson, *Clin. Chem.,* 1999, **45**, 901-904.

48 G. L. Squadrito, R. Cueto, A. E. Splenser, A. Valavanidis, H. W. Zhang, R. M. Uppu and W. A. Pryor, *Arch. Biochem. Biophys.,* 2000, **376**, 333-337.

49 B. N. Ames, R. Cathcart, E. Schwiers and P. Hochstein, *Proc. Natl. Acad. Sci. U. S. A.,* 1981, **78**, 6858-6862.

50 G. Kroemer, L. Galluzzi and C. Brenner, *Physiol. Rev.,* 2007, **87**, 99-163.

51 A. C. Rego, M. S. Santos and C. R. Oliveira, *J. Neurochem.,* 1997, **69**, 1228-1235.

52 S. Ahmad, A. Ahmad, M. Ghosh, C. C. Leslie and C. W. White, *J. Biol. Chem.*, 2004, **279**, 16317-16325.

53 Y. Pankratov, U. Lalo, A. Verkhratsky and R. A. North, *Pflugers Arch.*, 2006, **452**, 589-597.

54 K. Kovacs, K. Hanto, Z. Bognar, A. Tapodi, E. Bognar, G. Kiss, A. Szabo, G. Rappai, T. Kiss, B. Sumegi and F. Gallyas, *Mol. Cell. Biochem.*, 2009, **321**, 155-164.

55 R. M. Berne, *Circ. Res.*, 1980, **47**, 807-813.

56 T. Inoue, Z. S. Mu, K. Sumikawa, K. Adachi and T. Okochi, *Jpn. J. Cancer Res.*, 1993, **84**, 720-725.

57 K. Kita, S. Matsunami and J. I. Okumura, *J. Nutr.*, 1996, **126**, 1610-1617.

58 Z. W. Li, J. H. Wu and C. J. DeLeo, *IUBMB Life*, 2006, **58**, 581-588.

59 U. Rinas, K. Hellmuth, R. J. Kang, A. Seeger and H. Schlieker, *Appl. Environ. Microbiol.*, 1995, **61**, 4147-4151.

60 Y. B. Kim, C. M. Lew and J. D. Gralla, *J. Bacteriol.*, 2006, **188**, 7457-7463.

61 Q. Deng, L. M. Kauri, W. J. Qian, G. M. Dahlgren and R. T. Kennedy, *Analyst*, 2003, **128**, 1013-1018.

62 M. Kathiwala, A. O. Affum, J. Perry and A. Brajter-Toth, *Analyst*, 2008, **133**, 810-816.

63 R. Bravo and A. Brajter-Toth, *Chem. Anal.*, 1999, **44**, 423-436.

64 R. Boulieu, C. Bory, P. Baltassat and C. Gonnet, *Anal. Biochem.*, 1983, **129**, 398-404.

65 N. Arikyants, A. Sarkissian, A. Hesse, T. Eggermann, E. Leumann and B. Steinmann, *Pediatr. Nephrol.*, 2007, **22**, 310-314.

66 G. Rebentisch, S. Stolz and J. Muche, *Aktuelle Urol.*, 2004, **35**, 215-221.

67 C. Vidotto, D. Fousert, M. Akkermann, A. Griesmacher and M. M. Muller, *Clin. Chim. Acta*, 2003, **335**, 27-32.

68 F. A. Mateos, J. G. Puig, M. L. Jimenez and I. H. Fox, *J. Clin. Invest.*, 1987, **79**, 847-852.

69 V. Di Pietro, I. Perruzza, A. M. Amorini, A. Balducci, L. Ceccarelli, G. Lazzarino, P. Barsotti, B. Giardina and B. Tavazzi, *Clin. Biochem.*, 2007, **40**, 73-80.

70 H. A. Simmonds, *Clin. Chim. Acta.*, 1986, **160**, 103-108.

71 E. T. G. Cavalheiro, K. El-Nour and A. Brajter-Toth, *J. Braz. Chem. Soc.*, 2000, **11**, 512-515.

72 E. T. G. Cavalheiro and A. Brajter-Toth, *J. Pharm. Biomed. Anal.*, 1999, **19**, 217-230.

73 A. Brajter-Toth, K. Abou El-Nour, E. T. Cavalheiro and R. Bravo, *Anal. Chem.,* 2000, **72**, 1576-1584.

74 C. Hsueh, R. Bravo, A. J. Jaramillo and A. Brajter-Toth, *Anal. Chim. Acta,* 1997, **349**, 67-76.

75 B. E. K. Swamy and B. J. Venton, *Analyst,* 2007, **132**, 876-884.

76 W. G. Kuhr and R. M. Wightman, *Brain Res.,* 1986, **381**, 168-171.

77 J. O. Howell and R. M. Wightman, *J. Phys. Chem.,* 1984, **88**, 3915-3918.

78 M. Heien, P. E. M. Phillips, G. D. Stuber, A. T. Seipel and R. M. Wightman, *Analyst,* 2003, **128**, 1413-1419.

79 M. J. Logman, E. A. Budygin, R. R. Gainetdinov and R. M. Wightman, *J. Neurosci. Methods,* 2000, **95**, 95-102.

80 R. M. Wightman, *Science,* 1988, **240**, 415-420.

81 T. G. Strein and A. G. Ewing, *Anal. Chem.,* 1994, **66**, 3864-3872.

82 M. F. Suaudchagny, R. Cespuglio, J. P. Rivot, M. Buda and F. Gonon, J. Neurosci. Methods.,1993, **48**, 241-250.

83 K. Pihel, T. J. Schroeder and R. M. Wightman, *Anal. Chem.,* 1994, **66**, 4532-4537.

84 S. Adapa, V. Gaur and N. Verma, *Chem. Eng. J.,* 2006, **116**, 25-37.

85 J. B. Donnet and R. C. Bansal, *Carbon Fibers*, Marcel Dekker, New York, 1990.

86 K. Kinoshita, *Carbon: Electrochemical and Physical Properties*, Wiley & Sons, New York, 1988.

87 L. R. McCreery and K. K. Cline, *In Laboratory Techniques in Electroanalytical Chemistry*, Dekker, New York, 1996.

88 L. R. McCreery, *In Electroanalytical Chemistry*, Dekker, New York, 1991.

89 J. A. Stamford, *Trends Neurosci.,* 1989, **12**, 407-412.

90 P. S. Cahill, Q. D. Walker, J. M. Finnegan, G. E. Mickelson, E. R. Travis and R. M. Wightman, *Anal. Chem.,* 1996, **68**, 3180-3186.

91 K. Abou El-Nour and A. Brajter-Toth, *Analyst,* 2003, **128**, 1056-1061.

92 K. Abou El-Nour and A. Brajter-Toth, *Electroanalysis,* 2000, **12**, 805-810.

93 R. Bravo, C. Hsueh, A. Jaramillo and A. Brajter-Toth, *Analyst,* 1998, **123**, 1625-1630.

94 P. M. Kovach, A. G. Ewing, R. L. Wilson and R. M. Wightman, *J. Neurosci. Methods,* 1984, **10**, 215-227.

95 J. O. Howell and R. M. Wightman, *Anal. Chem.,* 1984, **56**, 524-529.

96 D. Garreau, P. Hapiot and J. M. Saveant, *J Electroanal Chem,* 1989, **272**, 1-16.

97 C. C. Hsueh and A. Brajter-Toth, *Anal. Chim. Acta,* 1996, **321**, 209-214.

98 M. Vonstackelberg, M. Pilgram and V. Toome, *Zeitschrift Fur Elektrochemie,* 1953, **57**, 342-350.

99 P. Tschuncky and J. Heinze, *Anal. Chem.,* 1995, **67**, 4020-4023.

100 T. Childers-Peterson and A. Brajter-Toth, *Anal. Chim. Acta,* 1987, **202**, 167-174.

101 B. Tavazzi, G. Lazzarino, P. Leone, A. M. Amorini, F. Bellia, C. G. Janson, V. Di Pietro, L. Ceccarelli, S. Donzelli, J. Francis and B. Giardina, *Clin. Biochem.,* 2005, **38**, 997-1008.

102 R. Tawa, M. Kito and S. Hirose, *Chem. Lett.,* 1981, , 745-748.

103 G. Ihler, A. Lantzy, J. Purpura and R. H. Glew, *J. Clin. Invest.,* 1975, **56**, 595-602.

104 E. R. Block, J. M. Patel and D. Edwards, *Am. J. Physiol.,* 1989, **257**, C223-C231.

105 J. Zak and T. Kuwana, *J. Am. Chem. Soc.,* 1982, **104**, 5514-5515.

106 R. C. Engstrom and V. A. Strasser, *Anal. Chem.,* 1984, **56**, 136-141.

107 K. W. Hathcock, J. C. Brumfield, C. A. Goss, E. A. Irene and R. W. Murray, *Anal. Chem.,* 1995, **67**, 2201-2206.

108 P. M. Kovach, M. R. Deakin and R. M. Wightman, *J. Phys. Chem.,* 1986, **90**, 4612-4617.

109 G. N. Kamau, W. S. Willis and J. F. Rusling, *Anal. Chem.,* 1985, **57**, 545-551.

110 C. Hildebrandt, H. Bueth and H. Thielecke, *Ann. Anat. -Anat. Anz.,* 2009, **191**, 23-32.

111 R. G. Humphrey, S. D. Smith, L. Pang, Y. Sadovsky and D. M. Nelson, *Placenta,* 2005, **26**, 491-497.

112 B. T. Pierce, P. G. Napolitano, L. M. Pierce, C. C. Apodaca, R. F. Hume and B. C. Calhoun, *Am. J. Obstet. Gynecol.*, 2001, **185**, 1068-1072.

113 P. C. Panus, R. Radi, P. H. Chumley, R. H. Lillard and B. A. Freeman, *Free Radic. Biol. Med.,* 1993, **14**, 217-223.

114 E. Park, G. SchullerLevis, J. H. Jia and M. R. Quinn, *J. Leukoc. Biol.,* 1997, **61**, 161-166.

115 P. H. Chen, M. A. Fryling and R. L. McCreery, *Anal. Chem.,* 1995, **67**, 3115-3122.

116 P. L. Runnels, J. D. Joseph, M. J. Logman and R. M. Wightman, *Anal. Chem.,* 1999, **71**, 2782-2789.

117 R. S. Kelly, D. J. Weiss, S. H. Chong and T. Kuwana, *Anal. Chem.,* 1999, **71**, 413-418.

118 D. T. Fagan, I. F. Hu and T. Kuwana, *Anal. Chem.,* 1985, **57**, 2759-2763.

119 K. J. Stutts, P. M. Kovach, W. G. Kuhr and R. M. Wightman, *Anal. Chem.,* 1983, **55**, 1632-1634.

120 M. Hadi, A. Rouhollahi, F. Taidy and M. Yousefi, *Electroanalysis,* 2007, **19**, 668-673.

121 B. E. K. Swamy and B. J. Venton, *Anal. Chem.,* 2007, **79**, 744-750.

122 G. P. Jin and X. Q. Lin, *Electrochem. Commun.,* 2004, **6**, 454-460.

123 G. la Marca, B. Casetta, S. Malvagia, E. Pasquini, M. Innocenti, M. A. Donati and E. Zammarchi, *J. Mass. Spectrom.,* 2006, **41**, 1442-1452.

124 E. S. Ford, C. Y. Li, S. Cook and H. K. Choi, *Circulation,* 2007, **115**, 2526-2532.

125 I. Ben-Zvi, Y. Green, F. Nakhoul, Y. Kanter and R. M. Nagler, *Nephron. Clin. Pract.,* 2007, **105**, 114-120.

126 A. A. Ejaz, W. Mu, D. H. Kang, C. Roncal, Y. Y. Sautin, G. Henderson, I. Tabah-Fisch, B. Keller, T. M. Beaver, T. Nakagawa and R. J. Johnson, *Clin. J. Am. Soc. Nephrol.,* 2007, **2**, 16-21.

127 E. Krishnan, C. K. Kwoh, H. R. Schumacher and L. Kuller, *Hypertension,* 2007, **49**, 298-303.

128 T. Kuhara, *J. Chromatogr. B,* 2002, **781**, 497-517.

129 T. Ito, A. B. P. van Kuilenburg, A. H. Bootsma, A. J. Haasnoot, A. van Cruchten, Y. Wada and A. H. van Gennip, *Clin. Chem.,* 2000, **46**, 445-452.

130 N. Cooper, R. Khosravan, C. Erdmann, J. Fiene and J. W. Lee, *J. Chromatogr. B,* 2006, **837**, 1-10.

131 L. Domanski, K. Safranow, M. Ostrowski, A. Pawlik, M. Olszewska, G. Dutkiewicz and K. Ciechanowski, *Arch. Med. Res.,* 2007, **38**, 240-246.

132 E. Causse, A. Pradelles, B. Dirat, A. Negre-Salvayre, R. Salvayre and F. Couderc, *Electrophoresis,* 2007, **28**, 381-387.

133 V. F. Samanidou, A. S. Metaxa and I. N. Papadoyannis, *J. Liq. Chromatogr. Rel. Technol.,* 2002, **25**, 43-57.

134 Q. C. Chu, M. Lin, C. H. Geng and J. N. Ye, *Chromatographia,* 2007, **65**, 179-184.

135 E. Palecek, *Anal. Biochem.,* 1980, **108**, 129-138.

136 J. L. Owens and G. Dryhurst, *Anal. Chim. Acta,* 1977, **89**, 93-99.

137 A. D. Lazareck, S. G. Cloutier, T. F. Kuo, B. J. Taft, S. O. Kelley and J. M. Xu, *Nanotechnol.,* 2006, **17**, 2661-2664.

138 R. Bravo, D. M. Stickle and A. Brajter-Toth, *Methods in Molecular Biology*, Humana Press Inc, Totowa, New Jersey, 2002,.ch 21.

139 J. X. Feng, M. Brazell, K. Renner, R. Kasser and R. N. Adams, *Anal. Chem.,* 1987, **59**, 1863-1867.

140 C. A. Goss, J. C. Brumfield, E. A. Irene and R. W. Murray, *Anal. Chem.,* 1993, **65**, 1378-1389.

141 J. C. O'Brien, J. Shumaker-Parry and R. C. Engstrom, *Anal. Chem.,* 1998, **70**, 1307-1311.

142 M. G. Sullivan, B. Schnyder, M. Bartsch, D. Alliata, C. Barbero, R. Imhof and R. Kotz, *J. Electrochem. Soc.,* 2000, **147**, 2636-2643.

143 N. Oya and D. J. Johnson, *Carbon,* 2001, **39**, 635-645.

144 M. X. Ji, C. G. Wang, Y. J. Bai, M. J. Yu and Y. X. Wang, *Polym. Bull.,* 2007, **59**, 527-536.

145 C. Kim, S. H. Park, J. K. Cho, D. Y. Lee, T. J. Park, W. J. Lee and K. S. Yang, *J. Raman Spectrosc.,* 2004, **35**, 928-933.

146 A. J. Bard and L. R. Faulkner, *Electrochemical Methods, Fundamentals and Applications*, 2nd Ed; John Wiley & Sons Inc; New York, 2001.

147 A. Vieira, J. P. Telo and R. M. B. Dias, *J. Chim. Phys*., 1997, **94**, 318-325.

148 A. Vieira and S. Steenken, *J. Chim Phys*., 1996, **93**, 235-243.

149 J. Santamaria, C. Pasquier, C. Ferradini and J. Pucheault, *Radiat. Res.,* 1984, **97**, 452-461.

150 G. Dryhurst, *J. Electrochem. Soc.,* 1972, **119**, 1659-1665.

151 K. N. Rogstad, Y. H. Jang, L. C. Sowers and W. A. Goddard, *Chem. Res. Toxicol.,* 2003, **16**, 1455-1462.

152 C. C. Hsueh and A. Brajter-Toth, *Anal. Chem.,* 1993, **65**, 1570-1575.

153 N. Marklund, B. Ostman, L. Nalmo, L. Persson and L. Hillered, *Acta Neurochir.,* 2000, **142**, 1135-1142.

154 L. S. Terada, D. Piermattei, G. N. Shibao, J. L. McManaman and R. M. Wright, *Arch. Biochem. Biophys.,* 1997, **348**, 163-168.

155 T. K. Hazra, T. Izumi, I. Boldogh, B. Imhoff, Y. W. Kow, P. Jaruga, M. Dizdaroglu and S. Mitra, *Proc. Natl. Acad. Sci. U. S. A.,* 2002, **99**, 3523-3528.

156 J. Laval, J. Jurado, M. Saparbaev and O. Sidorkina, *Mutat. Res*., 1998, **402**, 93-102.

157 H. Cai and D. G. Harrison, *Circ. Res.,* 2000, **87**, 840-844.

158 D. X. Zhang and D. D. Gutterman, *Am. J. Physiol. -Heart Circul. Physiol.,* 2007, **292**, H2023-H2031.

159 M. Quintero, S. L. Colombo, A. Godfrey and S. Moncada, *Proc. Natl. Acad. Sci. U. S. A.,* 2006, **103**, 5379-5384.

160 S. Therade-Matharan, E. Laemmel, S. Carpentier, Y. Obata, T. Levade, J. Duranteau and E. Vicaut, *Am. J. Physiol.,* 2005, **289**, R1756-R1762.

161 D. B. J. Bone and J. R. Hammond, *Am. J. Physiol. -Heart Circul. Physiol.,* 2007, **293**, H3325-H3332.

162 V. Ralevic and G. Burnstock, *Pharmacol. Rev.,* 1998, **50**, 413-492.

163 M. Papaspyrou, L. E. Feinendegen and H. W. Mullergartner, *Cancer Res.,* 1994, **54**, 6311-6314.

164 Q. C. Yu, W. J. Mergner, R. D. Vigorito and J. H. Resau, *Pathobiology,* 1990, **58**, 138-145.

165 M. H. Maguire, I. Szabo, I. E. Valko, B. E. Finley and T. L. Bennett, *J. Chromatogr. B,* 1998, **707**, 33-41.

166 M. Czauderna and J. Kowalczyk, *J. Chromatogr. B,* 1997, **704**, 89-98.

167 S. G. James, G. J. Appleby, K. A. Miller, J. T. Steen, E. Q. Colquhoun and M. G. Clark, *Gen. Pharmacol.,* 1996, **27**, 837-844.

168 Van Wylen, D. G. L. and S. A. Manthei, *Basic Res. Cardiol.,* 1997, **92**, 368-377.

169 F. Niklasson, *Clin. Chem.,* 1983, **29**, 1543-1546.

170 W. S. Waring, D. J. Webb and S. R. J. Maxwell, *QJM-Mon. J. Assoc. Physicians,* 2000, **93**, 707-713.

171 R. E. Handschumacher and A. D. Welch, *Cancer Res.,* 1956, **16**, 965-969.

172 J. Saevels, A. Z. Perez, A. S. Jauma, A. Van Schepdael and J. Hoogmartens, *Chromatographia,* 1998, **47**, 225-229.

173 R. T. Smolenski, Z. Kochan, R. McDouall, C. Page, A. M. L. Seymour and M. H. Yacoub, *Cardiovasc. Res.,* 1994, **28**, 100-104.

174 J. D. Loike, L. Cao, J. Brett, S. Ogawa, S. C. Silverstein and D. Stern, *Am. J. Physiol.,* 1992, **263**, C326-C333.

175 J. I. Ram and L. M. Hiebert, *In Vitro Mol. Toxicol. -J. Basic Appl. Res.,* 2001, **14**, 209-217.

176 J. Sevcik, T. Adam and H. Mazacova, *Clinica Chimica Acta,* 1996, **245**, 85-92.

177 J. Reutershan, I. Vollmer, S. Stark, R. Wagner, K. C. Ngamsri and H. K. Eltzschig, *FASEB J.,* 2009, **23**, 473-482.

178 H. K. Eltzschig, J. C. Ibla, G. T. Furuta, M. O. Leonard, K. A. Jacobson, K. Enjyoji, S. C. Robson and S. P. Colgan, *J. Exp. Med.,* 2003, **198**, 783-796.

179 R. Seifert and G. Schultz, *Trends Pharmacol. Sci.,* 1989, **10**, 365-369.

180 K. Kroll, T. R. Bukowski, L. M. Schwartz, D. Knoepfler and J. B. Bassingthwaighte, *Am. J. Physiol.,* 1992, **262**, H420-H431.

181 L. M. Schwartz, T. R. Bukowski, J. H. Revkin and J. B. Bassingthwaighte, *Am. J. Physiol. -Heart Circul. Physiol.,* 1999, **277**, H1241-H1251.

182 M. J. Bell, C. S. Robertson, P. M. Kochanek, J. C. Goodman, S. P. Gopinath, J. A. Carcillo, R. S. B. Clark, D. W. Marion, Z. C. Mi and E. K. Jackson, 2001, , 399-404.

183 J. Doukas, T. A. H. Cutler, C. A. Boswell, I. Joris and G. Majno, *Am. J. Pathol.,* 1994, **145**, 211-219.

184 A. Clement, U. Hubscher and A. F. Junod, *J. Appl. Physiol.,* 1985, **59**, 1110-1116.

185 S. Ahmad, A. Ahmad, E. Gerasimovskaya, K. R. Stenmark, C. B. Allen and C. W. White, *Am. J. Respir. Cell Mol. Biol.,* 2003, **28**, 179-187.

186 A. G. Tkachenko, *Biochem. -Moscow,* 2004, **69**, 188-194.

187 A. D. Hacker, D. F. Tierney and T. K. Obrien, *Biochem. Biophys. Res. Commun.,* 1983, **113**, 491-496.

188 C. A. Haven, J. W. Olson, S. S. Arcot and M. N. Gillespie, *Am. J. Respir. Cell Mol. Biol.,* 1992, **7**, 286-292.

189 N. A. V. Belle, G. D. Dalmolin, G. Fonini, M. A. Rubin and J. B. T. Rocha, *Brain Res.,* 2004, **1008**, 245-251.

190 H. C. Ha, N. S. Sirisoma, P. Kuppusamy, J. L. Zweier, P. M. Woster and R. A. Casero, *Proc. Natl. Acad. Sci. U. S. A.,* 1998, **95**, 11140-11145.

191 A. U. Khan, Y. H. Mei and T. Wilson, *Proc. Natl. Acad. Sci. U. S. A.,* 1992, **89**, 11426-11427.

192 B. Tadolini, *Biochem. J.,* 1988, **249**, 33-36.

193 B. Tadolini, L. Cabrini, L. Landi, E. Varani and P. Pasquali, *Biochem. Biophys. Res. Commun.,* 1984, **122**, 550-555.

194 H. Tabor, S. M. Rosenthal and C. W. Tabor, *Annu. Rev. Biochem.,* 1961, **30**, 579-&.

195 K. W. Minton, H. Tabor and C. W. Tabor, *Proc. Natl. Acad. Sci. U. S. A.,* 1990, **87**, 2851-2855.

196 E. Lovaas and G. Carlin, *Free Radic. Biol. Med.,* 1991, **11**, 455-461.

197 G. Drolet, E. B. Dumbroff, R. L. Legge and J. E. Thompson, *Phytochemistry,* 1986, **25**, 367-371.

198 E. Gerlach and B. F. Becker, *Topics and perspectives in adenosine research.* Springer-Verlag, Berlin, Heidelberg, New York, 1987.

199 S. J. Engle, M. G. Stockelman, J. Chen, G. Boivin, M. N. Yum, P. M. Davies, M. Y. Ying, A. Sahota, H. A. Simmonds, P. J. Stambrook and J. A. Tischfield, *Proc. Natl. Acad. Sci. U. S. A.,* 1996, **93**, 5307-5312.

200 D. Erlinge, J. Harnek, C. van Heusden, G. Olivecrona, S. Jern and E. Lazarowski, *Int. J. Cardiol.,* 2005, **100**, 427-433.

201 A. Mazzola, E. Amoruso, E. Beltrami, D. Lecca, S. Ferrario, S. Cosentino, E. Tremoli, S. Ceruti and M. P. Abbracchio, *J. Cell. Mol. Med.,* 2008, **12**, 522-536.

202 E. R. Lazarowski and R. C. Boucher, *News. Physiol. Sci.,* 2001, **16**, 1-5.

203 O. Culic, M. L. H. Gruwel and J. Schrader, *Am. J. Physiol. -Cell Physiol.,* 1997, **42**, C205-C213.

204 N. M. Elsayed and D. F. Tierney, *Arch. Biochem. Biophys.,* 1989, **273**, 281-286.

205 L. S. Terada, C. J. Beehler, A. Banerjee, J. M. Brown, M. A. Grosso, A. H. Harken, J. M. McCord and J. E. Repine, *J. Appl. Physiol.,* 1988, **65**, 2349-2353.

206 D. Dreher and A. F. Junod, *J. Cell. Physiol.,* 1995, **162**, 147-153.

207 H. T. Li, H. M. Cui, T. K. Kundu, W. Alzawahra and J. L. Zweier, *J. Biol. Chem.,* 2008, **283**, 17855-17863.

208 Z. Zhang, D. Naughton, P. G. Winyard, N. Benjamin, D. R. Blake and M. C. R. Symons, *Biochem. Biophys. Res. Commun.,* 1998, **251**, 667-667.

209 C. I. Jones, Z. S. Han, T. Presley, S. Varadharaj, J. L. Zweier, G. Ilangovan and B. R. Alevriadou, *Am. J. Physiol. -Cell Physiol.,* 2008, **295**, C180-C191.

210 L. Christa, J. Kersual, J. Auge and J. L. Perignon, *Biochem. J.,* 1988, **255**, 145-152.

211 K. Kaneko, S. Fujimori, T. Kumakawa, N. Kamatani and L. Akaoka, *Metab. -Clin. Exp.,* 1991, **40**, 918-921.

212 J. B. Wyngaarden and J. T. Dunn, *Arch. Biochem. Biophys.,* 1957, **70**, 150-156.

213 R. N. Goyal, A. Kumar and A. Mittal, *J. Chem. Soc.,* 1991, , 1369-1375.

214 V. C. Diculescu, J. A. P. Piedade and A. Oliveira-Brett, *Bioelectrochem*., 2007, **70**, 141-146.

215 R. N. Goyal and A. Mittal, *Indian J. Chem. Sect A-Inorg. Phys. Theor. Anal. Chem.,* 1993, **32**, 852-856.

216 B. T. Emmerson, R. B. Gordon and L. Thompson, *Aust. N. Z. J. Med.,* 1975, **5**, 440-446.

217 T. Wessel, C. Lanvers, S. Fruend and G. Hempel, *Journal of Chromatography A,* 2000, **894**, 157-164.

218 S. Sumi, K. Kidouchi, S. Ohba and Y. Wada, *J. Chromatogr. B-Biomed. Appl.,* 1995, **672**, 233-239.

219 T. Kojima, T. Nishina, M. Kitamura, N. Kamatani and K. Nishioka, *Clin. Chim. Acta,* 1989, **181**, 109-113.

220 R. N. Goyal and A. Sangal, *J Electroanal Chem,* 2003, **557**, 147-155.

221 R. N. Goyal and A. Sangal, *J Electroanal Chem,* 2002, **521**, 72-80.

222 E. E. Kelley, T. Hock, N. K. H. Khoo, G. R. Richardson, K. K. Johnson, P. C. Powell, G. I. Giles, A. Agarwal, J. R. Lancaster and M. M. Tarpey, *Free Radic. Biol. Med.,* 2006, **40**, 952-959.

BIOGRAPHICAL SKETCH

Ms Mehjabin Abdul Majid Kathiwala was born to Late Mr Abdul Majid Kathiwala and Mrs Naeema Kathiwala. After finishing her Master of Science in Bombay, India, Ms Kathiwala came to the United States in August 2000 to Louisville, Kentucky and attended the University of Louisville and earned her Master of Science in 2003 under the able guidance of Dr Cecilia M Yappert. That same year Ms Kathiwala moved to Gainesville, Florida. She married her longtime boyfriend Krupant Vora in 2003 and started her PhD at the University of Florida the following Fall semester.

During her PhD Ms Kathiwala also became a proud mother to Isa Vora in 2008. Ms Kathiwala completed her PhD in the summer of 2009 under the able guidance of Dr Anna Brajter-Toth. Her current research interests include analytical applications of electrochemical techniques and HPLC to measurements of stress and disease markers in biological fluids.